CFIRE

Wisconsin Study on the Impact of OSOW Vehicles on Complex Bridges

CFIRE 08-03
March 2016

National Center for Freight & Infrastructure Research & Education
Department of Civil and Environmental Engineering
College of Engineering
University of Wisconsin–Madison

Authors:
Jaime Yanez-Rojas, Jin Yu, and Professor Michael Oliva
University of Wisconsin–Madison

Principal Investigator:
Professor Michael Oliva
University of Wisconsin–Madison

Co-Principal Investigator:
Professor Teresa M. Adams
University of Wisconsin–Madison

This page intentionally left blank.

Technical Report Documentation

1. Report No. CFIRE 08-03	2. Government Accession No.	3. Recipient's Catalog No. **CFDA 20.701**	
4. Title and Subtitle Wisconsin Study on the Impact of OSOW Vehicles on Complex Bridges		5. Report Date **March 2016** 6. Performing Organization Code	
7. Author/s Jaime Yanez-Rojas, Jin Yu, and Michael Oliva		8. Performing Organization Report No. **CFIRE 08-03**	
9. Performing Organization Name and Address National Center for Freight and Infrastructure Research and Education (CFIRE) University of Wisconsin-Madison 1415 Engineering Drive, 2205 EH Madison, WI 53706		10. Work Unit No. (TRAIS) 11. Contract or Grant No. **0092-13-11**	
12. Sponsoring Organization Name and Address Wisconsin Department of Transportation Research and Library Services Section Division of Business Management 4802 Sheboygan Ave., Room 104 Madison, WI 53705		13. Type of Report and Period Covered **Final Report 08/08/2013 – 10/07/2015** 14. Sponsoring Agency Code	
15. Supplementary Notes Project completed by CFIRE with support from the Wisconsin Department of Transportation.			
16. Abstract Special purpose freight vehicles, which may weigh six times the normal legal limit, request special government permits for travel along selected highway routes. It is difficult for transportation agencies to determine the effects of these vehicles on some unique complex bridge structures. Errors in issuing travel permits may impact public safety or impede commerce through long detours. The goal of this study was to identify how complex bridges, unlike normal girder span bridges, respond to normal and oversize truck loading and then to develop methods that might be used for simply evaluating the impact of overweight trucks on bridges as part of the permit issuing process. Some of these results may also be useful in the bridge rating processes. Three long span arch bridges, one rigid frame bridge and two short span opening bascule bridges were examined in detail analytically to investigate their behavior; three of the bridges were also load tested to provide proof of the accuracy of the analytic methods used.			
17. Key Words Freight Vehicles, Travel Permits, Bridges, Oversize Trucks, Overweight Trucks, OSOW	18. Distribution Statement **No restrictions. This report is available to the public through the National Transportation Library Digital Repository.**		
19. Security Classification (of this report) **Unclassified**	20. Security Classification (of this page) **Unclassified**	21. No. of Pages	22. Price **-0-**

Form DOT F 1700.7 (8-72) Reproduction of form and completed page is authorized.

DISCLAIMER

This research was funded by the National Center for Freight and Infrastructure Research and Education. The contents of this report reflect the views of the authors, who are responsible for the facts and the accuracy of the information presented herein. This document is disseminated under the sponsorship of the US Department of Transportation, University Transportation Centers Program, in the interest of information exchange. The US Government assumes no liability for the contents or use thereof. The contents do not necessarily reflect the official views of the National Center for Freight and Infrastructure Research and Education, the University of Wisconsin–Madison, or the US DOT's RITA at the time of publication.

Wisconsin Study on the Impact of OSOW Vehicles on Complex Bridges

Professor Michael Oliva,
Jaime Yanez-Rojas,
Jin Yu,
Professor Teresa Adams

March 31, 2016

Funding provided by the Wisconsin Department of Transportation

National Center for Freight & Infrastructure Research & Education
College of Engineering
Department of Civil and Environmental Engineering
University of Wisconsin, Madison

SUMMARY

Objective:

Special purpose freight vehicles, which may weigh 6 times the normal legal limit, request special government permits for travel along selected highway routes. It is difficult for transportation agencies to determine the effects of these vehicles on some unique complex bridge structures. Errors in issuing travel permits may impact public safety or impede commerce through long detours.

The goal of this study was to identify how complex bridges, unlike normal girder span bridges, respond to normal and oversize truck loading and then to develop methods that might be used for simply evaluating the impact of overweight trucks on bridges as part of the permit issuing process. Some of these results may also be useful in the bridge rating processes.

Three long span arch bridges, one rigid frame bridge and two short span opening bascule bridges were examined in detail analytically to investigate their behavior; three of the bridges were also load tested to provide proof of the accuracy of the analytic methods used.

Critical Observations:

Very large overload vehicles, with total gross weights nearly seven times the weight of the truck used for bridge design, can be allowed to pass over most of the complex bridges examined. This may be particularly important for the long span arch bridges, such as the La Crosse Cameron Avenue tied arch**.** The Leo Frigo Memorial bridge over the Fox River in Green Bay was found to be slightly less robust, but even its truck capacity was not limited by the main structural elements: the arch and the tie beam. There were no cases, of the set of bridges examined, where vehicles with gross weight of up to 500,000lbs caused the arches, tie girders or hangers of these bridges to be overloaded.

As a general conclusion it appears that the bridge stringers, which support the concrete deck, and the floor beams, which support the stringers, are the critical components that need to be closely examined when an overload vehicle is crossing a complex bridge. The stringer force capacity limited the bridge load capacity in three of the five bridges that were closely examined. The floor beam force capacity controlled in one.

A close analytical examination of two complex parts of the bascule bridge, the midspan joint between leafs and the tail beam that prevents the bascule leafs from tipping downward, was not possible within the scope of this project. An indirect method of tail beam analysis, based on the empirical data from a Marinette bascule bridge load test combined with force predictions from analysis, did indicate that it is highly likely that the tail beam or tail lock could be severely overloaded (to nearly twice the yield stress) under both full factored HL-93 design truck loading and the oversize/overweight

(OSOW) special truck loading. The tail lock beam is an essential resisting element in a bascule bridge and needs to be guarded. It appears critical that further investigation of the tail beams on an array of bascule bridges be undertaken. Special care should be dedicated to the tail lock beam during annual bascule bridge inspections.

Two bascule bridges were examined analytically, one was load tested. Under the HL-93 design truck loading, the bridge capacity was found to be limited by the stringer strength in one case and the floor beam strength in the second case. When the large overweight vehicles pass over these bridges, however, the capacity is limited by the strength of the two main bascule girders that support the entire bridge.

Simplified Analysis Methods:

A general simplified method for estimating forces in stringers and floor beams was not satisfactorily achieved for all loadings. The portion of truck wheel loads carried by a stringer can be estimated by using an AASHTO defined distribution factor (from the AASHTO Standard Specifications) and the stringer moments calculated for HL-93 design truck loading will be acceptable for most bridges with standard proportions. When the span to spacing ratio of the stringers exceeds 4, as in the Frigo bridge, then use of the AASHTO factor may produce results that are 25% conservative.

Stringer moments are not successfully predicted for the heavy OSOW trucks using the same AASHTO distribution for the trucks examined. It is unlikely that the AASHTO factor would work with any vehicle that has wheel spacing on an axle substantially different from the AASHTO assumed 6ft. spacing. When OSOW trucks were on the bridges examined, the stringer moments could be conservatively predicted using an alternate method that overestimated by 16% to 124%. The alternate method estimates wheel loading on a stringer by considering the bridge deck to act as short simply supported spans between stringers. Calculated reactions from the deck on the stringers, due to wheel loads, are used to calculate the stringer moments. This method conservatively estimated stringer moments in all cases.

Floor beam forces were more difficult to predict than the stringer forces when using a simplified method. One of the primary difficulties is in accounting for the restraint applied to a floor beam by the supporting girders. In cases where the joint was by web connection only, the floor beam could be considered pin ended. When the floor beams were rigidly connected to the girders the assumed support condition was dubious. A fixed end assumption produced a calculation of negative end moments much larger than actually existed, and of course smaller positive moments. A pin ended assumption over-estimated the magnitude of the positive moments. The calculation process is further complicated by the assumption made regarding the wheel load distribution to the stringers as discussed above. Results for floor beam moment calculations in the bridges examined were acceptable with HL-93 loading present, except in the case of the Chippewa arch bridge. With OSOW vehicle loading the

moments were over estimated by 9% to 43% (except with the Chippewa bridge), a conservative result that may be acceptable for judging capacity.

A simple method for estimating moments in the main girders of bascule bridges was identified and provided very accurate results for HL-93 truck loading but was 20% to 30% conservative for the special OSOW trucks. Existence of an initial small gap in the midspan joint between leaves of a bascule bridge was found to have little effect on peak forces and stress. With a gap of 0.125in. in the Winneconne bridge, the resulting peak stresses change by only 8%. In bridges with well-maintained joints the effect of an initial gap on the member forces can be ignored.

Methodology:

Eight key steps were used in defining the effects of special oversize/overweight vehicles on unusual complex bridges. The main tool employed in the process was a specialized software program capable of refined 3-dimensional modelling of the complete bridge structures and moving various vehicles across the model bridges while tracking the impact of the vehicle on individual structural members. The steps in using this tool are as follow.

1. Four unique oversized/overweight (OSOW) vehicles were are identified, with advice from the WisDOT load permitting office and specialized freight shipping companies, that would serve as test load when solving for the bridge response.
2. Five critical highway routes through the State of Wisconsin were identified that frequently see requests for special load moving permits. Complex bridges along those routes were selected for in-depth study.
3. Amongst the identified complex bridges, three were selected to have load tests run. The test results would be compared to the analytic predictions to verify the capability of the modelling and software to provide accurate estimates of structural member loads.
4. Analytic models of the bridges for load testing were built based on available plan information. Trucks were run over the models, and critical locations in the bridges where structural members were highly loaded were defined. Those locations were places that were then chosen for placement of gages to be monitored during the load testing.
5. Three bridges were field inspected and load tests were conducted with strain and deflection data obtained to document the bridge performance.
6. The analytic models were compared with visual field inspections of the bridges and modifications to the models were made based on a better understanding of the as-built structural systems. Predicted member strain values from the models were compared with the collected strain data from test to validate the accuracy of the prediction method.
7. All of the selected critical complex bridges were modelled and loaded with the selected OSOW trucks in addition to the normal truck used in design. The results of the model analyses were used to find the most highly loaded structural members compared to their

load capacities. These members would usually control the size and type of loading that could be applied to the bridges.

8. Various simple methods, compared to the 3-D complex finite element analysis used in prior steps, were tested to see if they could approximate estimates of the forces likely to be experienced during future OSOW loading of the bridges. These are methods that the highway freight permitting authorities might use in judging the impact of a truck on a bridge and in issuing load permits for vehicles to cross specific bridges.

CONTENTS

1. INTRODUCTION

1.1 Background

Special overload vehicles, over legal limits in size or weight, need to travel highways as industry evolves and large items must be shipped. Transport of these large items, such as pressure vessels, wind turbines, electrical transformers and military equipment, often impose loads that exceed the normal interstate legal limit of 80 thousand pounds (80 kips). They may be substantially larger than loads assumed in bridge design. A vehicle with a million pound load is shown in Figure 1.1-1. In fact the gross weight of these trucks, as seen in the load of Figure 1.1-2, may weigh more than five to six times the design truck load. Consequently, transportation agencies are asked to provide special permits for these vehicles. Permit approval entails checking capacity of bridges along the intended route.

Figure 1.1-1. OSOW special vehicle. Reprinted from Perkins STC.

Because of the unusual axle configurations and excessive loading of these trucks, checking the capacity may involve an analysis to insure that forces in bridge components do not exceed their operating limits. This is usually a direct process for bridges with common configurations. For unusual or complex bridges an extraordinary time-consuming analysis may be required. Conducting such an analysis may be an unreasonable demand in the special case of complex bridges. The Wisconsin Department of Transportation (WisDOT) seeks simplified methods in evaluating the impact of OSOW vehicles for those cases.

In a previous project sponsored by the National Center for Freight and Infrastructure Research and Education (CFIRE), working with WisDOT, a simplified analysis method to predict the effects of these OSOW vehicles on normal girder span bridge systems was successfully developed in 2009 [1]. This report focuses on analysis methods for unusual or complex bascule, arch and rigid frame bridges.

1.2 Purpose, Objectives and Scope

The research objective of this project is to simplify the overload permitting process executed by WisDOT engineers for complex bascule, arch and rigid frame bridges subjected to OSOW vehicles located on critical freight routes in Wisconsin. The effects of vehicles on bridges are usually found by evaluating the forces that the loading causes in individual members of the bridge. The American Association of State Highway and Transportation Officials (AASHTO) in their *LRFD Bridge Design Specifications* [2] provide factors to predict the portion of load from a bridge lane that will be resisted by a single girder in normal short girder span bridges. However, those factors are not intended for use with unusual complex bridges. Thus, this research project focuses on developing means to predict the force effects caused by OSOW vehicles on complex bridges to provide reliability in permit issuance and to ensure safety of crossing for OSOW freight vehicles on bridge structures.

Though it would be valuable to have simple methods of analysis that could apply to all complex bridges, the substantial differences in behavior of different bridge configurations would require an in depth study of a multitude of bridges to develop general guidelines. The scope of this project was limited to examine a small set of critical Wisconsin complex bridges. Simple methods for analysis will be explored but the small sample size will make generalizations speculative. The primary aim will be to provide WisDOT with tools to evaluate the most critical bridges.

Four critical routes in the State of Wisconsin and a fifth one along the Mississippi River were selected as target pathways with complex bridges. The critical routes were selected by examining WisDOT's historical permit issuing records for locations where overload permit applications most frequently occurred. As might be expected, these routes connected the large metropolitan cities: Minneapolis – St. Paul, Milwaukee, Marinette-Green Bay and Madison with other out-of-state destinations. Figure 1.2-1 shows these critical routes in a Wisconsin highway map.

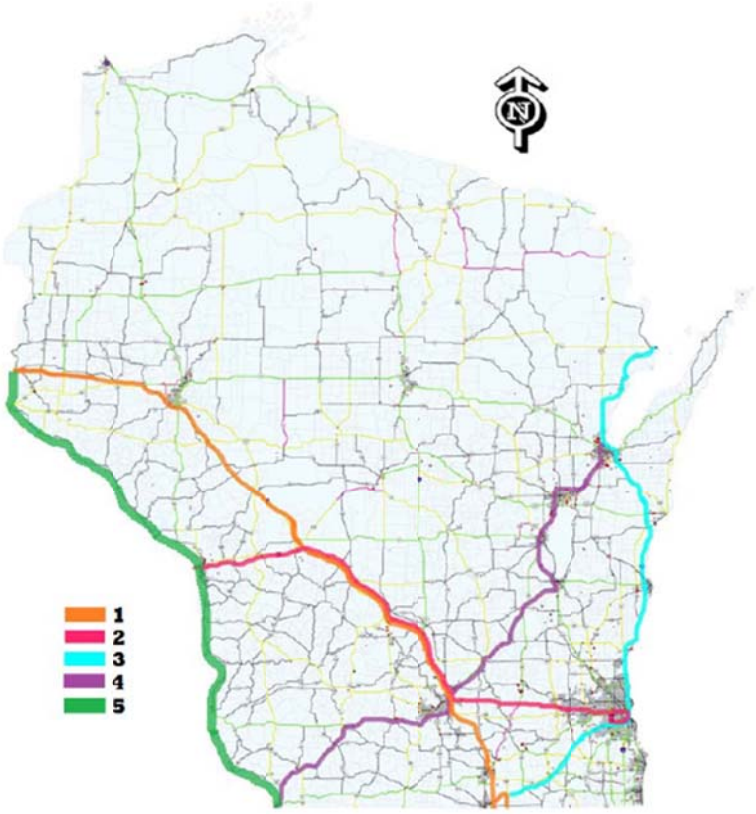

Figure 1.2-1. Critical routes for OSOW truck permitting in Wisconsin.

In cooperation with WisDOT, seven complex bridges, most on the critical routes, were selected for OSOW loading and force analysis:

i) Twin rigid frame bridges on I-90/I-94 over Mirror Lake in Sauk County (B-56-0048) on critical routes 1&2,
ii) Tied arch bridge over the Fox River on IH 43 in Green Bay (B-05-158-0010) on critical route 3,
iii) Tied arch bridge on STH64 and Bridge St. over the Chippewa River (B-09-0087) not on a critical route,
iv) Tied arch bridge on US 14/16/61 over the Mississippi in La Crosse (B-32-0202-0002) on the Mississippi critical route,
v) Steel truss bridge on USH 14/61/16 over the Mississippi (B-32-300) in La Crosse on the Mississippi critical route,
vi) Double-leaf bascule bridge on Ogden St. over the Menominee River (B-38-16-0003) in Marinette-Menominee near critical route 3, and
vii) Double-leaf bascule bridge on STH116 and main St. over Wolf River (B-70-913-0002) in Winneconne, Winnebago County near critical route 4.

1.3 Literature Review

This study is focused on analyzing the effects of overload vehicles on rigid frame, arch, truss and bascule bridges using three-dimensional finite element modeling (3DFEM). A brief description of useful previous work done in this area and the relevance of each to this study is explained.

Chung and Sotelino [3] investigated 3DFEM techniques for composite steel girder bridges focusing on the flexure behavior of the system. Four 3D FE bridge models were examined to understand geometric modeling errors, incompatibility and accuracy. This paper was useful to this research in understanding different modeling techniques to simulate composite action between girders and decks.

Bae and Oliva [1] evaluated the effects of overload vehicles on bridges. The report was primarily focused on multi-girder bridges, and included the analysis of two complex bridges: the Mirror Lake Bridge (also analyzed in this report) and the Bong Bridge. This study was relevant to the present research efforts in learning 3DFEM techniques and understanding the overload effects on partially composite girders. Load combinations representing OSOW vehicles identified in that report were selected for use in this study.

WisDOT Bridge and Structure Inspection manuals were fundamental in understanding behavior and structural components of bascule and rigid frame bridges. A book by Koglin [8] on movable bridge engineering was also helpful for understanding the functions of elemental components of bascule bridges such as tail beams and center locks.

2. METHODOLOGY

2.1 Procedure

The research objective is to identify and predict how specific complex bridges respond under OSOW vehicles. This information may later be used in the WisDOT permitting process to evaluate the safety in allowing OSOW freight vehicles to cross the bridges. The following five tasks are utilized to accomplish the project objective: analytic modeling, field instrumentation test, analysis verification, OSOW effect examination and examination of simplified methods.

Analytic Modeling

For the development of computer bridge models, WisDOT and project personnel selected the commercial CSiBridge analysis software [5]. CSiBridge is versatile software package with integrated 3DFEM analysis, design and rating functions. Each of the target bridges is initially modelled using the software. Initial modelling is used, with HL-93 truck loading, to identify critically loaded components in the bridges and truck positions on the bridge likely to cause the largest force effects.

Field Test Instrumentation Plan

Load tests are conducted on a subset of the selected bridges. One frame, arch and bascule bridge is tested. The bridges are instrumented to measure force conditions in critical components. The test data then provides a data base to judge and verify the quality of the analytic predictions of response and the analytical modelling. The Mirror Lake, Marinette and La Crosse bridges are selected as the rigid frame, bascule and tied-arch respectively to perform the field tests. The procedures used in testing and the test results are provided in this report.

Resistive foil and vibrating wire strain gages are placed, with the help of WisDOT personnel, on critical members of the selected bridges in order to detect large strains. Both reach-alls and loaded dump trucks are used as the test vehicles.

Analysis Verification

Comparative analysis is conducted by examining the predicted bridge response from the initial analytic models and the measured bridge data from the field test. Stresses in the members calculated from axial and bending moment diagrams provided by the software are converted to strains and compared to the data from the strain gages.

The initial analytic models are created based on the available recorded bridge plans, engineering judgment/assumptions, and experience. Changes made to the analytic models are done after on-site bridge inspections when the information on the plans isn't clear about the behavior and geometry of members and joints. The intent is to match the analytical model with the as-built bridge.

Where the exact behavior of the bridge is unclear, such as the degree of composite action between beams and decks, data obtained from the field test is used to improve assumptions initially made for the model. These particular changes are also described in more detail.

OSOW Vehicle Analysis

Each of the target bridges will be subjected to the passing of a series of OSOW vehicles analytically with the software. In this analysis the bridges are modelled as complex 3D structures with a combination of frame, shell and link FEM elements to accurate simulate the bridge response. Two types of overload vehicles, single lane and dual lane trailers are selected for use in this study. These are vehicles used in a previous OSOW study [1] and based on data obtained from trucking firms that provide special trucks for transporting OSOW loads. The transverse wheel spacing of the trucks is shown in Figure 2.1-1. Single lane trailers have constant 8-ft. spacing between centers of dual wheels. For the dual lane trailer, the spacing between the centers of the middle dual wheels are assumed to be 2 ft., 6 ft. and 10 ft. for the analysis since the actual OSOW truck configurations can vary depending on the loads carried.

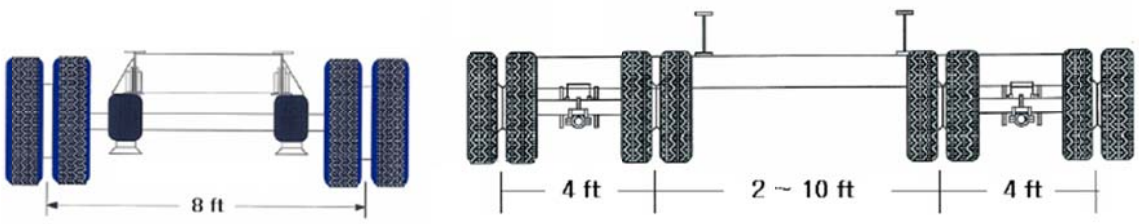

(a) (b)

Figure 2.1-1. Transverse wheel spacing of the (a) single and (b) dual lane trailers. Reprinted from Bae, H. and Oliva, M. [1].

The longitudinal axle spacings for the OSOW vehicles are also taken from the previous study. The longitudinal axle configurations for the OSOW vehicles are shown in Figure 2.1-2 for (a) a 313-kip truck, (b) a 446-kip truck, (c) a 500-kip truck, and (d) a 486-kip truck.

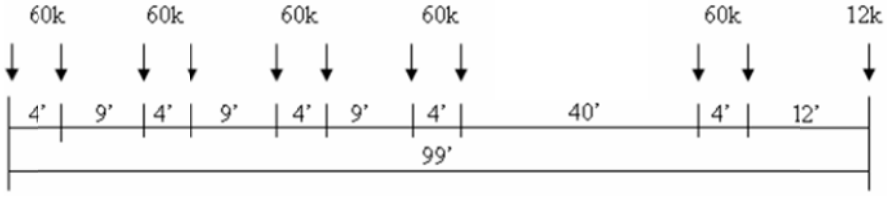

(a)

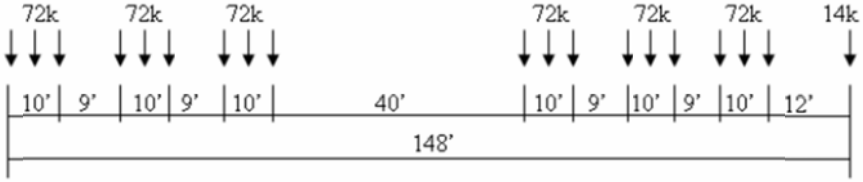

(b)

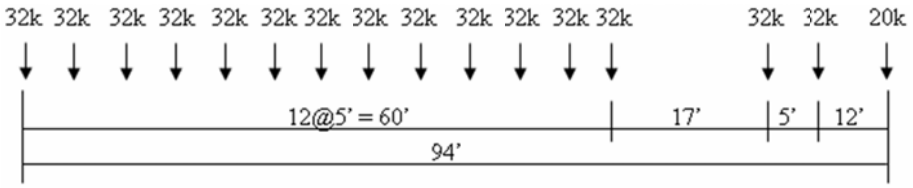

(c)

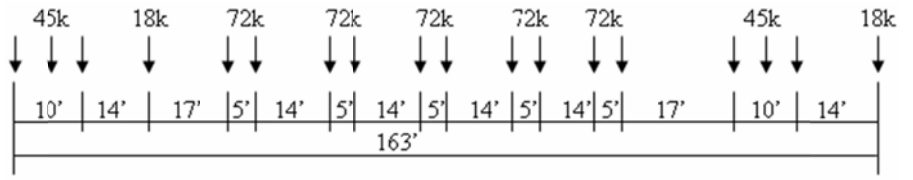

(d)

Figure 2.1-2. Axle spacing of selected overload vehicles. (a) & (b) Single lane loading, (c) & (d) dual lane loading. Reprinted from Bae, H. and Oliva, M. [1].

In addition, the current design vehicular load used by AASHTO, designated as the HL-93, is also included in the analysis of this bridge to provide a basis for judgement of the severity of the overload vehicles. The HL-93 live load consists of 5 different load types: design truck (72 kips), design tandem (50 kips), design lane, double truck and fatigue truck. These loads are then combined and scaled to generate six live load combinations. The LRFD live load factor of 1.75 for the Strength I limit state is applied to the HL93 truck with an impact factor of 33 percent in the design process. Both lanes may be loaded when the HL-93 truck is used – compared to a single OSOW vehicle assumed on the bridge at any time. The only load type not considered in this analysis is the double truck, which is used for negative moments at the support of continuous bridges. A picture describing the loads used in this project is shown in Figure 2.1-3.

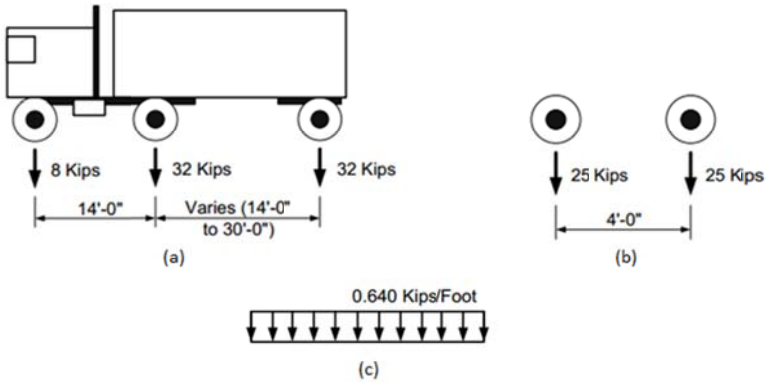

Figure 2.1-3. AASHTO HL-93 (a) design truck, (b) design tandem and (c) design lane. Fatigue truck is the same as design truck but with a fixed space between back and middle axle of 30 ft. Reprinted from WisDOT Bridge Manual [4].

For the 3DFEM analysis, AASHTO standard HL-93 combinations are driven in one or more lanes, considering that the truck is only 10-ft. wide with a 6-ft. wheel spacing on each axle and each lane is 12-ft. wide. In the case of OSOW trucks, single and dual lane trailers are driven alone on the bridge due to weight and speed special considerations. Single lane trailers and the dual lane trailer with 2-ft. transverse spacing are driven in one of the 12-ft. wide lanes on the bridge. Dual lane trailers with 6-ft. and 10-ft. transverse spacing are driven down the centerline of the bridge due to the inability to fit in a single lane. Figure 2.1-4 clarifies lane loading used in the bridge models. A table summarizing type of vehicle and different factors used in the bridge analysis is shown in Table 2.1-1.

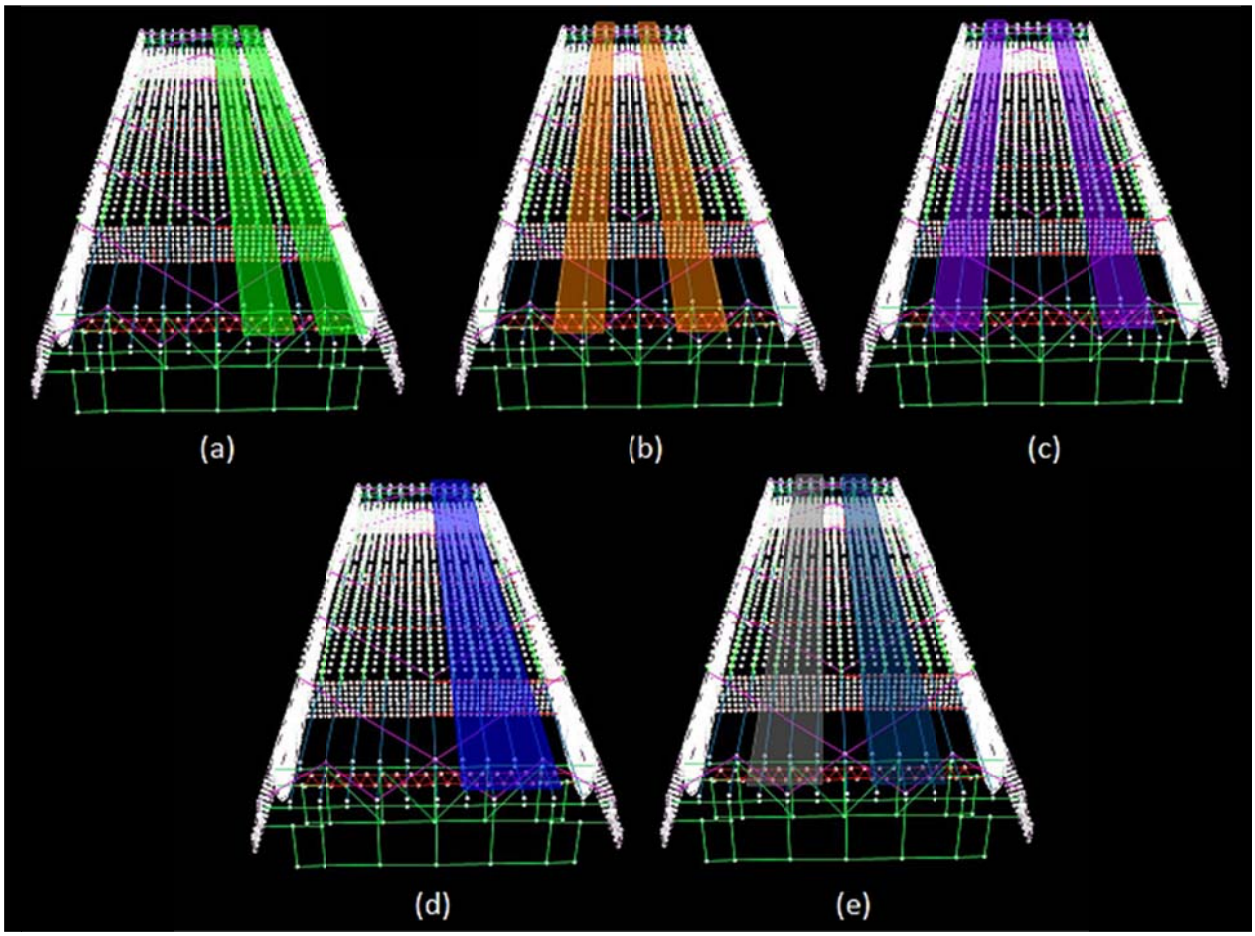

Figure 2.1-4. Example of lane loading on 3D Winneconne Bridge model. (a) Dual lane truck 2', (b) Dual lane truck 6', (c) Dual lane truck 10', (d) Single lane truck and (e) HL93 truck pathway.

Table 2.1-1. Vehicle classification for model analysis with LRFD load factors.

Type of Vehicle	Characteristics
AASHTO standard HL-93 strength design load	- Gross weight = 72 kips - Negative moment truck train was not included - 1 lane and 2 lane loading

	- Multiple presence factor was considered (1.2 one lane, 1.0 two lanes, 0.85 three lanes and 0.65 if >3) - 33% of dynamic allowance was considered - Load factor = 1.75
Single lane trailers	- Gross weight = 312 & 446 kips - 1 lane loading - Multiple presence factor was NOT considered - 0% of dynamic allowance was considered - Load factor = 1.35
Dual lane trailers	- Gross Weight = 486 & 500 kips - 1 lane loading - Multiple presence factor was NOT considered - 0% of dynamic allowance was considered - Load factor = 1.35 - Transverse wheel spacing: 4’ + 2’ + 4’ 4’ + 6’ + 4’ 4’ + 10’ +4’

Simplified Analysis Method

After completing the 3DFEM analysis of the previous step, the critical members in the bridges with high force values are identified along with the loadings causing those force effects. Then simplified methods that might be used to quickly estimate the same force values are tested. Simplified methods that successfully predict the OSOW effects are recommended for possible use in approving OSOW permits for bridge crossings.

2.2 Assumptions.

During the progress of this research several assumptions are made based on the best available knowledge of material behavior, modeling experience and understanding of the bridge structures. The main assumptions are classified into material and modeling ones.

Material

Steel and concrete are assumed to behave as homogeneous-isotropic linear elastic materials. Additionally, deterioration due to fatigue, corrosion, or residual stresses is not considered. Concrete deck strength is assumed to be 4000 psi whenever it wasn’t specified in the plans provided by the WisDOT data base or Michigan Department of Transportation (MDOT) [10]. Steel used in the fabrication of the bascule bridges (ASTM A709) is assumed to have the same stiffness properties as current ASTM A36 material.

3D-Modeling

Assumptions regarding loading, connections and supports during the development of the 3D model are necessary. In many instances the original information on bridge plans is incomplete or unreadable, requiring such assumptions. Vehicle wheel loads are modeled as point loads or area pressures on the decks. Only fully restrained moment or pin connections are used between members. No partially restrained moment connections are assumed. Composite behavior is assumed between flexural members and the bridge deck when composite connectors are shown on bridge plans. Supports are assumed to behave ideally as pinned or rollers. All elements defined in the modeling software are assumed to as shown in the plans with no defects or fabrications errors. Other assumptions are discussed in more detail in the specific description for each bridge.

2.3 Delimitations.

In order to evaluate the effects of OSOW vehicles on the selected bridges, individual members of the bridge are evaluated under the loadings imposed on them. Typically for simpler and smaller structures an analysis of every single member is performed, but for complex bridges like the ones analyzed on this report it is very time consuming. Consequently, it is necessary to set some boundaries on which elements are going to be examined. For this report, only primary members such as girders, floor beams and stringers are examined for overloading since in most of the cases these may be the controlling ones in term of stresses. Supports/substructures, connections, diaphragms, bracing, stiffeners and other secondary elements are not examined within the scope of the project.

2.4 Limitations.

As mentioned previously, instrumentation and load testing of bridges is essential in this research project in order to verify the quality of the 3D analysis developed with CSiBridge. However, due to the large selection of bridges and considering the preparation time for field testing, only three bridges are load tested. Because of this, modeling assumptions used on the verified bridges are also used in modelling the bridges that are not load tested.

3. MIRROR LAKE FRAME BRIDGE

3.1 Mirror Lake: Introduction and Structural Components

The Mirror Lake bridges, built in 1961, are two identical unique steel rigid-frame bridges over Mirror Lake in Sauk County, Wisconsin. They were built to carry traffic in both directions of a divided I-90/94 highway. The bridge being analyzed on this research project corresponds to the one on I-90/94 Eastbound, covering only southeast bound traffic. The shape of this superstructure can be seen in Figure 3.1-1.

Rigid-frame bridges have superstructure members that are rigidly connected to form a frame, making the structure continuous from deck to foundation. They were originally developed in Germany, and quickly expanded to USA in the 1930's. Among their numerous advantages is that moments at midspan are usually smaller than the ones in a continuous beam superstructure, so member sections can be reduced or longer spans can be accomplished. Moreover, structural complex details for connections at abutments are not needed since the whole structure is one piece. However, these types of structures are externally statically indeterminate and consequently harder to design and analyze.

The most common rigid-frame bridge is the Batter-Post type, like the Mirror Lake Bridge, in which the supports (column legs) run from the deck to the abutments in an angle. They are very effective for rivers and valley crossings eliminating the need for a mid-support in the water body. Firm foundations are essential so that these bridges do not suffer from uneven settlement and induced internal moments. The Mirror Lake bridges are on rock foundations. Steel plate girders are widely used in long span bridges of 100 to 300 ft., like the Mirror Lake bridges, to achieve girder depths deeper than possible with rolled steel sections. These are very effective structures while carrying the loads primarily in flexure.

The Mirror Lake Bridge has a total span length of 324 ft. with a deck width of 35 ft. covering two traffic lanes. Each lane is 12 ft. wide with a 4 ft. wide shoulder on both sides. The steel bridge uses two main plate girders with varying depth in a parabolic shape in the center span. The two girders support a total of 17 transverse floor beams, which in turn support 3 stringers running in the longitudinal direction.

In 1991, the concrete deck was entirely replaced with the intention of having a partially composite structure. The main girders are partially composite with the deck in the positive moment regions of the structure. In the negative moment regions there are no shear connectors, to avoid fatigue failure of the steel (because of the welding) with tension in the deck and girder top. The floor beam and stringers are near to fully composite with the deck. No studs were provided above the floor beams over a distance of 3 ft. from either end where the beam attaches to the girder. No studs were installed at the ends of the stringers over a 4-ft. distance where they join the floor beams.

An elevation, framing plan and cross-sectional view (after 1991 concrete deck replacement) are shown in Figure 3.1-2 from the original plans of the structure.

Figure 3-1.1. Mirror Lake Bridge (Steel rigid frame bridge, span = 324 ft.)

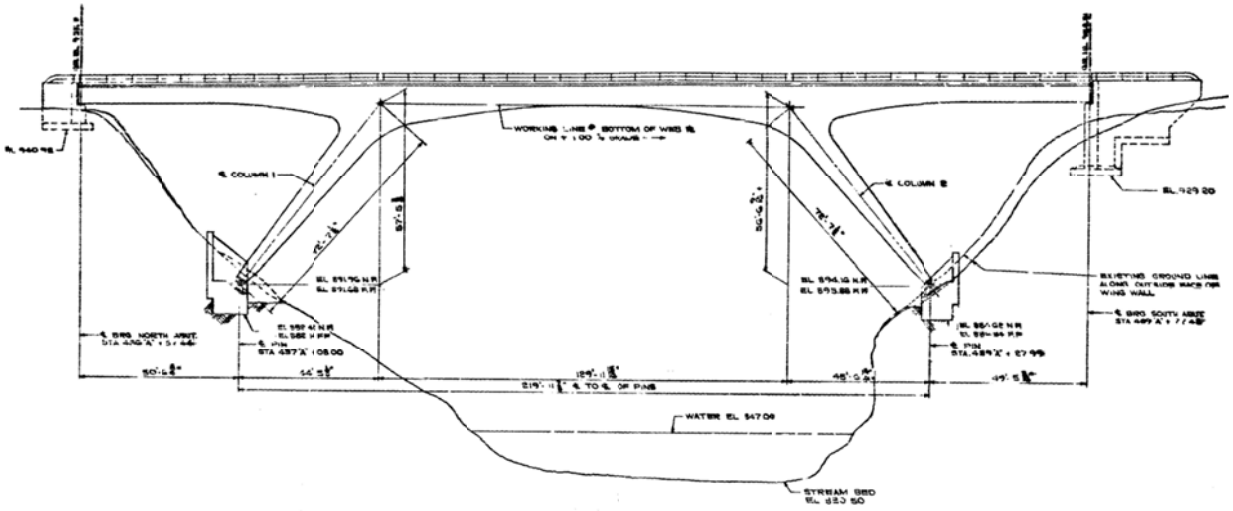

(a)

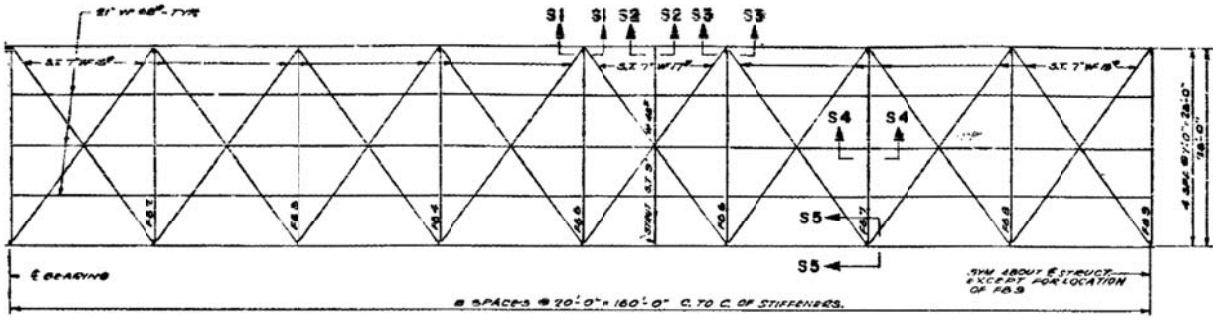

(b)

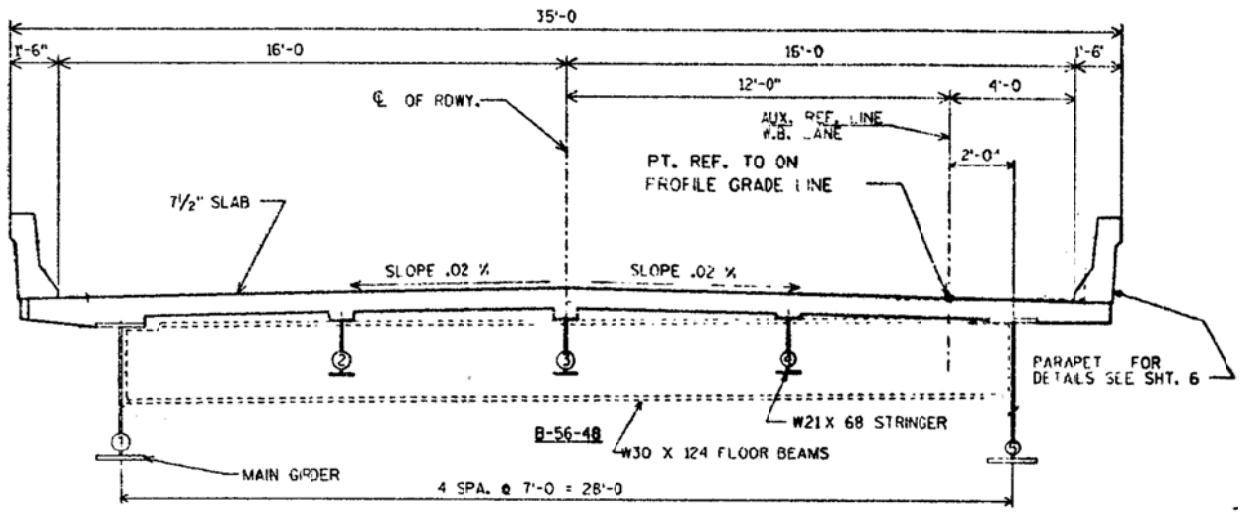

(c)

Figure 3.1-2. Mirror Lake Bridge original plans. (a) Elevation view. (b) Framing plan (half of the bridge total span). (c) Cross sectional view. Adapted from WisDOT HSI database [10].

Structural Components

A close examination of the bridge components is necessary to build a satisfactory analytical model. The main structural members of the bridge were made of steel with the exception of the concrete deck. The girders, floor beams, stringers, and bracing were all steel components with different properties. The plates and web of the girders were made of steel conforming to ASTM designation A242, F_y = 50 ksi. The floor beams conform to ASTM designation A373, F_y = 36 ksi. All other steel members were made of steel conforming to ASTM A7, F_y = 36 ksi. A summary of the main steel structural members can be seen in Table 3.1-1.

The plate girders on this bridge are designed as I-shaped sections built up from two flange plates and one web plate welded together. To avoid local buckling, vertical web stiffeners (typically 8 by 1.5-in. plates) are provided approximately every 5 ft. along the girder as shown in Figure 3.1-3. These I-shaped plate girders have a variable section throughout most of their span, varying depth and thickness. The girder's depth starts at the abutment bearing with 60 in. and increases to 117 in. where it meets the leg. On the opposite side of the leg it is 180 in. and tapers down to 72 in. at midspan. An original plan showing the side view of the plate girder can be seen in Figure 3.1-3.

Floor beams and stringers are common W-shape sections with constant section along their axis. The W30x124 floor beam webs are connected to the stiffener of the girder web by bolts. This web to web connection might be considered as "pin" ended for the floor beam. The W21x68 stringer webs are bolted to the webs of the floor beams through angles welded to the stringer web and bolted to the floor beam webs (see Figure 3.2-2a), again implying a pinned end. Vertical cross-bracings are composed of structural angles and are only provided in the zones where the column leg meets the plate girder, on

floor beams 6, 7, 8, 11, 12 and 13 (with beam number 1 starting from the northwest end of the bridge, at the left of Figure 3.1-2b. The lower lateral bracing between girders is provided by cross-bracing using structural angles and tees. Vertical and lower lateral bracing are connected to the girders by bolts, both used to prevent lateral torsional buckling of the girders.

The slant legs are also designed as plate girders with a variable section along their axes. They have plates as web stiffeners every 5 ft. to prevent local buckling, and cross bracing made of W-shaped beams to provide lateral stability. Bolts are provided for connections. All of the main structural elements are listed in Table 3.1-1.

Table 3.1-1. Main structural elements description and dimensions.

Member Name	Type	Dimension
Girder	Plate girder with parabolic shape	Variable Section
Floor beams	Simple span W-shape from cl to cl of girders	W30x124
Stringers	Simple spans W-shape framed on the web of floor beams	W 21×68
Vertical bracing	X pattern structural angles connecting the two girders	L 3½ x 5 x $^{7}/_{16}$
Lower Lateral bracing	X pattern structural angles + tees connecting the two girders	L 6 x 3½ x $^{5}/_{16}$ ST9 WF 48
Column bracing	X pattern W-shape beams connecting the column legs	21 WF 62

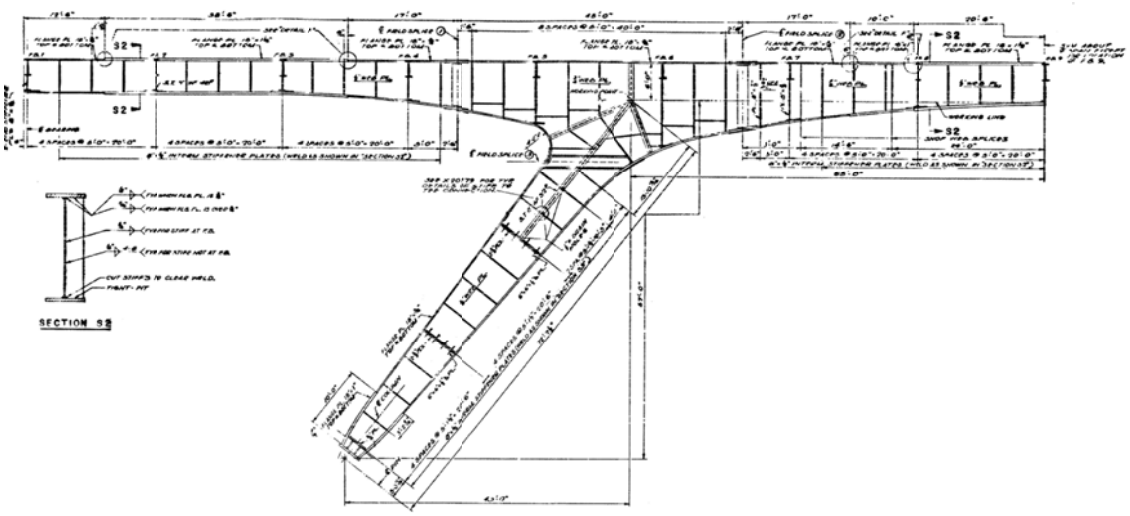

Figure 3.1-3. Girder side view. Stiffeners every 5 ft. and a variable cross section along the bridge axis Adapted from WisDOT HSI database [10].

The bridge deck is designed as a 7.5-in. thick reinforced concrete slab. It is 35-ft. wide with a 2% slope from the centerline of the bridge to the parapets. The concrete slab is haunched above the

girders, floor beams and stringers. The concrete design stress is 4000 psi and the steel reinforcement is grade 60, F_y = 60 ksi.

As described in the introduction, the Mirror Lake Bridge has partially composite action between the deck and the main girders. It has shear connectors at 1.5ft. in the positive moment region, which is defined as the first 63 ft. from the centerline of the abutments and the 24 ft. on each side of midspan. The negative moment region, on top of the slant legs, extends for a total of 71 ft. where no studs were used.

For the 28-ft. long floor beams, the spacing of the studs is uniform at 2 ft., starting at a distance of 3 ft. from the centerline of the girders. For the stringers, the studs' spacing is uniform at 1.5 ft., without studs 4 ft. from the centerline of the floor beams throughout the entire bridge span length. Details for the shear studs and their placement can be seen at Fig. 3.1-4.

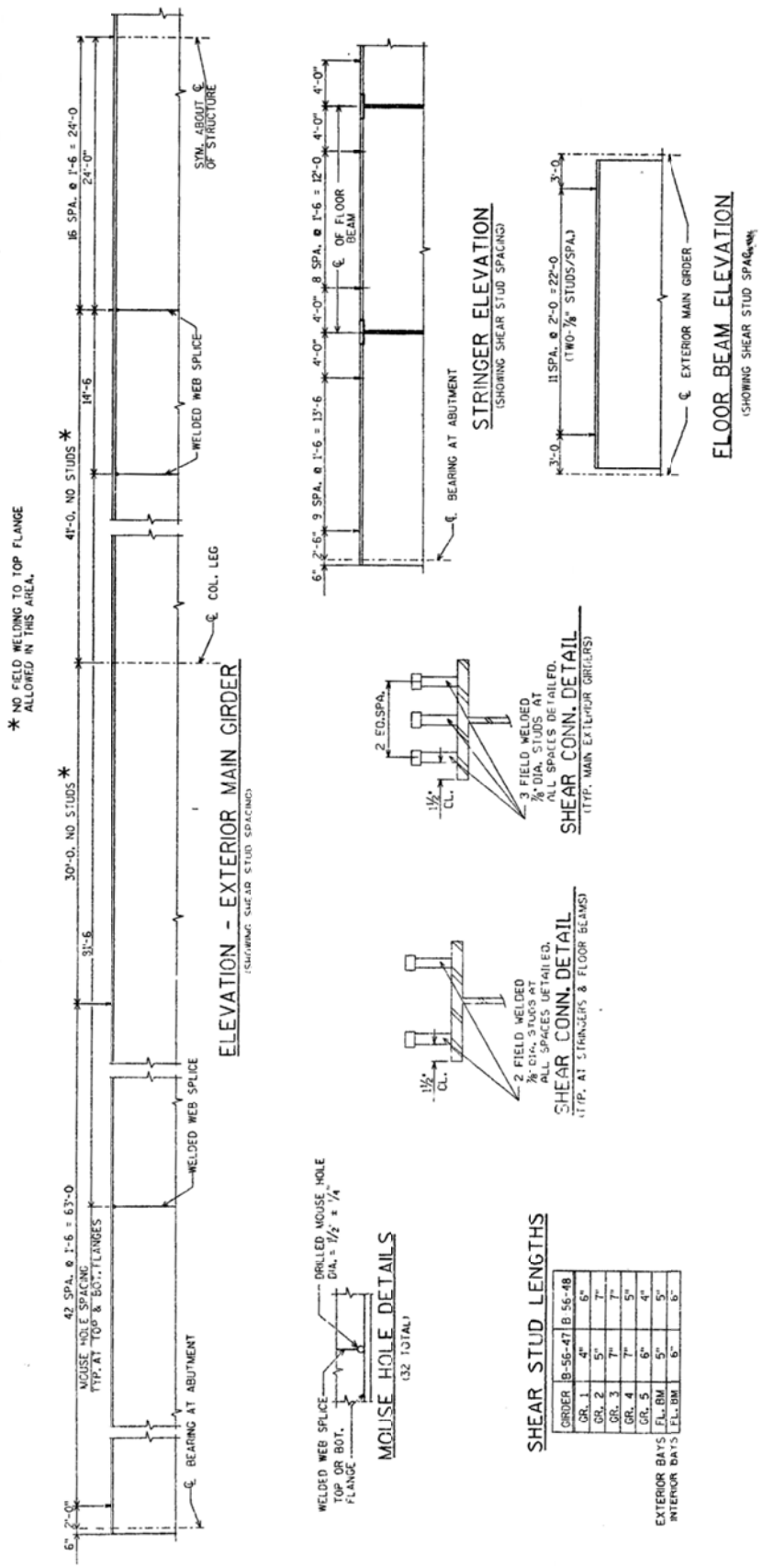

Figure 3.1-4 . Shear connector details on Mirror Lake Bridge. Adapted from WisDOT HSI database [10].

3.2 Mirror Lake: Field Load Testing

Field testing was conducted on this bridge to provide a comparative basis to judge the accuracy of analytical models to be used in simulation of the bridge response under OSOW trucks. Though the intent of the project is to be able to predict the bridge response to various oversize/overweight vehicles, such vehicles were not available for a load test. Instead standard trucks with measured wheel locations and weights were employed to load the structure while strains were measured in selected locations of the structure. Since the trucks were not extremely heavy, the strains were expected to be generally low. Key locations where the highest strains could be expected were estimated from an initial model analysis under HL93 loading and used to place strain gages. A final analytical model with the same loading as actually applied in the field is then compared with the measured response to validate its quality. That final model is then used to predict the bridge response to a wide series of different oversize/overweight vehicles.

Selection of Test Location

Accurately measuring very low levels of strain in structural members is difficult in the field, so selected locations were chosen because they were expected to have high strain values. After building and running a preliminary analytic model of the structure, four critical locations were chosen for gage placement. The west girder at midspan, floor beam #14 and the center stringer between floor beams 13 and 14 were instrumented using vibrating wire (VW) strain gages. The girder-knee joint was instrumented using a triaxial foil strain gage. Figure 3.2-1 shows a side and plan view of where the gages were placed.

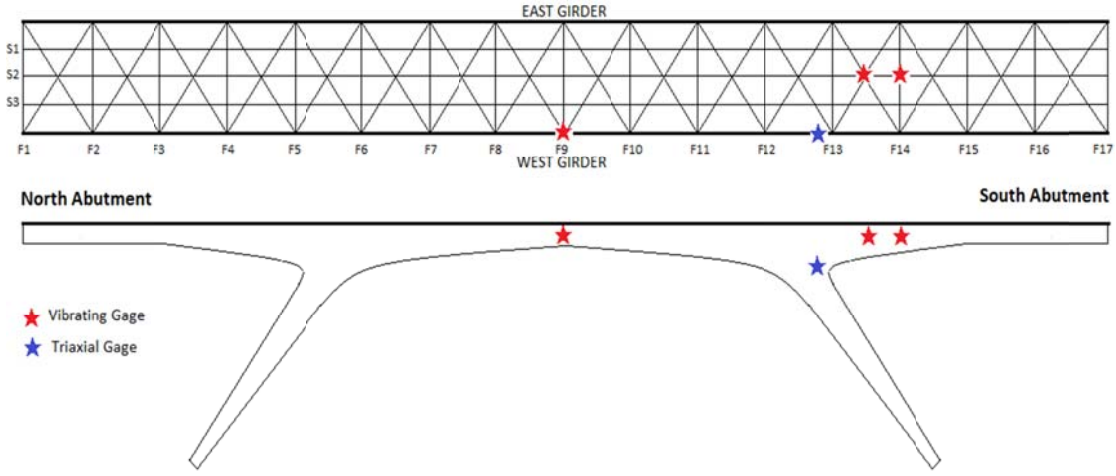

Figure 3.2-1. Gage locations on girder at midspan, F.B. #14, stringer #2 and girder knee.

Vibrating wire gages were installed in pairs at each location, symmetrically above and below the centroid of the steel section. This was done to obtain compression and tension data due to the combined axial deformation and bending of the members. They were installed parallel to the beam axis. For the VWs on the girder web at midspan, both gages were installed at a distance of 32 in. from the centroid of the steel section. On the floor beam, the gages were placed 10 in. from the steel section centroid. Finally, on the stringers, the pair of gages were installed at 6.75 in. from the centroid of the

steel stringer. The triaxial gage was placed just above the web splice near the knee joint. These details are shown in Fig. 3.2-2.

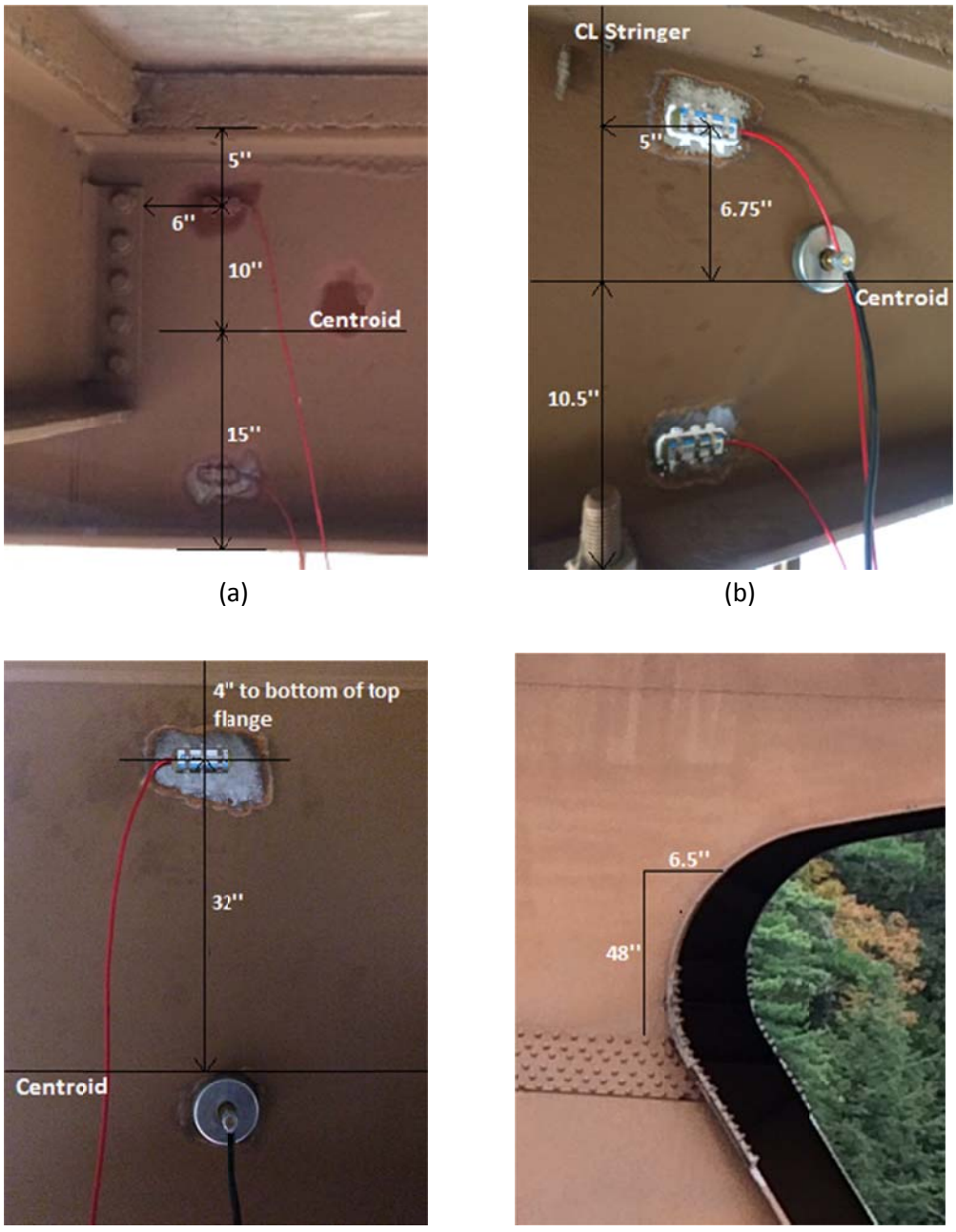

(a) (b)

(c) (d)

Figure 3.2-2. Location of gages for field test. (a) Vibrating strain gages at floor beam #14, 6 in. from stringer #2 web connection. (b) Vibrating strain gages at stringer #2, 115 in. from F.B #14. (c) Vibrating strain gage at girder, 90 in. south from bridge centerline. (d) Triaxial strain gage at knee-column, approximately 966 in. from south abutment and 135 in. from girder top flange.

Loading Regime

Two Sauk County loaded dump trucks, as shown in Fig.3.2-3 (a), were used to impose a stationary live load when moved onto the bridge. For truck #1, the heavier one, the front axle carried 19,700 lbs. and both the back axles 19,129 lbs. Truck #2 front axle carried 18,782 lbs. and both the back axles 18,229 lbs.

The locations of the trucks were intended to create the highest stresses in the members of interest. First, both dump trucks were located with the center of the two back axles on top of the midspan floor beam (F.B #9), with the front wheels heading towards South/East, and one truck very close to the parapet wall (center of wheels at 30 inches). This was selected to obtain high strain values at the web of the midspan west girder. Then, both trucks were moved and located with their back axle on top of floor beam number 14, to produce high strains on the girder-knee joint, floor beam #14 and the center stringer. Figure 3.2-3 (b) shows the exact location of the trucks during the field test.

(a)

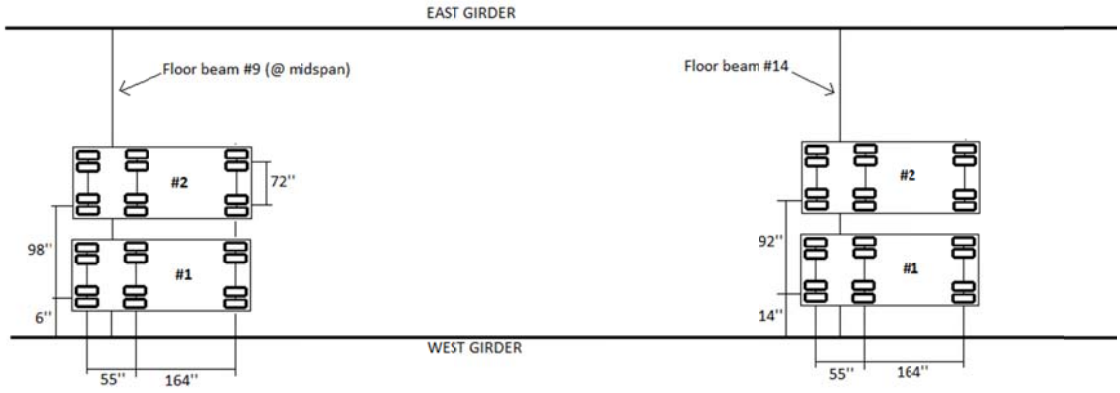

(b)

Figure 3.2-3. Trucks used on the field test. (a) Dump Trucks provided by the county. (b) Location of the trucks during testing (measurements from centerline of west girder). Position 1 is at midspan and position 2 is at floor beam #14.

Gage Installation

Two types of gages were used for strain analysis on the Mirror Lake Bridge. Geokon 4100 Vibrating Wire gages with a 2-inch gage length were installed in the three critical locations discussed above: girder at midspan, floor beam #14 and stringer #2 between floor beam #14 and 15. A Tokyo Sokki Kenkyujo WFRA-6-11 (11 mm or 0.43 in.) waterproof 3 element strain gage rosette was installed at the girder-knee joint to allow determination of the principal strain directions.

For the VW gages, the installation set-up started by identifying the location where the gage will be located. Then, the zone was ground to remove the paint until the steel surface was exposed. With sand paper, a smoother surface was obtained and alcohol was applied to clean the area. Then, the gage was welded to the steel element using a Sunstone Pulse Tack Welder. After the plastic protective coil cover was on, waterproofing caulk was applied around the edges of the cover. Finally, a paint primer was applied to the grind area and to the gage to prevent steel corrosion. Figure 3.2-4 recapitulates this process on a floor beam gage.

(a) (b)

(c)

Figure 3.2-4. Vibrating Wire gages on Mirror Lake Bridge. (a) Grinding the floor beam for gage installation. (b) VW gage welded after surface was cleaned. (c) Plastic cover/lead wire placement.

For the 3-element strain gage rosette, the procedure was similar to the VW gages. First, the surface is ground to expose the steel web. Then, the surface is cleaned with alcohol and water-based alkaline/acidic surface cleaners. Instead of using the tack welder, cyanoacrylate glue is used to attach the gage on the defined location. Lastly, primer is applied to the ground surface and to the gage to prevent corrosion of the steel. Figure 3.2-5 shows the only triaxial strain gage used in the Mirror Lake Bridge.

Figure 3.2-5. Triaxial strain gage at girder-knee joint.

Data Collection Scheme and Results

The installed strain gages on the bridge were then connected to a data acquisition system located next to the south abutment under the bridge. After getting initial readings from all the gages, the test was ready to begin. Since the Mirror Lake Bridge is located in a major Interstate highway, it was not an option to close the bridge and detour the traffic during testing. There were two ramp entrances within 4 miles north from the bridge that had to be blocked during testing. For those vehicles that were already on the I-90/94 beyond he ramps, a rolling roadblock was performed with the help of the State Patrol to reduce the speed limit from 60 to 20 mph starting at a ramp beyond that 4 mile range, allowing for a 10 minute gap in traffic to perform the load test before the traffic again reached the bridge. State Traffic Operations also requested that the testing be conducted after midnight when the traffic was somewhat reduced.

The test plan was divided in four stages. In stage one, an initial reading of all the gages was taken with no vehicles on the bridge. In stage two, the two loaded dump trucks were driven into their position, with the center of the two back axles on top of floor beam No. 9 (at midspan) and the front wheels facing south. The strains under the stationary truck loading were collected in all the gages. While

taking the readings, the exact truck axle locations with respect to the west girder were recorded in order to place the truck later on in the CSiBridge analytical model. In stage three, the two loaded dump trucks were driven into their second position, with the center of the two back axles on top of floor beam No. 14. Again, all the data from the gages and the exact location of the axles were taken. Finally, in stage four, data was gathered again without any vehicles on the bridge.

Stages one and four were done to establish a base line reading with no load. Results from stages two and three were then adjusted by the base line reading to determine the change in strain which could be compared with the strains found in the CSiBridge analytical model under only stationary live load.

Strain Data

A total of 28 scans were taken during the four stages. During each test step (and also in transition between stages) the strain gages were scanned every 12 seconds. The data obtained from the uniaxial strain gages on the floor beam, stringer and the girder web is shown in the Table 3.2-1. Positive values indicate tension in the member and negative compression.

Table 3.2-1. Strain data obtained from field test.

	Girder		**Floor Beam**		**Stringer**	
	Top	Bottom	Top	Bottom	Top	Bottom
Trucks at midspan	-4	47	0	0	-3	1
Trucks at F.B14.	0	-4	-14	46	0	5

Note: Values in microstrain already adjusted with base line reading.

As seen in Table 3.2-1, the strains are all very small and the floor beam and stringer values when the trucks were located at midspan are insignificant. This was expected since the loaded floor beam No. 9 is 100 ft. away from the gages located at floor beam 14 and stringer. The reverse occurs when the trucks were moved to floor beam 14, girder values are practically zero. It is also noticeable from the floor beam and girder data that they are acting in a composite way with the deck since the top and bottom strains are different indicating that the neutral axis is shifted to the upper part of the members. The stringer strains are all at an insignificant level.

All the VW data gathered during the field test was plotted in a graph, Fig. 3.2-6. The first 5 scans correspond to stage one, with no trucks on the bridge. Scans 15 to 18 represent stage two when the trucks are at midspan. Scans 22 to 26 denote stage three when the trucks are 60 ft. from south abutment. Finally, scan 28 corresponds to stage four with no trucks on the bridge. Scans in between stages show strain picked up when the trucks were moving into their positions.

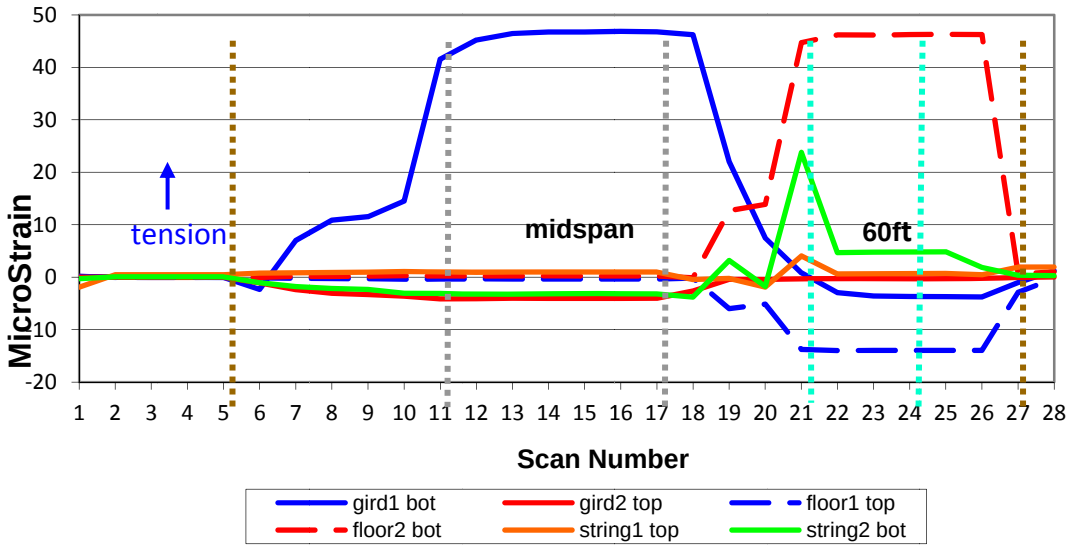

Figure 3.2-6. Strain gage values from field test.

A picture detailing the triaxial Rosette gage is shown in Figure 3.2-87 with one gage grid placed in the direction of the beam axis and the other two rotated from the first by 45 degrees. Raw data from the field test is shown in Table 3.2-2. Positive values correspond to tension in the member, negative is compression.

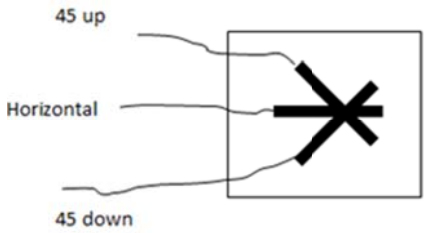

Figure 3.2-7. Rosette strain gage.

Table 3.2-2. Rosette strain data.

		Loads at midspan	Loads at 60ft
Horizontal	e	-19	1
45 degree up	e up	12	-14
45 degree dw	e down	-21	-52
Shear strain	gamma	-29	68
Principal Strains	e-1	17	6
	e-2	-26	-72
Direction	angle 1	-66	-15
	angle 2	24	75

With the three linearly independent strain measurements, and using Mohr's Circle equations, the direction and magnitude of principal stresses/strains was calculated as shown in Table 3.2-2. The angle for the principal direction is measured from the horizontal. Graphical representation of the direction of principal stresses is shown in Figure 3.2-8 with the principal compression at 75^{o} from horizontal.

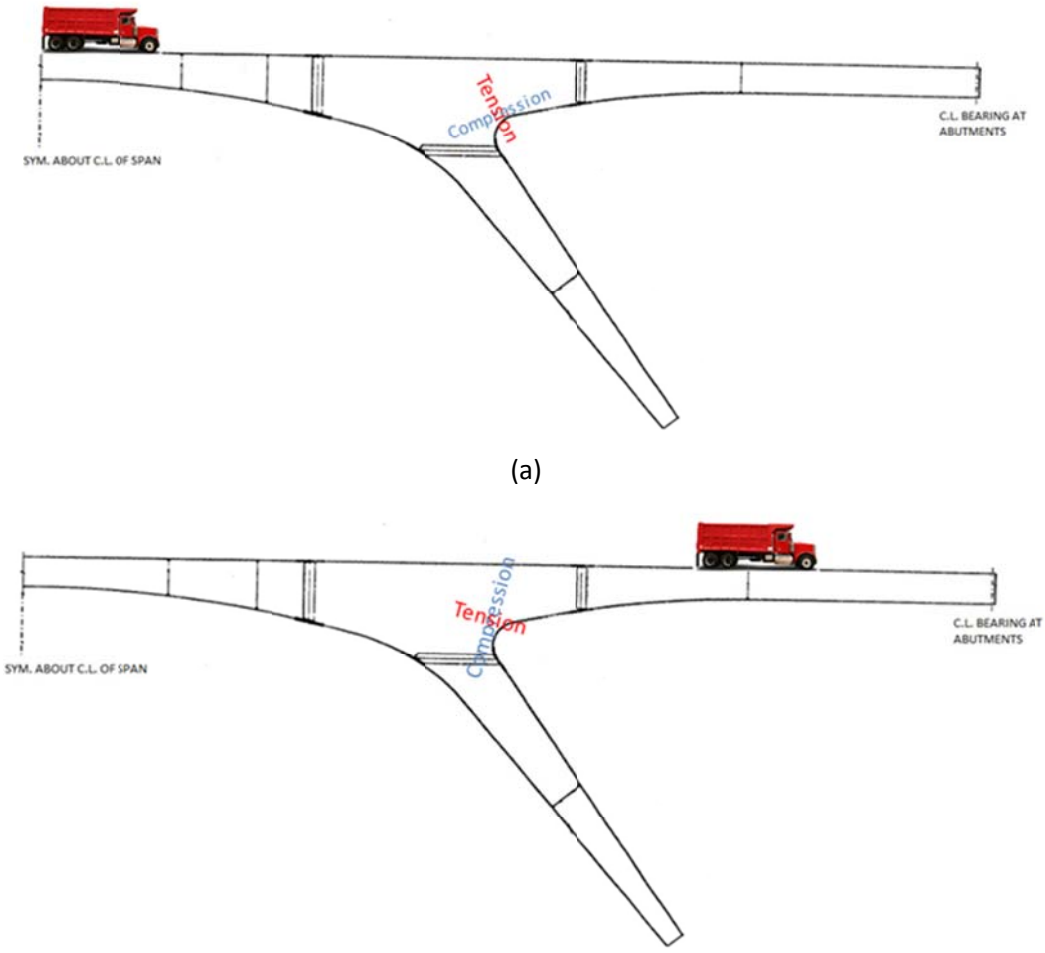

Figure 3.2-8. Direction of principal stresses at girder-knee point under loaded dump trucks. (a) Trucks at midspan (Position 1) and (b) trucks at 60 ft. from south abutment (Position 2).

3.3 Mirror Lake: Development of Three Dimensional Finite Element Model.

To predict the bridge structural response, an initial three-dimensional finite-element-model (3DFEM) was created according to the design plans. The 3DFEM model of the bridge was created using the commercial CSiBridge software.

After the field test was concluded, the truck loading scheme from the field test was replicated on the analytical model. By comparing the measured strains from the 3D FEM model and the field test, an evaluation of the model's accuracy was attained. The analysis results did not match the measured data as expected. The plans for the bridge were further examined and particular details such as the support conditions and the degree of composite action between deck and beams were evaluated and modified.

With the revised analytical model the accuracy was again be verified, and then oversize-overload loads (simulating known OSOW vehicles) were applied to the analytic model to evaluate the actual bridge performance. Then, critical members with high stress to capacity ratios were identified. Those were then recommended as the members to consider in the issuing of permits for future OSOW vehicles.

Initial Model Development

Frame, shell and link elements were used to model different sections of the Mirror Lake Bridge. The selection of these elements was done after considering the advantages of every element type in modeling.

Floor beams, stringers, bracing elements and the girders were modeled using frame elements. Detailed modeling of the connections and bolts was not done. Instead, connections between these members were simulated. Links with different directional stiffness, as explained by Chung and Sotelino [3], are effective especially for linking the deck and the flexural members for composite action. Links were necessary since individual members, such as the stringer and floor beam, had their centroids at different locations so they could not be joined directly. Frame elements were used for the girders and slant legs. At the knee joint the girder and leg frame elements were assumed to join where their centroids coincided. This assumption will underestimate the joint stiffness. An alternative would be to assume the slant leg portion between the bottom of the girder and girder centroid to be rigid. The concrete deck was modeled using thin shell elements. Bridge geometry was taken from WisDOT design and shop drawings [10].

In the initial model, the concrete deck to stringer, and concrete deck to floor beam connections were assumed to be rigid in flexure assuming full composite action. Even though studs were not provided on portions of the members, under low loading it was suspected that friction would be sufficient to provide composite action. Links were applied throughout the whole bridge over the stringers and floor beams. However, for the girders links were only used in the positive moment regions

since there were no studs over a substantial length of the girder in the negative moment zones. The connections were modeled by using fixed linear links, rigidly linking displacement and rotation in every direction. These links were defined from the centroid of each member. In the case of the floor beam to girder connection and stringer to floor beam connection, rigid links were also used between the centroids of each member.

The floor beams were attached to the girders through full depth web plates as noted earlier. The stringers were attached to the floor beams by bolted full depth web plates. Normally a web only connection would be considered as “pin ended” with no moment resisting capacity. On a deep member, like the 30” floor beam, a full depth web connection will provide some moment capacity. In a case where the flexural member is composite with a deck the character of the joint must be considered further. The composite action is achieved by transferring shear through the deck to beam connection. The deck develops tension (under negative moment) and the beam has combined axial compression and bending. The joint between two composite flexural members will automatically simulate this condition if the beam connection is considered as pinned and the deck is continuous. End flexure releases were used between beam and girder and between stringer and beam to simulate a pin end connection.

Support restraints were applied over the abutments at the ends of the girders and at the bottom of the slant legs. The connection between girder and the abutment, a rocker and bearing plate, was modeled using a roller support. The joint between the slant leg and the foundation, a true pin, was modeled by using a pinned connection. A picture of the initial extruded model can be seen in Figure 3.3-1.

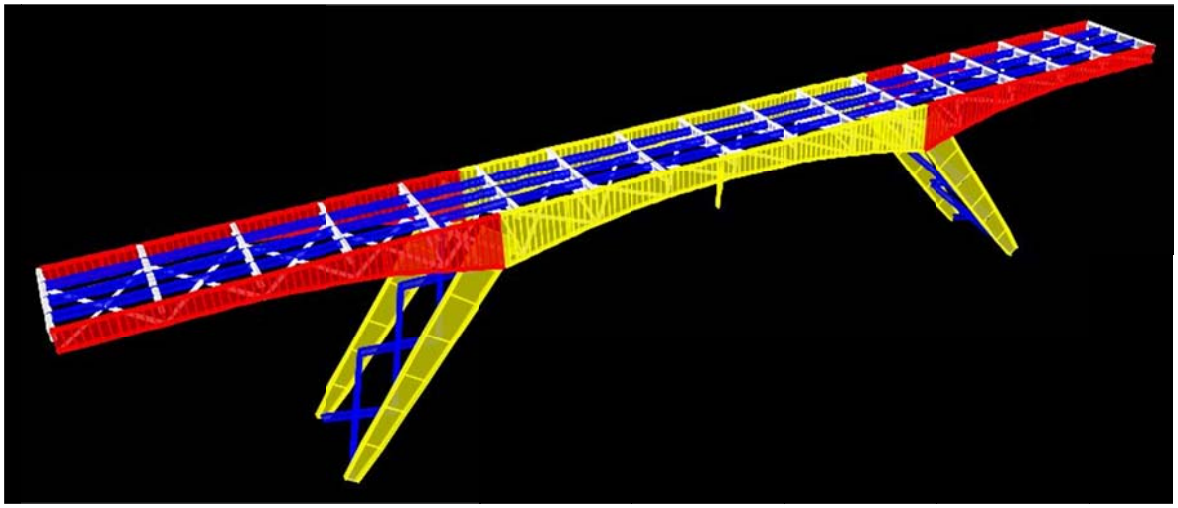

Figure 3.3-1. Initial extruded 3-D Model of Mirror Lake Bridge. Girder modeled as frame element.

Comparison with Field Strain Measurements

The results obtained from the initial model are compared with the measured data in Table 3.3-1 for strain data. Positive values indicate tension and negative compression.

Table 3.3-1. Strain data comparison between field data and 3-D model values.

TRUCKS AT MIDSPAN							MODEL	GAGES
		Moment (kip-ft.)	Axial (kip)	Inertia (in^4)	Area (in^2)	Stress (Ksi)	Micro-Strain	Micro-Strain
Floor Beam	Top	-0.23	-0.17	5360	36.5	0.00	0	0
	Bottom					-0.01	0	0
Stringer	Top	-0.01	-0.21	1480	20	-0.01	0	1
	Bottom					-0.01	0	-3
Girder	Top	700	-4.64	88493	90	-3.23	-111	-4
	Bottom					3.13	108	46

Note: Moment, Axial, Inertia, Area and Stress listed on tables are based on the values found in the CSiBridge Model.

TRUCKS AT 60 FT							MODEL	GAGES
		Moment (kip-ft.)	Axial (kip)	Inertia (in^4)	Area (in^2)	Stress (Ksi)	Micro-Strain	Micro-Strain
Floor Beam	Top	37.5	38.4	5360	36.5	0.21	7	-14
	Bottom					1.89	65	46
Stringer	Top	0.63	2.6	1480	20	0.09	3	1
	Bottom					0.16	6	5
Girder	Top	-80.5	-5.3	88492.5	90	0.31	11	-0
	Bottom					-0.42	-15	-4

Note: Moment, Axial, Inertia, Area and Stress listed on tables are based on the values found in the CSiBridge Model.

As evident from the tables, the model results did not match the data obtained from the field test. When the trucks are located at midspan, modeled strains on the main girder are significant greater than the ones obtained from the gages. It can also be seen that composite action is not working between the concrete deck and girder since the model strain values show that the neutral axis is located near mid depth of the girder element. Better results were obtained when the trucks are located at 60 ft. from the south abutment. Floor beam and girder data obtained from the model get closer to the field values.

Since the girders and columns were approximately modeled as frame elements joining where their centroids coincide, stresses around the girder knee region could not be accurately attained and a refinement of the model was done.

Adjustment to the Model Based on Closer Examination of Design Details

The first change in the model was the type of element that it was used to model the girders. In the initial model the main girders were modeled as frame elements as suggested by Chung, W. and Sotelino, E. [3]. An attempt to model the girders with fine shell elements was done to obtain more accurate results by using finite element meshing.

Another refinement in the model was the location of the composite links. In the initial model only the positive moment regions had links between the girder and the concrete deck. Now, links every 5 ft. were defined in the negative moment region considering that in reality there is a partially composite action due to the friction contact between those two surfaces.

Finally, joint restraint between the girder and the abutment was changed. Instead of using a roller support a new element was introduced with the purpose of only restraining downward deflection. This compression only element called a "gap" [5] acted as a roller support but with the ability to deflect upwards whenever it is necessary. This was done after looking closely the support in the bridge field test and realizing that a heavy live load at the midpsan of the bridge, without including dead loads, can produce an uplifting of the supports. Figure 3.3-2 displays the new model with the applied changes.

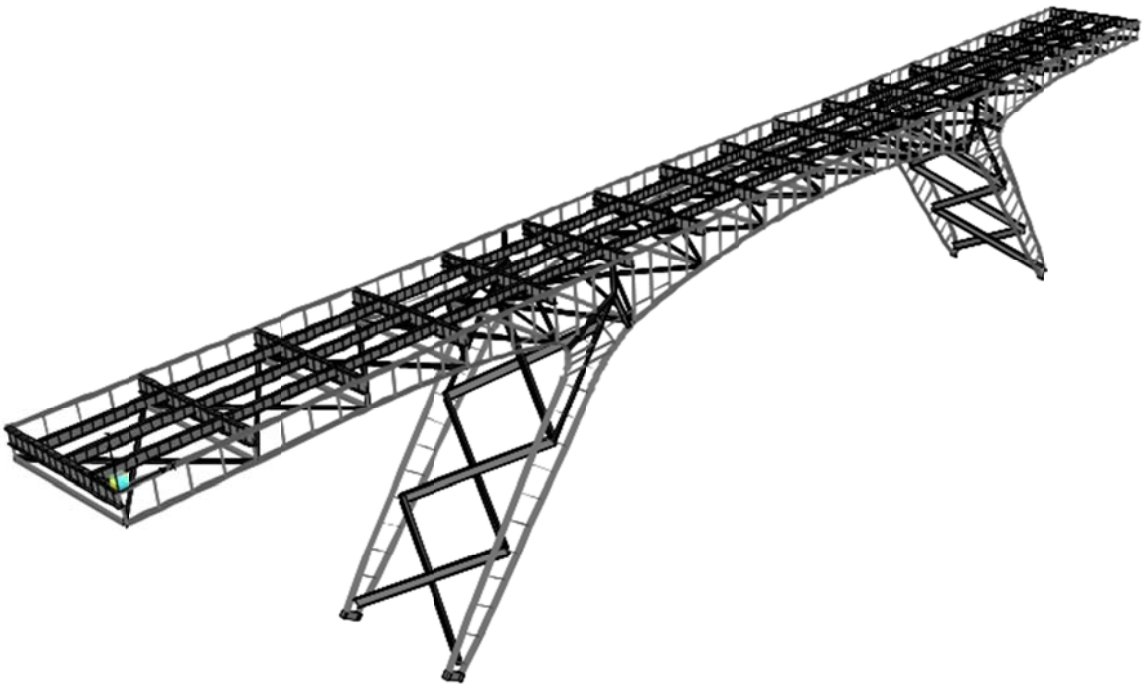

Figure 3.3-2. 3D FEM of the Mirror Lake Bridge. Web of the main girders defined as thin shell elements, flanges and stiffeners as frame elements.

The results obtained after implementing the changes described above are shown in Table 3.3-2. The girder row in the table does not contain any values in moment, axial, inertia and area cells since now we are using fine shell elements. The software provides these values only for frame elements. In the case of shell elements, stress values are taken directly from the software. A positive value denotes tension in the member and negative compression.

Table 3.3-2 Strain values measured and predicted.

TRUCKS AT MIDSPAN		Moment (kip-ft.)	Axial (kip)	Inertia (in^4)	Area (in^2)	Stress (Ksi)	MODEL Micro-Strain	GAGES Micro-Strain
Floor Beam	Top	-0.0735	-0.159	5360	36.5	0.00	0	0
	Bottom					-0.01	0	0
Stringer	Top	0.1102	0.342	1480	20	0.01	0	1
	Bottom					0.02	1	-3
Girder	Top	Not output by model				-0.90	-31	-4
	Bottom					3.50	121	46

Note: Moment, Axial, Inertia, Area and Stress listed on tables are based on the values found in the CSiBridge Model.

TRUCKS AT 60 FT		Moment (kip-ft.)	Axial (kip)	Inertia (in^4)	Area (in^2)	Stress (Ksi)	MODEL Micro-Strain	GAGES Micro-Strain
Floor Beam	Top	69.5029	84.232	5360	36.5	0.75	26	-14
	Bottom					3.86	133	46
Stringer	Top	0.729	0.488	1480	20	-0.02	-1	1
	Bottom					0.06	2	5
Girder	Top	Not output by model				0.05	2	0
	Bottom					-0.69	-24	-4

Note: Moment, Axial, Inertia, Area and Stress listed on tables are based on the values found in the CSiBridge Model.

Some improvement can be seen with respect to the first approximate initial model. The floor beam and girder show composite action and values are closer to the data from the field. However, there is still big difference in results and the adjusted analytic model does not provide satisfactory results.

Regarding triaxial data obtained, the comparisons with the results from the FEM model are also unsatisfactory. Table 3.3-3 shows the values predicted versus the measured ones. Positive values indicate tension and negative compression.

Table 3.3-3. Triaxial data predicted vs measured.

		Values from triaxial gage		Values from CSiBridge Model	
		Loads Midspan	Loads at 60ft	Loads Midspan	Loads at 60ft
Max Strains	ε1	17	6	17	-51
	ε2	-26	-72	-8	-89

Note: Values in microstrain.

Strain data when both trucks were located at midspan get closer to the ones obtained in the field test. Results when the trucks were located at 60 ft. from south abutment differ with the ones calculated from the triaxial gages. Orientation of the principal directions was also off as seen in Table 3.3-4. Since the model is not accurate enough it was not possible to continue the experimentation with the OSOW vehicles. Development of an improved model is left for future research work.

Table 3.3-4. Orientation of principal strains.

		Principal direction derived from triaxial gage		Principal direction derived from CSiBridge Model	
		Loads Midspan	Loads at 60ft	Loads Midspan	Loads at 60ft
Direction	θ_1	-66	-15	-80	-44
	θ_2	24	75	10	46

Note: Values in degrees.

Three completely separate models of the Mirror Lake bridge were built using the CSiBridge software. In one model all of the structural elements were modelled using frame or beam elements, except the concrete deck was modelled with shell elements. This approach was simple, but an approximation since the actual rigid frame members were replaced by 1 dimensional linear elements placed at the centroids of the actual frame members. Where the legs and top girder of the frame members joined, very deep sections existed, and the joint region was poorly modelled with the overlapping beam elements. In the other two models the main rigid frames were completely modelled using shell elements. There was no overlap in the leg to girder connection region.

Unfortunately none of the models were successful in simulating the types of strains that were actually measured during the load testing. Part of the inaccuracy was contributed by composite action between the structural framing members and the composite concrete bridge deck. This seems apparent in the girder strain data listed in Table 3.3-2 with the trucks at midspan. The predicted girder strains are much larger than measured. Horizontal thrusts from the leg reactions of the rigid frame, acting a bit like

an arch, should be causing high compressive strains in the girder. But the actual data shows small strains with the model values somewhat higher. The only explanation for the low strains is a good portion of that compressive thrust is being resisted by the bridge deck even though only a midspan portion of the girder has a designed composite connection with the deck.

Since the errors in model accuracy were not satisfactory, the results of OSOW truck loading analyses that were conducted on the Mirror Lake bridge will not be provided here.

4. MARINETTE BASCULE BRIDGE

4.1 Marinette: Introduction and Structural Components

The Marinette Bridge, B-38-16, is a double leaf Bascule Bridge over the Menominee River in Marinette, Wisconsin. Designed by the Michigan DOT and built in 1973, it connects Ogden St. in Marinette, WI. and 1st St. in Menominee, MI. Bascule bridges have the flexibility of providing crossings that can be temporarily removed by having one or two movable spans

Three types of steel bascule bridges are found in modern design: the fixed-trunnion bascule bridge, the rolling lift trunnion and the Rall bascule type. The Marinette Bridge corresponds to a Rolling Lift Trunnion bascule, also called "Scherzer" rolling lift due to its creator in 1894. Figure 4.1-1 shows the main components of a Scherzer rolling bascule. It raises the leaf by rotating the pinion, forcing it to roll back along a fixed rack (using electric motors) while the tread rolls along the track, retreating from the front edge of the pier to increase the navigable width of the water body. In the Marinette bridge the bascule girder rolls back 9ft. when in the full open position. To make lifting the bascule easier, with less power, the dead weight of bascule leaf is counterbalanced. The counter weight is usually made of concrete and is located below the deck of the bridge, although in some cases (typically single leaf bascule bridges) it is located above the deck.

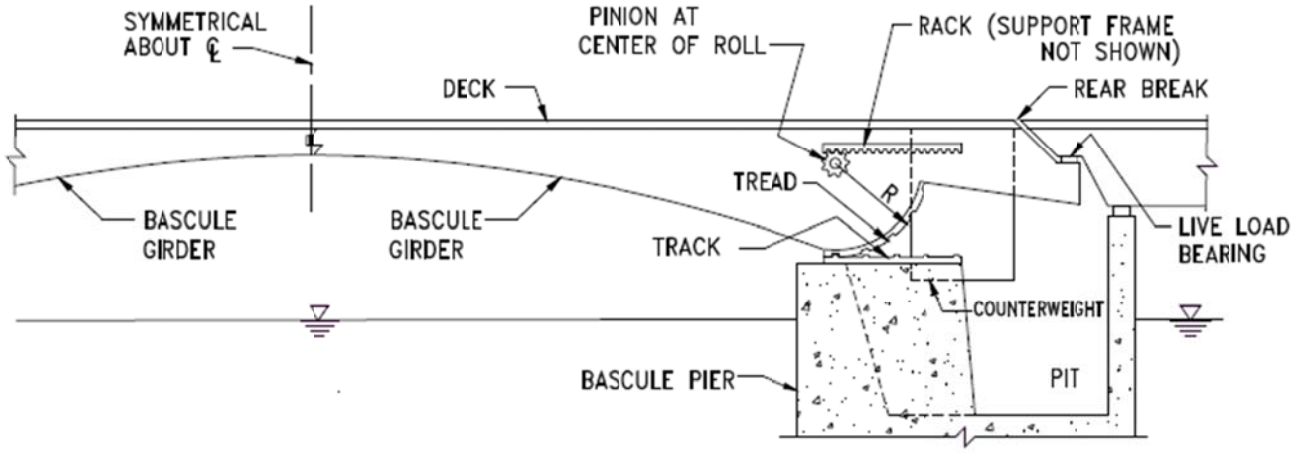

Figure 4.1-1. Double leaf Rolling Bascule Bridge configuration. Reprinted from WisDOT Structures Inspection Manual.

Center locks are used to allow the leafs to share load resistance. They are required to transfer vertical shear between the two leaves and to assure proper lateral and vertical alignment. Sherzer-type rolling lift bascules are characterized by having a fixed center lock replacing motor-driven locking mechanisms. Based on the tongue-in-groove principle, the center lock consists of a protruding

horizontal tooth on the end of one leaf, which is designed to fit into a horizontally slotted jaw on the end of the other leaf [8].

The function of the live load bearing (tail lock/tail beam) is to prevent the tail from rising, and the bridge leaf from rotating down, when large live loads are present on the bridge. An upward reaction, due to the unbalanced live load, is applied by the tail lock to the approach span beam transferring vehicular live load from the bascule to the approach span when the leaves are in the closed position [8]. Whenever a vehicle is on the leaf, the track and treads acts like a roller support with only an upward reaction and the tail beam needs a downward reaction. The couple from these two reactions balances the moment from live loading near the mid-joint.

The Marinette Bridge has a total span length of 143 ft. Each lift span of the bridge extends 66 ft. Deck width is 30 ft. covering two traffic lanes in opposite directions. Each lane is 15-ft. wide with a 5.67-ft. wide sidewalk on both sides. The operator's house is located on the right side of the south leaf. A picture of the bascules being lifted is shown in Fig. 4.1-2 with the south leaf on the left.

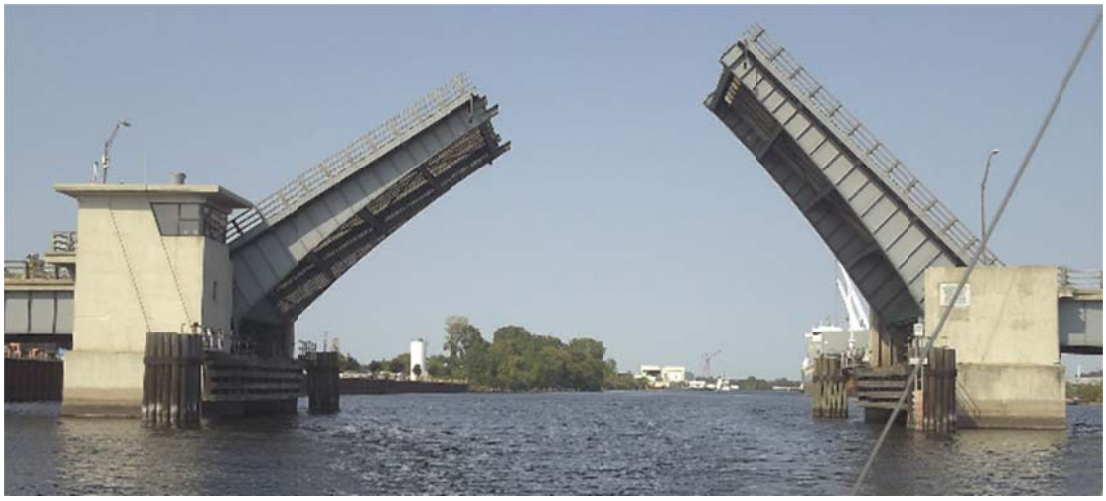

Figure 4.1-2. Marinette Bridge (Wisconsin, HIS ID: B38016, Bascule bridge, span = 143 ft.). Reprinted from BridgeHunter.com

The bridge has two main bascule girders that vary in depth with a parabolic shape along the bridge length. Besides the two bascule girders, there are 8 stringers running in the longitudinal direction on a total of 5 transverse floor beams per leaf running perpendicular to the girders. An elevation view from the original plans of the structure, framing plan and cross-sectional view from 1995 deck replacement plans are shown in Figure 4.1-3 and a structural photo in 4.1-4. Major work performed after first construction involved stringer replacement, painting, overlay concrete work and cleaning of expansion joints.

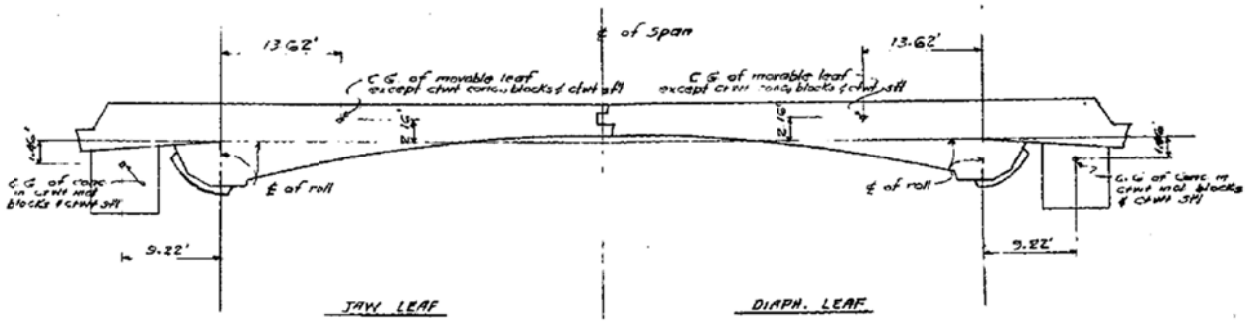

(a)

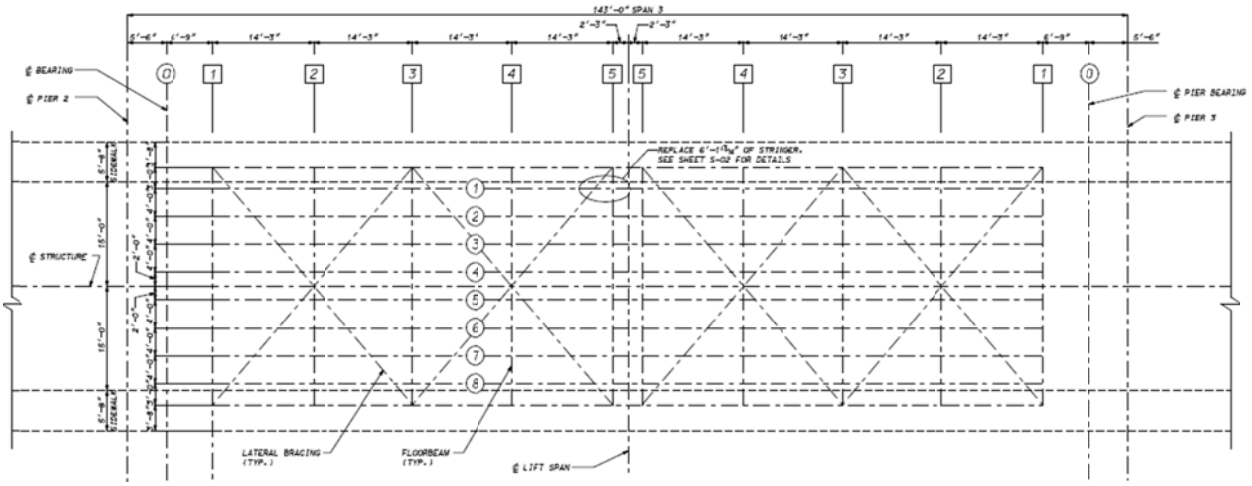

(b)

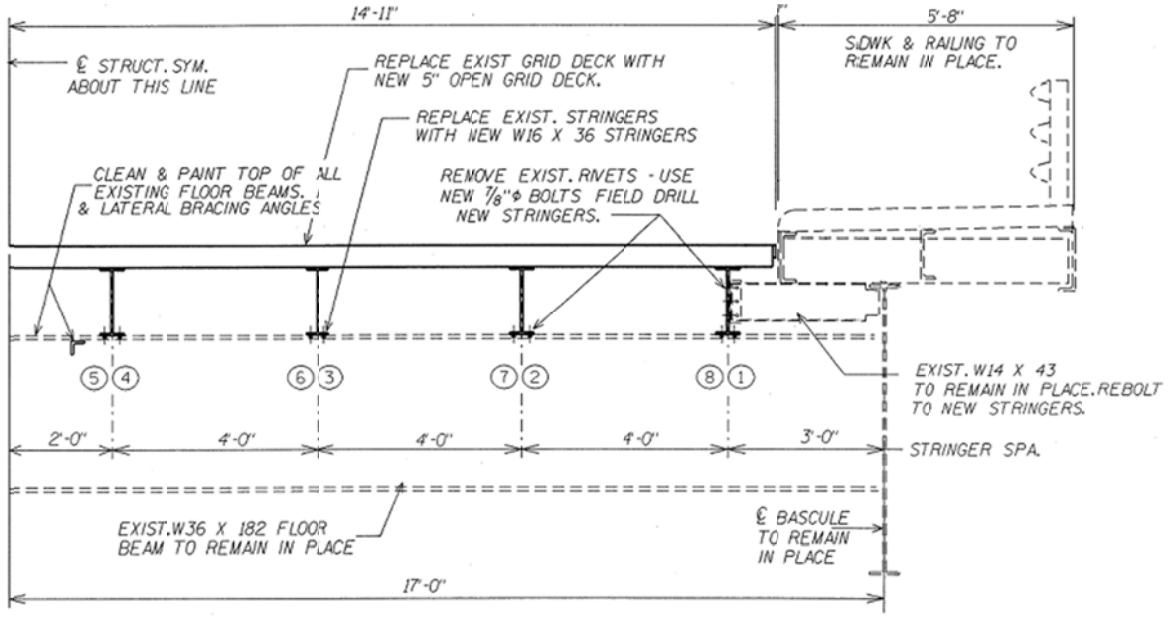

(c)

Figure 4.1-3. Marinette Bridge plans. (a) Elevation view with North to right (b) Framing plan. (c) Cross sectional view (half of the bridge). Adapted from WisDOT HSI database [10]

Figure 4.1-4. View of Marinette framing from below leaf and joint locking mechanism at the open end of the bascule girder.

Structural Components

The main structural members of the bridge are made of steel. The girders, floor beams, stringers, and bracing are all made of steel conforming to ASTM designation A709 grade 36. A summary of the main steel structural members can be seen in Table 4.1-1.

The plate girders on this bridge are built up from angles and flange plates riveted together to the web plate. To avoid local web buckling, vertical stiffeners (typically double angles, 2L 3½ x 5 x $^{5}/_{16}$) are provided approximately every 3.5 ft. along the girders as shown in Figure 4.1-5. Furthermore, additional cover plates typically 14 in. by 0.5 in. are riveted on top of the flanges in required zones. These plate girders have a variable section throughout their span, varying depth and thickness. The girder's depth varies from 48 in. at floor beam No. 5 to 126 in. at floor beam No. 1 (with 1 being closest to the pier). An original plan showing the beam numbering and side view of the plate girder can be seen in Fig.4.1-3a and b.

Floor beams and stringers are common W-shape sections with constant section along their axis. Floor beams webs are connected to the plate girder through bolts and a stub bracket (below the bottom flange). The stringers are alternately continuous over the floor beams – that is one will be continuous

over one floor beam and then simply supported on two others while the adjacent stringer is continuous over an alternate floor beam. Stringers are thus broken once or twice depending on the stringer. The stringers sit above the floor beams and their top flange is bolted to the steel metal deck and the bottom one connected to the floor beam flanges by bolts. This layout is apparent in Figure 4.1-6.

Lateral bracing is provided with a cross-bracing formed by structural angles along the bridge axis. Both the vertical and lower lateral bracing are connected to the girders by bolts, both used to prevent lateral torsional buckling of the girders.

Table 4.1-1. Main structural elements description and dimensions.

Member Name	Type	Dimension
Girder	Plate girder with parabolic shape	Variable Section
Floor beams	Simple span W-shapes from cl to cl of girders, spaced at 14ft-3in	W36x182 (F.B. No. 2 to 4) W33x220 (F.B. No.5)
Stringers	Simple spans W-shape framed on top of the floor beams, spaced at 4ft	W16×36
Lower Lateral bracing	X pattern structural angles connecting the two girders	L 6 x 3½ x $^{3}/_{8}$ L 4 x 3½ x $^{3}/_{8}$ L 3½ x 3 x $^{3}/_{8}$
Side Walk	C-shape channels connected to top of the bascule girder	12 C 30 15 C 33.9
Counter-Weight trusses	Combination of Tee sections and double angles supporting the concrete counter-weight	ST 4 WF 24 ST 5 WF 16.5 ST 6 WF 39 2L 7 x 4 x $^{5}/_{8}$ 2L 8 x 8 x 3⁄4 2L 4 x 3½ x 3⁄8

Figure 4.1-5. Bascule Girder view. Stiffeners every 3.5 ft. and a variable cross section along the bridge.

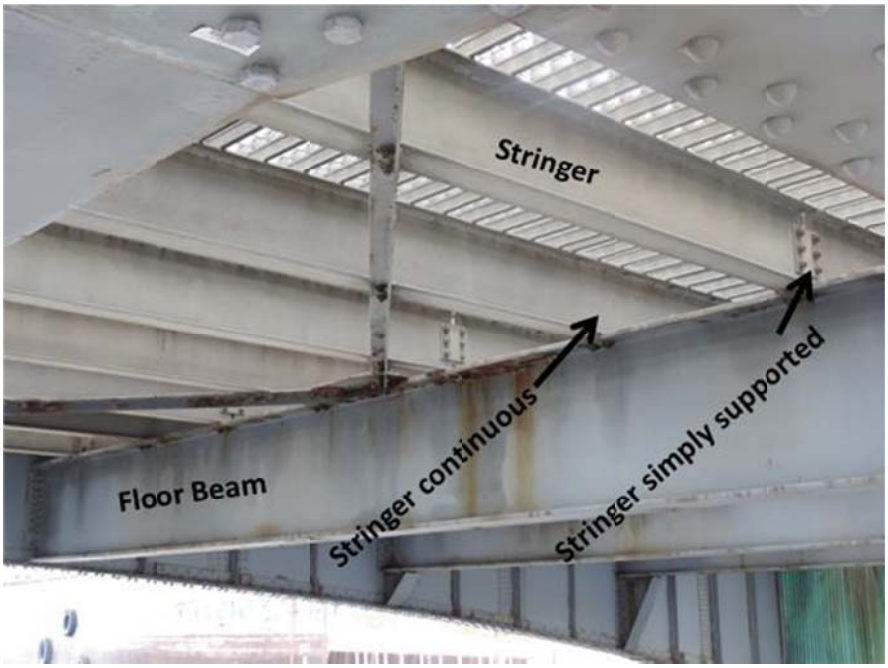

Figure 4.1-6. Marinette - alternate supports for stringers.

The deck of each leaf is a galvanized 5-in. steel open welded grid flooring (ASTM A36). It is fastened to the stringers with stainless bolts approximated every 1 ft. A picture detailing the deck flooring is shown in Fig. 4.1-7.

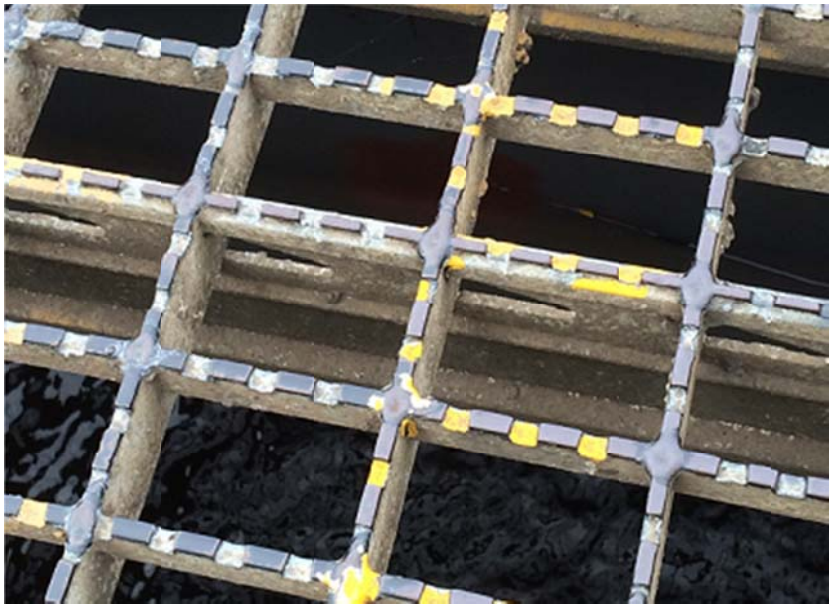

Figure 4.1-5. 5-in. steel open welded grid flooring.

4.2 Marinette: Field Load Testing

A field test of the bridge, with stationary truck loading, was conducted to obtain strain data for critical members. These strains were compared to predicted strains from an analytical model to verify the quality of the model. The analytical model was then used to calculate the effects of various oversize/overweight vehicles on this bridge.

Selection of Test Location

After running a preliminary analytical model of the structure, three critical locations were chosen for gage placement. The east bascule girder on the south leaf of the bridge (Figure 4.1-3) between floor beam No. 2 and 3, and the floor beam No. 5 were instrumented using uniaxial strain gages. The tail beam was instrumented using triaxial gages. Figure 4.2-1 shows a side and plan view of where the gages were placed.

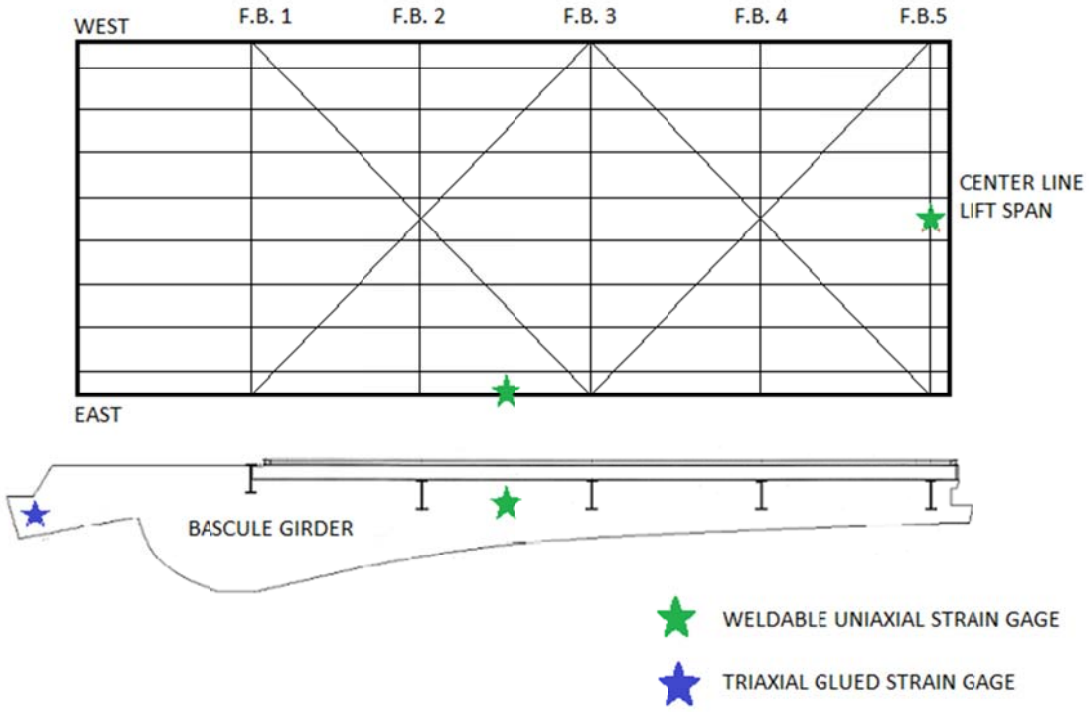

Figure 4.2-1. Gage locations at F.B. No.5, bascule girder web and tail beam.

Weldable uniaxial foil strain gages were installed in pairs at both locations on the girder and floor beam. The ones on the floor beam were placed 12.5 in. symmetrically above and below the centroid of the steel section. At the girder web the gages were located 30.5 in. symmetrically above and below mid-depth of the steel section. This was done to obtain compression and tension data due to axial deformation and the curvature of the member. At the tail beam, two triaxial gages were installed symmetrically 10 in. above and below mid-depth of the steel section where it slimmed down to the tail beam dimension. The 3 element tail beam gages were oriented with one element in the direction of beam axis and the other two at 45^{o} above/below the first. Figure 4.2-2 shows gages on the Marinette Bridge.

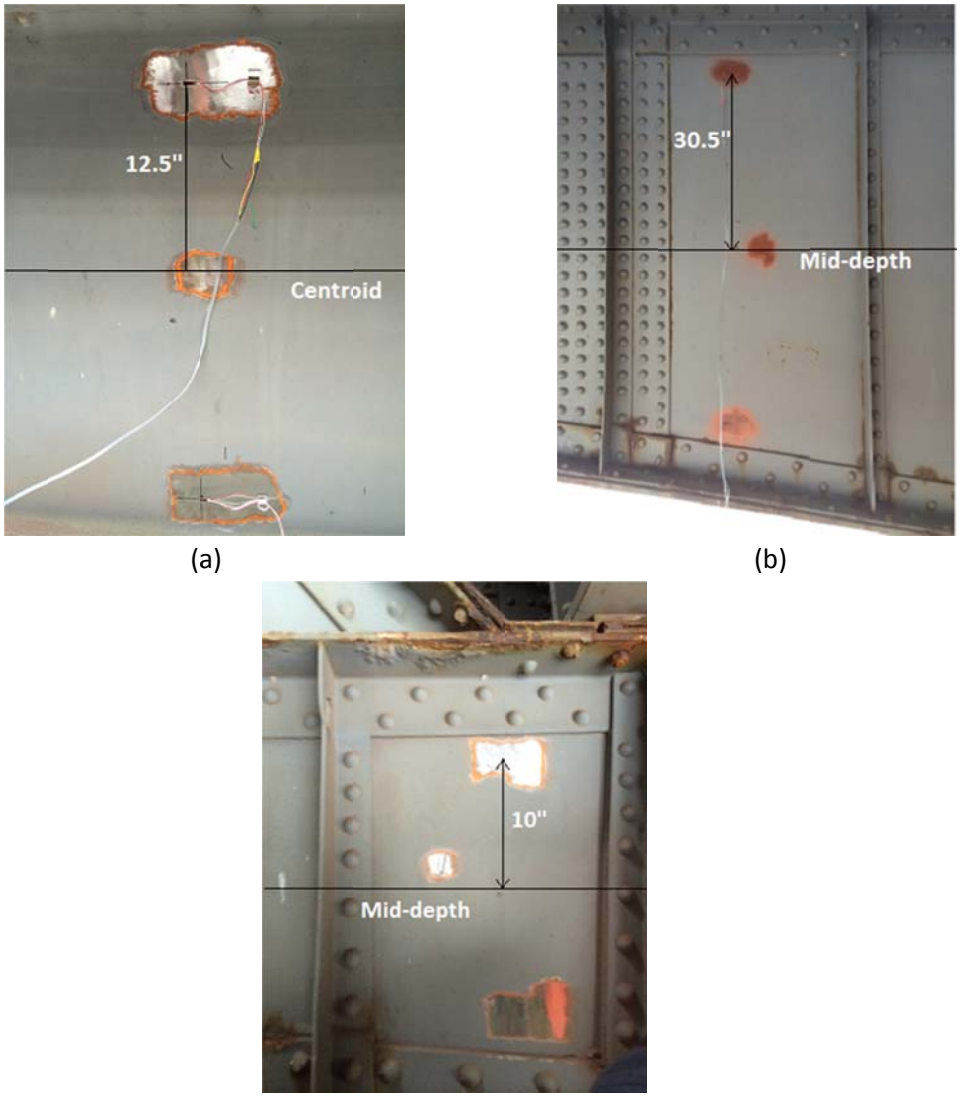

(a) (b)

(c)

Figure 4.2-2. Location of gages for field test. (a) Uniaxial weldable strain gages at floor beam #5, centerline of the bridge. (b) Uniaxial strain gages at bascule's girder web, 65.375 in. from floor beam No.2 towards centerline of lift span. (c) Triaxial glued strain gages at tail beam, 21.5 in. from tail beam end (tail beam bearing on approach span is at top right).

Behavior of the mid-joint connection in bascule bridges was also of interest in defining the behavior of the bridge. Therefore, the deck elevations on either side of the joint section were measured using a total station. The purpose of using the total station was to detect relative displacements between the two leaves due to lack of tightness in the joint. Four targets for the surveying equipment were placed on sides of the joint. Two of them were placed on top of the west girder, one on each side of the mid-joint connection. The other two were place on top of the east girder, following the same pattern on either side of the joint. Figure 4.2-3 clarifies the location of the targets.

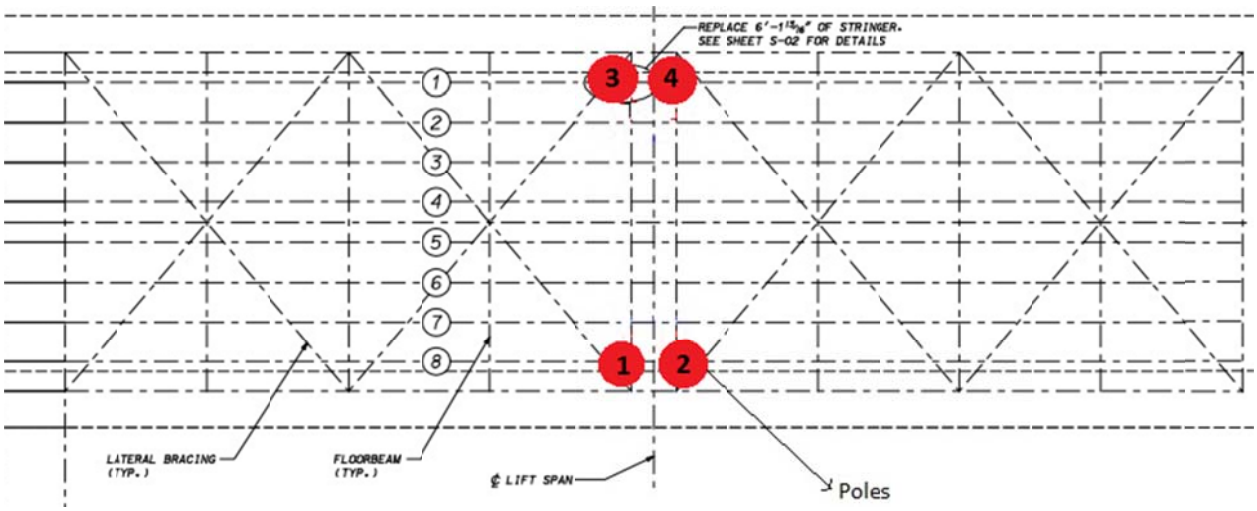

Figure 4.2-3. Deflection target locations during the bridge test.

Loading Regime

A loaded County dump truck (DT-A) and a reach-all truck (UB-60) were used to impose the stationary live load on the bascule bridge. The weights of the front and back axles of each truck were recorded before the testing. For the reach-all truck, the heavier one, the front axle weighed 21,880 lbs. and both the mid and back axles 21,000 lbs. (the fourth axle was lifted). The dump truck front axle weighed 19,140 lbs. and both the back axles 18,590 lbs. (the mid axle was lifted).

The location of the trucks was intended to create the highest stresses on the members of interest. First, the reach-all truck was located with its front axle on top of floor beam No. 5 (south leaf), and the back half on the same leaf. This was done to obtain high strain values in all the gages placed on the bridge. Subsequently, the dump truck was also added with its back axle on top of the same floor beam (No. 5). Figure 4.2-4 shows the exact location of the trucks during the field test.

(a)

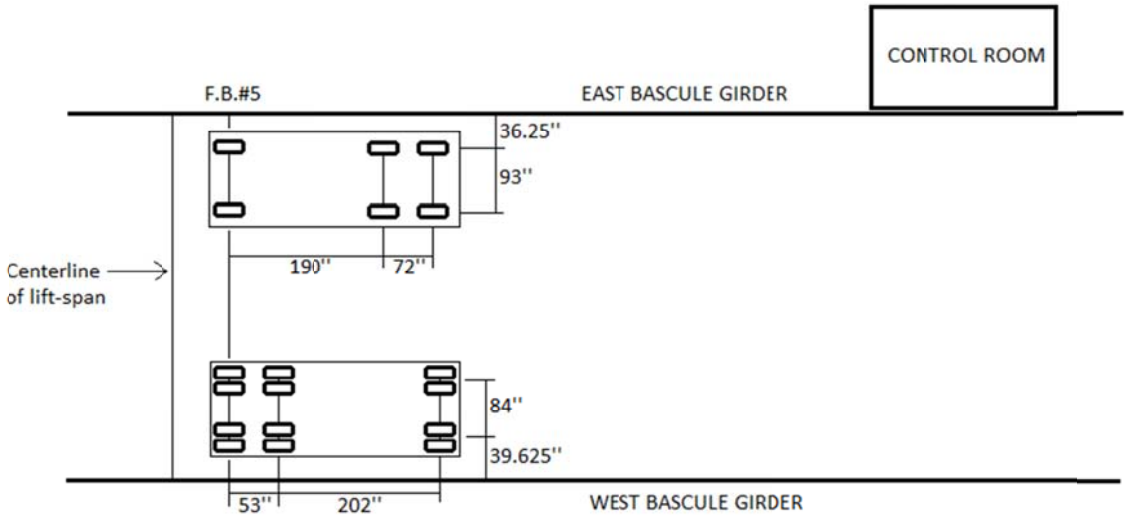

(b)

Figure 4.2-4. Trucks used on the field test. (a) Reach-all Truck and Dump Truck provided by the county. (b) Location of the trucks in the South leaf. Lifted axles are not shown in the figure. Reach-all Truck next to the east bascule girder, dump truck next to the west bascule girder.

Gage Installation

Two types of gages were used for strain analysis on the Marinette Bridge. Micro-Measurements LWK-XX-W250B-350 ¼ inch strain gages were installed on floor beam No. 5 and the girder web. Tokyo Sokki Kenkyujo WFRA-6-11 0.43 inch waterproof 3 element strain gage rosettes were installed on the tail beam. Both installations were previously featured in Figure 4.2-2.

For the Micro-Measurements weldable uniaxial gages, the installation involved grinding and welding. First, the zone was ground to remove the paint until the steel surface was exposed. With sand paper, a smoother surface was obtained and alcohol was applied to clean the area. Then with a clean surface the gage was spot welded to the steel element using a Sunstone Pulse Tack Welder. Finally, a primer was applied to the ground area and to the gage to prevent steel corrosion. Figure 4.2-5 recapitulates this process on the Marinette Bridge. These gages were not intended to remain in performance beyond the load test.

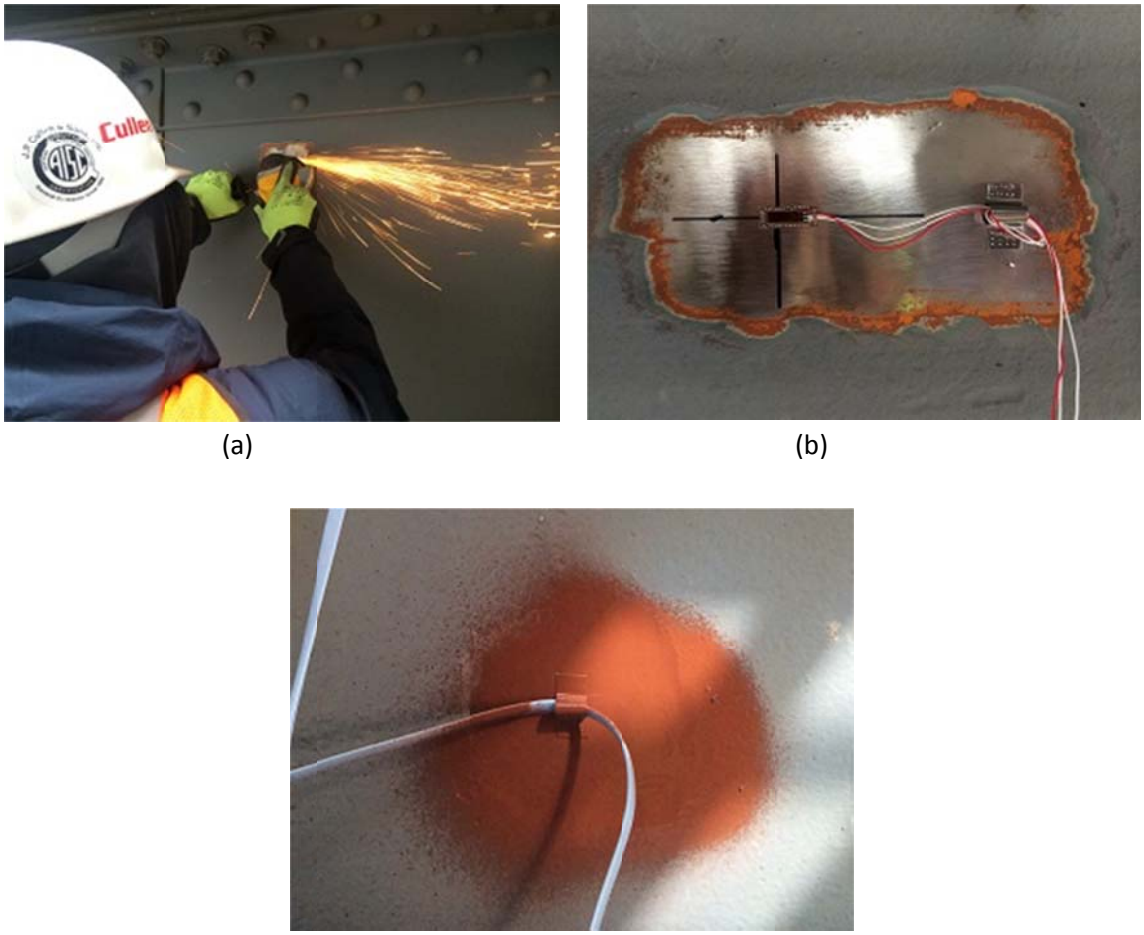

(a) (b)

(c)

Figure 4.2-5. Weldable uniaxial strain gages on Marinette Bridge. (a) Grinding steel web for gage installation. (b) Strain gage welded after surface was cleaned. (c) Primer applied to work area.

The 3-element strain gage rosette is the same type used in the Mirror Lake Bridge. First, the surface is ground to expose the steel web. Then, the surface is cleaned with alcohol and water-based alkaline/acidic surface cleaners. Cyanoacrylate glue is used to place the gage on the defined location. Lastly, primer is applied to the grind surface and to the gage to prevent corrosion of the steel. Figure 4.2-6 shows a rosette strain gage used on the tail beam of the Marinette Bridge.

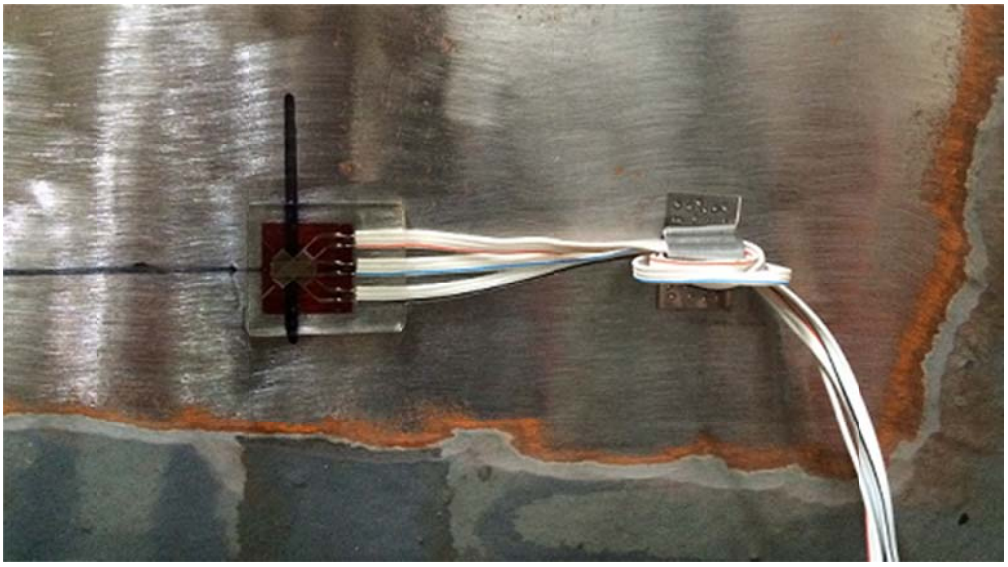

Figure 4.2-6. Triaxial strain gage at tail beam.

Data Collection Scheme and Results

The installed strain gages on the bridge were connected to a data acquisition system located in the bridge operation control room. After getting initial readings from all the gages, the test was ready to begin. The County closed the bridge and detoured the traffic. The test plan was divided in four stages. In stage one, an initial reading of all the gages and midspan deflections was taken with no vehicles on the bridge. In stage two, the reach-all (UB60) truck was driven into its position, next to the east girder and on top of floor beam No. 5. The strains under the stationary truck loading were collected in all the gages as well as the readings taken from the deflection targets. While taking the readings, the exact truck axle locations with respect to the east girder were recorded in order to place the truck later on in the CSiBridge analytical model. In stage three, the dump truck was driven into its position, near the west girder, and the UB-60 stayed in place. Again, all the data from the gages and targets plus the exact location of the axles were taken. Finally, in stage four, data was gathered again without any vehicles on the bridge.

In addition to the strain data gathered in every stage, the elevation of the mid-joint was read using the total station. Each target was measured once per load stage adding up to a total of 16 readings.

Stage one and four were done to establish a base line reading with no load. Results from stage two and three were then adjusted by the base line reading to determine the change in strain which could be compared with the strains found in the CSiBridge analytical model under only stationary live load.

Strain Data

A total of 211 scans were taken during the four stages. The first 60 scans represent the data with no load on the bridge. The following 50 scans show the data with the reach-all truck parked on the west side of the South bascule leaf. The next 50 scans represent the data with the reach-all truck plus the loaded dump truck on the east side of the South bascule leaf. The last 60 scans correspond to the data with no load on the bridge. During each test step the strain gages were read at a scan rate of 2 scans/second. The time to read elevations was approximated 5-10 minutes, and the strain gage data was collected at the beginning and end of this period. Strain gage data obtained from the field test was reliable and consistent with a standard deviation of less than 1 microstrain. The average data obtained from the uniaxial strain gages on the floor beam and the girder web is shown in the Table 4.2-1. Positive values correspond to tension in the member, negative is compression.

Table 4.2-1. Strain data.

	Floor Beam		**Girder**	
	Top	Bottom	Top	Bottom
Strain due to reach-all truck	-20	20	38	-55
Strain due to reach-all truck + dump truck	-48	53	42	-63

Note: Values in microstrain already adjusted with base line reading.

As seen in Table 4.2-1, strain on the floor beam top and bottom increases and more than doubles in magnitude between stage 2 and 3 of the testing. This was expected since floor beam No.5 is picking up stresses from both trucks, and they have approximately the same weight.

The same response wasn't observed with the data from the girder gages. The increment in microstrain from stage 2 to stage 3 is very small, approximate 12%. This was likewise expected since these strain gages were located on the east bascule girder. In stage three, the dump truck is located in the far lane, closer to the west bascule girder. The stresses due to the dump truck are picked up mostly by the west girder, generating a small increase in strain in the strain gages of the east girder. All the data gathered on the field test was plotted on the following graphs, Fig. 4.2-7 for floor beam data and Fig. 4.2-8 for the girder. Scans 60 to 110, and 111 to 160 represent the data with only the reach-all truck and both trucks, respectively.

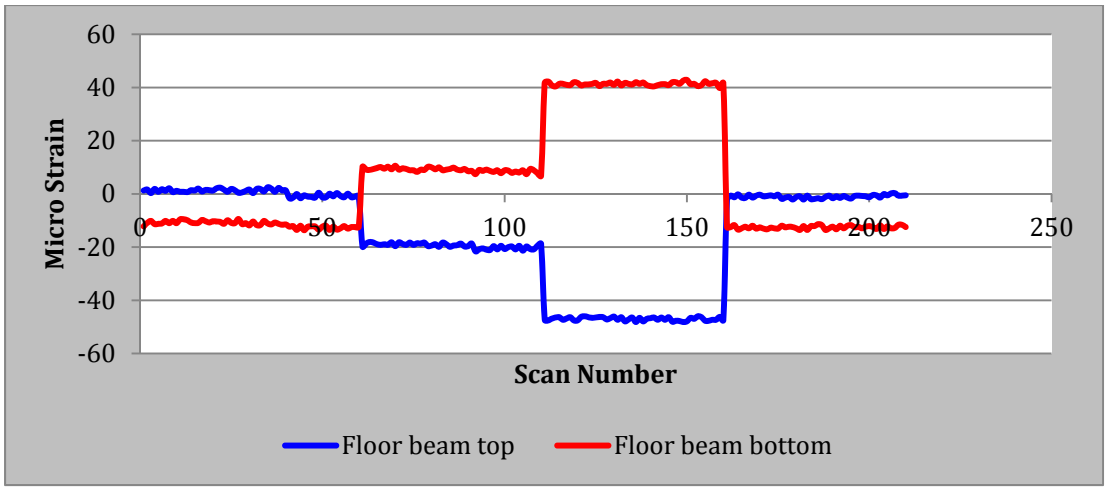

Figure 4.2-7. Strain gage from floor beam No.5.

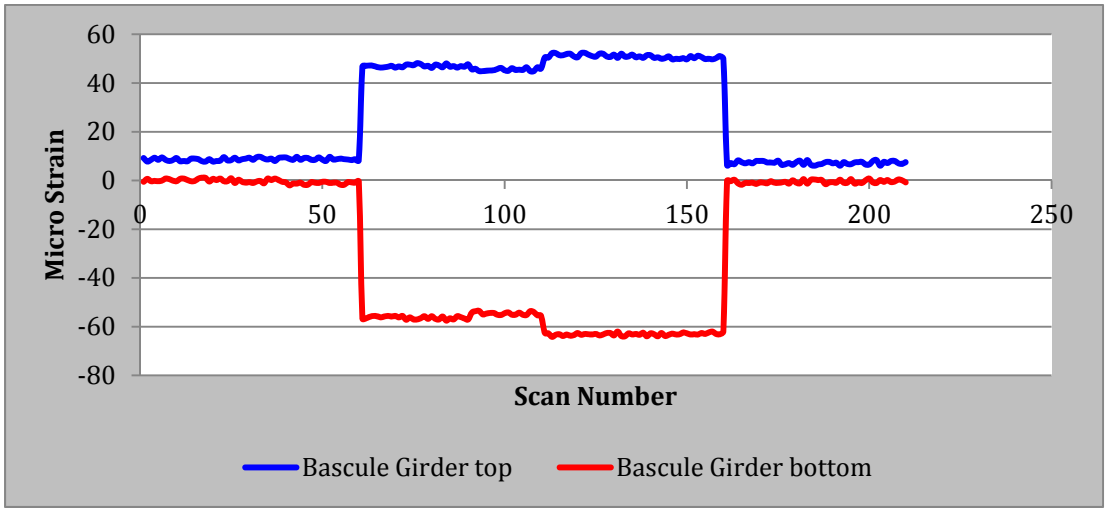

Figure 4.2-8. Strain gage from bascule girder.

The data obtained from the triaxial gages at the tail beam are shown in Table 4.2-2. Positive values indicate tension, negative compression. Figure 3.2-7 in Section 3 describes the notation used for the triaxial gages and their shape.

Table 4.2-2. Rosette data at Tail beam.

		Reach-all truck	Both trucks
Top	45 down	-81	-149
	horizontal	-11	-29
	45 up	134	239
Bottom	45 down	-89	-167
	horizontal	-45	-87
	45 up	72	138

Note: Values in microstrain already adjusted with base line reading.

From Table 4.2-2 the strains experienced by the tail beam web are largest of all the data gathered on the field test. The peak stress reached a value of 7.3 ksi, assuming a Young's modulus of 29,000 ksi. This could be explained by the key role that the live load bearing (Figure 4.1-1) plays, transferring load to the approach span using a complicated built-up tail section with multiple riveted angles as stiffeners. Strain data shows that the tail stub is working as a shear strut rather than as a bending member. In addition to vertical bearing force between the two bearing plates at the tail beam, friction between both surfaces may also induce stresses in the tail beam zone. The abrupt change of section could create a stress concentration notch, as illustrated in Figure 4.2-9, but since the stub is not acting in flexure this effect is of lesser importance.

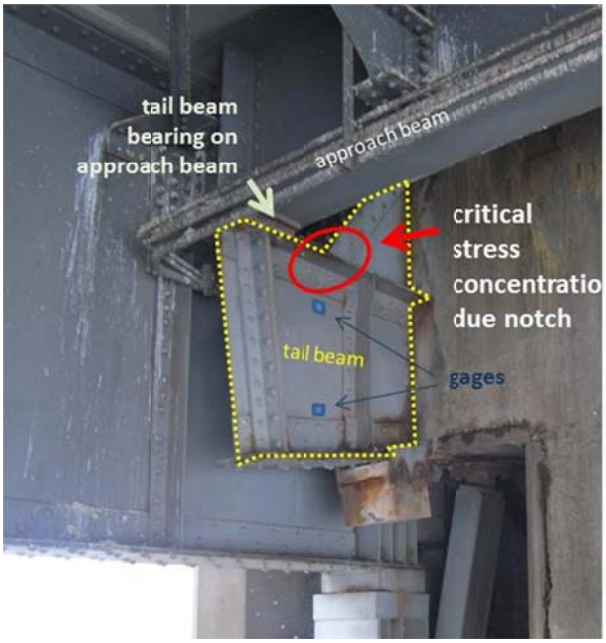

Figure 4.2-9. Tail beam region with bearing and notch.

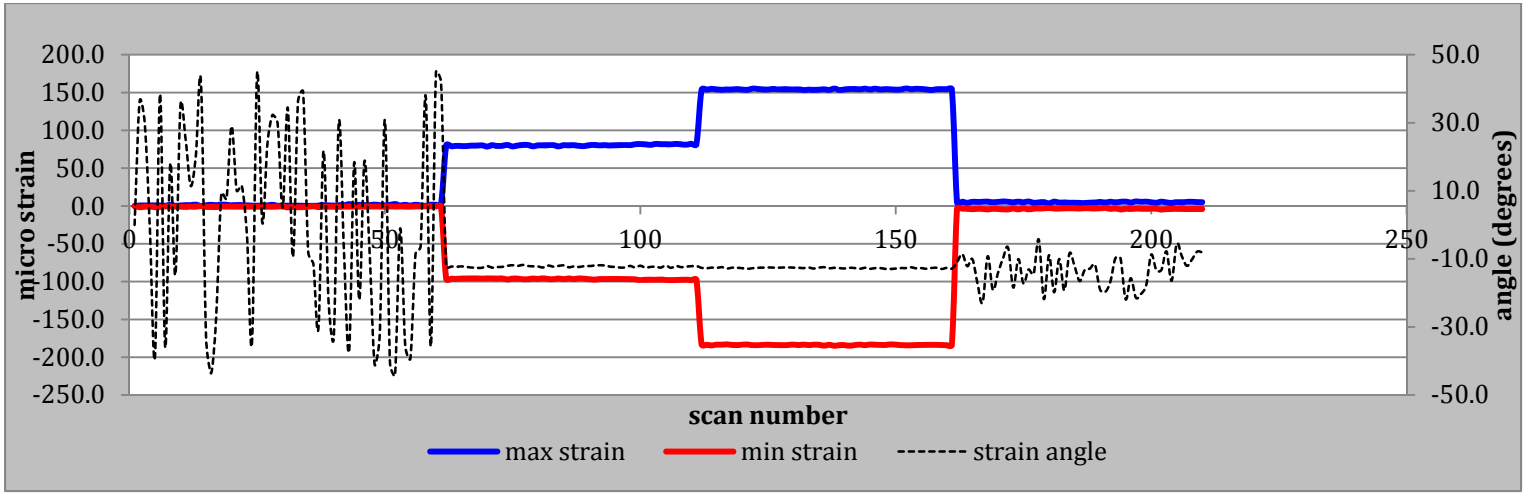

Figure 4.2-10. Tail beam top principal strains

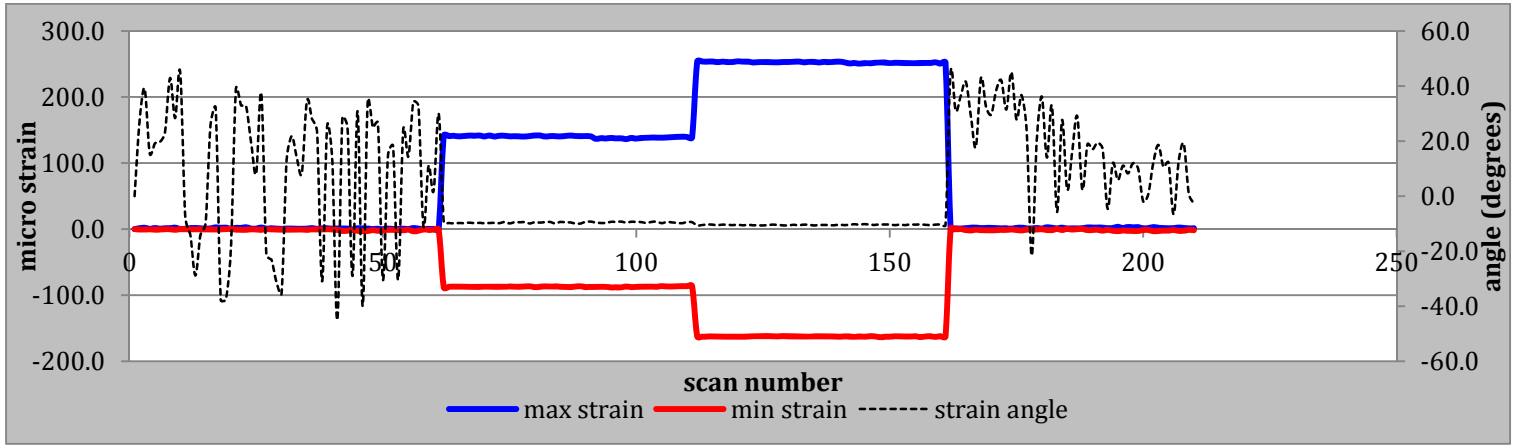

Figure 4.2-11. Tail beam bottom principal strain.

With the three linearly independent strain measurements from Table 4.2-2, and using Mohr's Circle equations, the direction and magnitude of principal stresses/strains were found as shown in Figures 4.2-10 for the top triaxial gage and 4.2-11 for the bottom triaxial gage. Red and blue solid lines represent the principal strains obtained from the field test data. The principal angle where the principal strain occurs was also calculated. For the tail beam top gage the angle is approximated -10 degrees, and for the bottom one -13 degrees (- indicating counter-clockwise from the gage axes).

A graphic representation of the principal direction and magnitude of the stresses at the tail beam is shown in Figure 4.2-12.

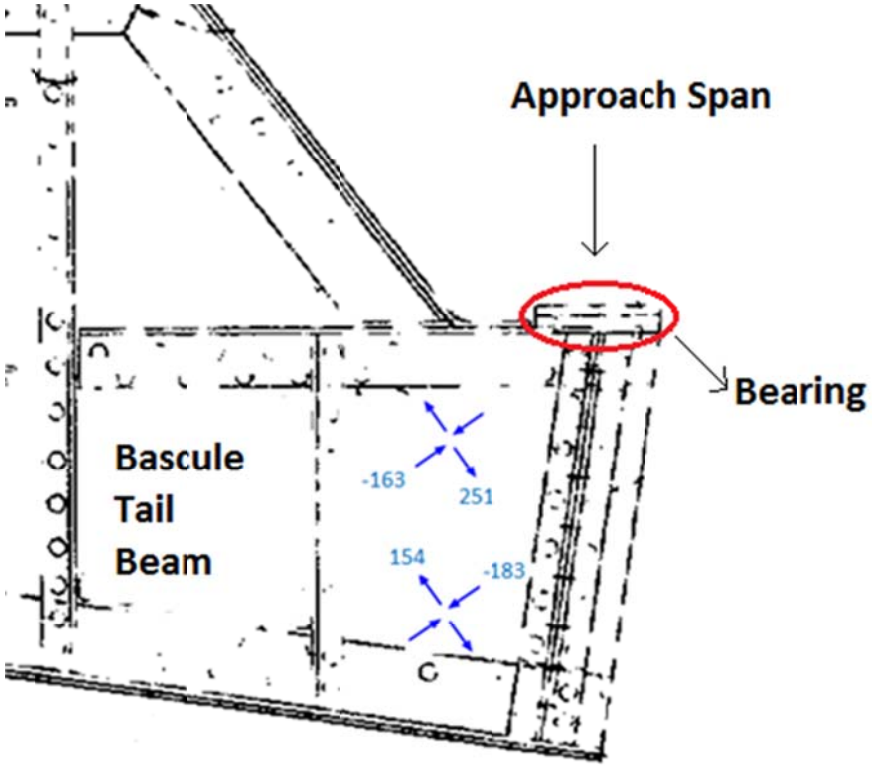

Figure 4.2-12 Tail beam principal strains phase 3. Positive sign is tension, negative is compression.

As is clear in Figure 4.2-12, principal strains at both locations occur at approximately the same angle. The maximum value is tension and happens at the top location near the live load bearing with a value of 251 microstrain (7.3ksi). These strains are part of a complex strain pattern since this region of the tail beam is a "disturbed" region where the reaction, multiple stiffeners, and abrupt section change cause unusual force flow. The FEA modelling used for the entire bridge is not sufficiently fine in the tail beam region to produce exact strain values. Better strain estimates would require detailed modelling of just the region shown in Figure 4.2-12.

The strains shown in the tail beam could be interpreted as resembling a truss mechanism, with diagonal tension members in the web at nearly 45 degrees from horizontal and 45^{o} compression

diagonals. The four 0.5in. thick angle stiffeners at the end, below the bearing, likely absorb most of the vertical bearing force and transfer it into the web as the force moves down through the angles along the web. The downward force transferred from the angles to the web is balanced by the upward component of the tension diagonal pulling on the angle and the upward component of the compression diagonal pushing on the angles. The difference in strains between the top gage and bottom suggests normal beam action with flexural stress is not occurring. The low flexural stress reduced the possibility that stress concentration will develop at the inner part of the tail beam where the section depth suddenly starts to increase.

Deflection Data

With the data taken from the surveying equipment, deflections at the four targets on poles were calculated using trigonometric relationships. The processed data is presented in Table 4.2-3 and a key to the target locations was provided in Figure 4.2-3 (Raw data from surveying equipment can be found in the Appendix). Stations 1 and 3 were on the loaded bridge leaf and stations 2 and 4 were on the unloaded opposite leaf. With just the reach-all truck, the deflections of the loaded leaf were 0.07 to 0.03 in. greater than the unloaded leaf. This difference appears to indicate a certain amount of "play" in the mid-joint before load is transferred across the joint. The value at Station 4 under double truck load (0.81 in.) appears to be unexpectedly high creating doubts on its accuracy. Positive values correspond to downward deflections.

Table 4.2-3. Mid-joint deflections under truck loading.

		Deflections (in)
Reach-all Truck	Station 1	0.55
	Station 3	0.25
	Station 2	0.48
	Station 4	0.22
Reach-all Truck + Dump Truck	Station 1	0.68
	Station 3	0.71
	Station 2	0.61
	Station 4	0.81

4.3 Marinette: Development of Three Dimensional Finite Element Model.

As described in Section 4.2, an initial 3D FEM was created according to design plans to predict the bridge structural response. The 3D FEM model of the bridge was created using the commercial

CSiBridge software. From this model, critical locations where high strains were expected were identified as a means of selecting locations to place the strain gages.

After the field test was concluded, the truck loading scheme from the field test was replicated on the analytical model. By comparing the measured strains from the 3D FEM model and the field test, an evaluation of the model's accuracy was attained. The analysis results did not match the measured data as was expected. The plans for the bridge were further examined and information on particular details such as the stiffness of the grid deck, the rigidity of connections between flexural members, the degree of composite action between deck and beams, and the tightness of the midspan joint, were re-considered from field observations and were evaluated and modified if there was doubt as to the accuracy of the first modeling method.

With the revised analytical model the accuracy was again verified, and then oversize-overload (OSOW) loads (simulating known OSOW vehicles) were applied to the analytic model to evaluate the actual bridge performance. Critical members with high stress to capacity ratios were identified. Those are then recommended as the members to consider in the issuing of permits for future OSOW vehicles.

Initial Model Development

Different elements were used to model different sections of the Marinette Bridge. The selection of these elements was done considering the advantages of every element type. Frame, shell and link elements are the most common ones.

Floor beams, stringers, bracing elements and stiffeners, angles and flanges of the two girder sections were modeled using frame elements (see Table 4.1-1 for specific member sizes). The steel open grid deck, girder web and counterweight concrete area were modeled using thin shell elements. Finally, connections between these members were bolted in reality but detailed modeling of the bolts was not done. Instead, connections were simulated by links with different directional stiffnesses. The links were necessary since individual members, such as the stringer and floor beam, had their centroids at different locations. The links connected the centroid of a stringer, over the floor beam, to the centroid of the floor beam to resemble the actual geometry as accurately as possible.

Bridge geometry was taken from Michigan State Highway Department design and shop drawings [10], but the poor quality of the old drawings made understanding of some details difficult. The initial model was constructed using known member sizes and assumed connection behavior as detailed in the following.

The bridge stringers were modelled as 2 span frame elements, continuous over the center floor beam and simple supported at the end floor beams. These model configurations of 2 span stringers were alternated – with one stringer continuous over a floor beam and the adjacent stringer non-continuous.

In the initial model, the steel deck to stringer and stringer to floor beam connections were assumed to be rigid in flexure. A flexural rigid connection implies full composite action. As noted earlier, the deck was bolted to the stringers at 1ft. intervals making composite action possible. The two connections were modeled by using fixed linear links, rigidly linking displacement and rotation in every direction. These links extended between the centroids of each member. The floor beam to girder connection was assumed to transfer only shear since the actual connection consisted of bolting between the beam web and a girder stiffener. A link element wasn't necessary because the floor beam ends (frame element) and the girder web (shell element) shared the same nodes. End releases were used at both ends of the floor beam in order to obtain a shear-only connection.

The bridge's mid-joint between bascule leaves was assumed to only allow the transfer of vertical shear forces between the two leaves. The connection was modeled using partially fixed linear links, transferring zero moment between leaves but fully transferring any displacements.

The counterweight is a large concrete block with embedded steel truss members. The assumed rigid behavior of the counterweight was modeled by using very high stiffness values with the concrete shell areas. No counterweight truss elements were simulated in the model, only the stiff shell areas connected rigidly to the girder web by sharing the same nodes.

Joint restraints were applied to the bascule girders. The connection between bascule girder and the pier was modeled assuming that the bascule girder can rotate only about the transverse axis of the bridge. Vertical movement at the contact point between the "tread" and "track" (see Figure 3.1-1) was assumed to be zero and modeled as a pin support. The contact between the tail beam and the approach span beam was modeled by using a pinned connection, this assumption prevented horizontal and vertical movement at that point and is based on the assumption that horizontal friction will develop between the bearing plates. Finally, the bascule pinion was also restricted from displacements assuming that its stays always in the same place. A picture of the initial analytical model can be seen in Figure 4.2-13.

Comparison with Field Strain Measurements

The results obtained from the initial model are compared with the measured data in Table 4.2-4 for strain and 4.2-5 for deflection data. Positive values indicate tension, negative is compression.

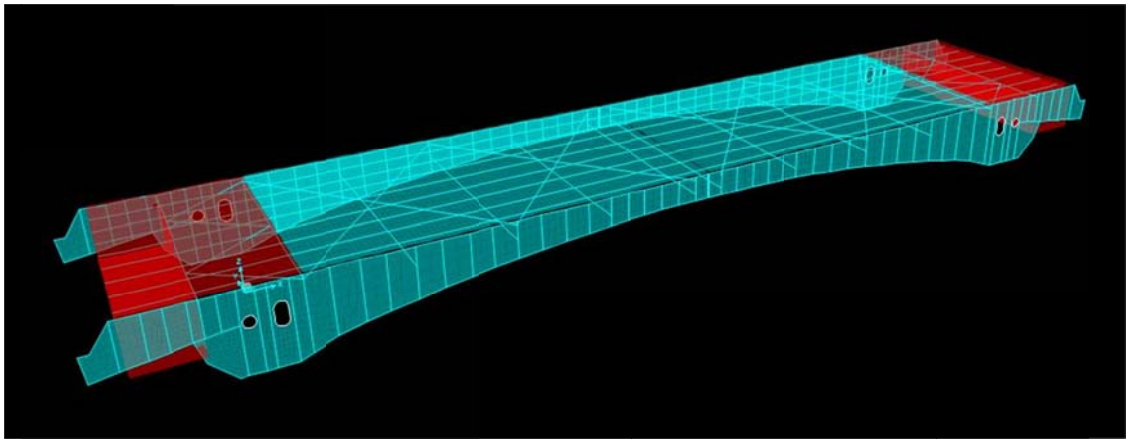

Figure 4.2-13. 3D FEM of Marinette Bridge. Concrete counterweight shown in red and the steel members in cyan.

Table 4.2-4 Strain values measured and predicted.

REACH-ALL TRUCK							MODEL	GAGES
Element	Location	Moment (kip-ft.)	Axial (kip)	Inertia (in^4)	Area (in^2)	Stress (Ksi)	Micro-Strain	Micro-Strain
Floor Beam	Top	19.7	45.9	12178	64.1	0.47	16	-20
	Bottom					0.96	33	20
Girder	Top	Not output by model				0.10	3	38
	Bottom					-0.94	-32	-55
Tail Beam	Top					0.70	24	-11
	Bottom					-0.56	-19	-45

Note: Moment, Axial, Inertia, Area and Stress listed on tables are based on the values found in the CSiBridge Model

REACH-ALL + DUMP TRUCK							**MODEL**	**GAGES**
Element	Location	Moment (kip-ft.)	Axial (kip)	Inertia (in4)	Area (in2)	Stress (Ksi)	Micro-Strain	Micro-Strain
Floor Beam	Top	31.2	74.4	12178	64.1	0.78	27	-48
	Bottom					1.54	53	53
Girder	Top	Not output by model				0.12	4	42
	Bottom					-1.15	-40	-63
Tail Beam	Top					0.92	32	-29
	Bottom					-0.72	-25	-87

Note: Moment, Axial, Inertia, Area and Stress listed on tables are based on the values found in the CSiBridge Model.

All the measured strains and induced stresses are very low values with the loading used. Modeled strain results obtained with the reach-all truck and both trucks disagree with the measured values and the error (in the tail beam) is equivalent to 3200psi of stress.

In terms of deflections, the results obtained with the initial model are shown in Table 4.2-5. The positions 1&3 are on the loaded leaf and 2&4 are on the opposite unloaded leaf. Positive values indicate downward deflection.

Table 4.2-5. Deflection values at mid-joint connection.

		Deflections (in)	
		Surveying equipment	CSiBridge Model
Reach-all Truck	Station 1	0.55	0.47
	Station 3	0.25	0.13
	Station 2	0.48	0.46
	Station 4	0.22	0.13
Reach-all Truck + Dump Truck	Station 1	0.68	0.58
	Station 3	0.71	0.58
	Station 2	0.61	0.58
	Station 4	0.81	0.58

As expected, the deflections at the different stations in our analytical model after the two trucks were placed on the bridge were the same, 0.58 in. This was attributed to the use of rigid links in between the two bascules leaves, transferring shear forces from one leaf to the other. A change in the mid-joint connection is necessary for more accurate results. Measured results from Table 4.2-5 show that the connection between the two leaves is not rigid, considering that the south lift span (locations #1 and #3) deflected more than the north one (except for the large value of 0.81 in. at location #4 – which might possibly be an errant data point).

Although the strain values were quite inaccurate and the deflection values differ a little bit from the ones measured in the field test, the initial model served as a good starting point

Adjustment to the Model Based on Closer Examination of Bridge Details

During the load testing a close inspection was made of the bridge components and connections that led to needed changes in the analytic model – which was based on poorly preserved original bridge plans. The first adjustment needed for the model was in the mid-joint connection between bascule girders. The original assumption of a complete vertical locking between the two leaves was incorrect. The degree to which the leaves are locked together depends on a tight adjustment of the bearing plates in the joint. With repeated traffic these joints are known to become loose and are regularly tightened (at least annually) as part of the bridge maintenance. To more reasonably model the joint, instead of using rigid linear links, a hook link element was used. A hook element is a partially linear link element that

transfers tension only [5]. It can be defined with an initial opening between the two elements where the stiffness of the link is zero. A pre-defined linear stiffness of the link takes action after the link has stretched more than the defined initial gap. This modelling may be essential in modelling the connection between bascule bridge leaves.

The hook element in the model was defined with an initial opening of 0.07 in. (in this case to match the difference between the measured deflection of the two spans) and a very high stiffness value to simulate rigidity once the gap closes**.** Typically the joint is adjusted at least once per year to eliminate gaps, but with repeated loading the gaps in bearings do grow again. Conservative modelling, to predict maximum forces in the loaded leaf, might best use a gap opening of ¼ inch which could develop if the joint is not adjusted frequently. Figure 4.2-14 shows the joint in the bridge at the time of load testing. There appears to be some lack of contact between the tooth (on right) and the bearing plate (at bottom).

Figure 4.2-14. Joint between leaves of Marinette bascule bridge.

Another refinement in the model was a change in the assumed connection behavior between the stringers and floor beams. In the initial model, this connection was modeled using fixed links, preventing differential rotations and displacements between the members (a shear and moment rigid joint). A close consideration of the bridge plans, and inspection in the field, revealed that the stringers are attached to the floor beams by bolts between the lower flange of the stringer (which sits above the floor beam) and the upper flange of the floor beam. It is doubtful whether this connection is capable of restricting relative rotation between the two elements. The connection should restrain differential displacements, but not rotations. The floor beam will not develop any composite action with the stringers and the deck. The connection between these members (deck to stringer and stringer to floor beam) was changed from fixed to partially fixed links, preventing only the relative vertical displacement.

After field inspection and observation of the open grid decking, shown in Figure 4.1-5, it was apparent that the grid itself sat on small inverted T section purlins that ran perpendicular across the stringers. The T is visible in the figure. The bottom flange of this T is bolted to the top flange of the stringer. Shear developed, for composite action, would have to be transferred to the grid through torsion of the T section. That section was judged to have insufficient stiffness to develop composite action with the orthotropic grid. The link between stringers to the decking was changed to the same form as the link described above for the stringer-beam connection.

Joint restraint between the tail beam and the approach span was changed from pinned to a roller connection. Examination of the tail beam during bridge inspection hinted that horizontal motion (and friction) between the bearing plates would be minimal. The joint between the girder and the Bascule pinion was released after realizing that the pinion actually moves horizontally along the rack (Figure 4.1-1).

Finally, the counterweight was redefined. There was some concern as to whether the stiff shell elements originally employed could adequately simulate the rigidity of the large reinforced concrete block. Counterweight steel trusses were introduced and the whole system was link together by applying a “rigid body constraint.” These changes were expected to increase the counterweight stiffness, showing a more rigid behavior. Figure 4.2-15 displays the new model with the applied changes.

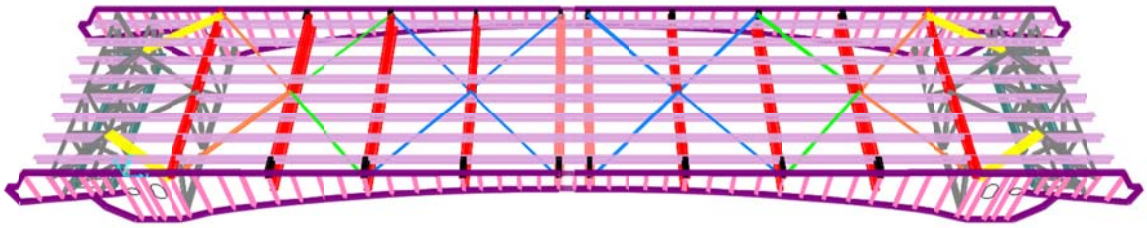

(a)

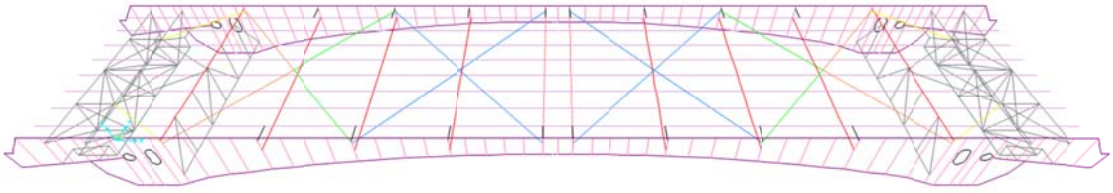

(b)

Figure 4.2-15. (a) Extruded model. (b) Analytic model.

The results obtained with the refined model of the Marinette Bridge, after implementing the changes described above, are shown in Table 4.2.6. A positive value indicates tension in the member, a negative one compression.

Table 4.2-6 Strain values measured and predicted.

REACH-ALL TRUCK							MODEL	GAGES
Element	Location	Moment (kip-ft.)	Axial (kip)	Inertia (in^4)	Area (in^2)	Stress (Ksi)	Micro-Strain	Micro-Strain
Floor Beam	Top	72.7	1.8	12178	64.1	-0.87	-30	-20
	Bottom					0.92	32	20
Girder	Top	No output by model				1.12	39	38
	Bottom					-2.22	-77	-55
Tail Beam	Top					-0.07	-2	-11
	Bottom					-0.4	-14	-45

Note: Moment, Axial, Inertia, Area and Stress listed on tables are based on the values found in the CSiBridge

REACH-ALL + DUMP TRUCK							MODEL	GAGES
Element	Location	Moment (kip-ft.)	Axial (kip)	Inertia (in^4)	Area (in^2)	Stress (Ksi)	Micro-Strain	Micro-Strain
Floor Beam	Top	156.4	4	12178	64.1	-1.86	-64	-48
	Bottom					1.99	69	53
Girder	Top	Not output by model				1.31	45	42
	Bottom					-2.65	-91	-63
Tail Beam	Top					-0.1	-3	-29
	Bottom					-0.51	-18	-87

Note: Moment, Axial, Inertia, Area and Stress listed on tables are based on the values found in the CSiBridge

The new predictions are more consistent with the measured data, though not exactly identical. Floor beam strains at top and bottom are nearly equal, as expected with a non-composite behavior. Strains at the girder top location correlated very well with the values obtained in the field, with differences less than 3 microstrain. However, strain values predicted for the bottom location were higher than the ones obtained in the field test by 22 to 28$\mu\varepsilon$ for a 780psi error.

Strain values at the tail beam are not consistent with the data obtained from the model. This is likely due to the complexity of the region where the gages were placed. This area is highly congested by angle stiffeners with rivets and an abrupt section change. Moreover, friction between the tail beam bearings may still induce some stresses on the tail beam. All of these produce a very complex stress distribution on the tail beam. It is not possible to model this disturbed region with minimum element size of 10 by 7.5 inches as used in the girder web here. A more refined model, i.e. 3-D Finite Element small scale analysis of the isolate area, is required to simulate the actual strains. That will be left to future research work.

Deflections with the refined model show an improved correlation with respect to the field test measurements. As seen in Table 4.2-7, with the introduction of the Hook to model the gap at the midspan joint, there is a better agreement in deflections at the 4 targets (except for the large value of

0.81 at location #4 – which is likely an errant data value since deflections in the unloaded leaf should not be larger than in the loaded leaf). Positive values correspond to downward deflections.

Table 4.2-7. Deflection values at mid-joint connection.

		Deflections (in)	
		Surveying equipment	CSI Bridge Model
Reach-all Truck	Station 1	0.55	0.55
	Station 2	0.48	0.46
	Station 3	0.25	0.16
	Station 4	0.22	0.13
Reach-all Truck + Dump Truck	Station 1	0.68	0.65
	Station 2	0.61	0.56
	Station 3	0.71	0.68
	Station 4	0.81	0.59

4.4 Marinette: Impact of OSOW Vehicles.

Six dual lane trailers, two single lane trailers and the HL-93 trucks, as described in Chapter 2, were analytically driven across the Marinette bascule bridge to measure the vehicle's force impact. Each of these vehicles was described earlier along with the geometry of the loaded lanes. Critical members where high stresses developed were identified. The dead load of the bridge was included in the analysis for all the load combinations. The response of only principal members, such as stringers, floor beams and girders, were examined in this project. Joints, bracing, diaphragm and deck members were not included in the scope. The OSOW vehicle loads are factored by 1.35, HL-93 by 1.75 and dead load by 1.25. The AASHTO multi-presence factor is used with the Hl-93 loads, but no the OSOW load.

The results obtained from the analyses are summarized in Table 4.4-2. The notation in the tables for single and dual trailers is as follows and is detailed further in Table 4.4-1:

- ***Single312*** represents the 312 kips gross weight single trailer,
- ***Single446*** represents the 446 kips gross weight single trailer,
- ***Dual486*** represents the 486-kip gross weight dual trailer,
- ***Dual500*** represents the 500-kip gross weight dual trailer.

Table 4.4-1. Notation used in results of OSOW analysis.

Truck Notation	Description
HL-93	AASHTO HL-93 truck combinations
Single312	312 gross weight single trailer
Single446	446 gross weight single trailer
Dual500-2	500 gross weight dual trailer with 2 ft. transverse wheel spacing
Dual500-6	500 gross weight dual trailer with 6 ft. transverse wheel spacing
Dual500-10	500 gross weight dual trailer with 10 ft. transverse wheel spacing
Dual486-2	486 gross weight dual trailer with 2 ft. transverse wheel spacing
Dual486-6	486 gross weight dual trailer with 6 ft. transverse wheel spacing
Dual486-10	486 gross weight dual trailer with 10 ft. transverse wheel spacing

Figures 4.4-1 and 4.4-2 show a moment and axial force envelope for the different flexural members under moving load combinations. The first plot shows floor beam and moment envelopes. The second plot shows axial force in the girder flanges.

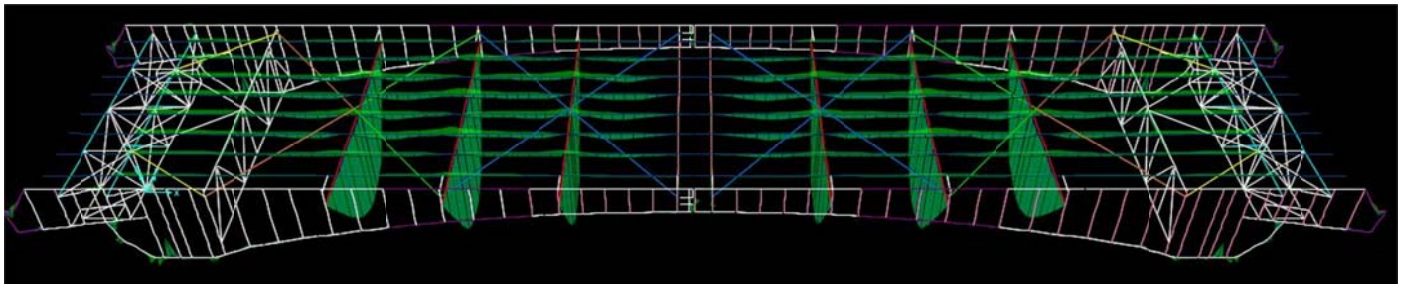

Figure 4.4-1. Moment envelope of critical members under OSOW/HL-93 truck combinations.

Figure 4.4-2. Axial force envelope of girder flanges under OSOW/HL-93 truck combinations.

The flanges of the girders, under axial load, provide most of the girder moment resisting capacity. In Figure 4.4-2, axial forces are plotted in every flange along the girder when OSOW trucks are driven down the load lanes. Axial forces in top flanges are almost entirely in tension, except close to the

mid-joint connection. Bottom flanges are the opposite in compression all along the girder and with larger values than the top flanges.

Values seen in Table 4.4-2 were obtained with the axial and bending moment envelopes (as shown above) under each load combination. Different members, such as various stringers, showed the maximum stress under different vehicle loadings. The stringer or beam with the largest stress is listed.

Table 4.4-2: Max.member stresses - Marinette Bridge under HL-93 and OSOW trucks and dead load. Tension is positive, compression negative; moment causing compression at top is positive. (Note: "flange" refers to flange of the main girders.)

Load Combination	Controlling Member	Max. Moment (kip-in)	Max. Axial (kip)	Min. Axial (kip)	Max Tension (ksi)	Max Compression (ksi)
HL-93	F.B. No. 4	13943	1	0	23	-23
	Stringer No. 24	1619	1	-3	29	-29
	Flange	0	452	-627	16	-22
Dual500-2	F.B. No. 3	9586	5	0	16	-16
	Stringer No. 23	881	1	-1	16	-16
	Flange	0	540	-792	19	-28
Dual500-6	F.B. No. 3	10093	6	0	17	-16
	Stringer No. 14	752	0	-4	13	-13
	Flange	0	399	-587	14	-21
Dual500-10	F.B. No. 3	8555	5	0	14	-14
	Stringer No. 22	720	1	-2	13	-13
	Flange	0	399	-588	14	-21
Dual486-2	F.B. No. 3	6052	3	0	10	-10
	Stringer No. 24	697	0	-1	12	-13
	Flange	0	358	-548	13	-19
Dual486-6	F.B. No. 3	6344	4	0	10	-10
	Stringer No. 22	572	1	-2	10	-10
	Flange	0	271	-415	10	-15
Dual486-10	F.B. No. 3	5397	3	0	9	-9
	Stringer No. 22	557	1	-2	10	-10
	Flange	0	271	-415	10	-15
Single312	F.B. No. 4	7619	1	0	12	-12
	Stringer No. 26	649	4	1	12	-12
	Flange	0	366	-511	13	-18
Single446	F.B. No. 4	7436	1	0	12	-12
	Stringer No. 20	679	0	-2	12	-12
	Flange	0	361	-500	13	-18

Axial load in the stringers and moment in the girder flanges were negligible and do not contribute in a significant way when calculating maximum stresses on those members. From the table, the girder flanges developed the maximum stress under all the OSOW truck combinations while the HL-93 load combination caused the highest overall maximum in stringer 6 of Figure 4.1-3 (Elem #24) between floor beams 4 and 5. The floor beam numbering is visible in Figures 4.1-3 & 4.2-2.

The maximum stringer stress, among all the truck combinations, was under the HL-93 load combination with a value of 29 ksi in compression and tension. The HL-93 load used an LRFD load factor of 1.75, where the OSOW truck used a 1.30 factor. The OSOW Dual500-2 truck induced the second largest with a value close to 16 ksi, a 46% decrease with respect to the stresses under the HL-93 truck. The Dual500-6, 500-10, Dual486-2 and Single446 all showed a decrease of approximately 58% compared to the HL-93 truck stresses. Finally, truck combinations Dual486-6, 486-10 and Single312 created the lowest stress in the stringers among all the trucks, with a 65% decrease with respect to the HL93 value.

An OSOW truck loading creates the highest girder flange stress. The maximum girder stress value was under the load combination Dual500-2, reaching a value of 28 ksi in compression, nearly the same as the maximum stringer stress of 29ksi. The other loads - HL-93, Dual500-6, 500-10, Dual486-2, Single312 and single446 created girder stress values that fluctuated between 22 to 18 ksi, a decrease of 21 to 37% with respect to the maximum value from the Dual500-2. Finally, lower stresses were seen in load combinations Dual486-6 and 486-10 with values of 15 ksi, a 48% decrease from Dual500-2.

Floor beam stresses were lower than stringers and girders under all the trucks loads. The largest floor beam stress was observed in floor beam No. 4 under th HL-93 load combination, reaching a value of 23 ksi in compression. Then, Dual500-2 and Dual500-6 followed with values of 16 ksi, a 30% decrease with respect to the HL-93 value. The Dual500-10, Single312 and Single446 had a decrease ranging from 37 to 47% compared to the HL-93, with values between 14 and 12 ksi. The Dual486-2, 486-6 and 486-10 produced the lowest stresses in floor beams, with a value below 10 ksi and a percentage of decrease between 55 and 61% with respect to HL-93 values.

The steel members on this bridge have a yield stress of 36 ksi, so no yielding was expected in any main member of the Marinette Bascule Bridge even under the heaviest OSOW trucks (29ksi). Since most of the biggest stresses are in compression, however, special consideration needs to be given to local buckling – which wasn't examined here.

Though the FEM analysis was not useable for predicting stresses in the tail lock beam, as evident in Table 4.2-6, an alternate estimate of the behavior was determined. Since the tail lock beam stress under the test loads is known and the stresses in the bascule girder are known, an extrapolation can estimate the tail beam stress under factored HL-93 loading and factored OSOW loading. The strain gage data showed that a principal stress of 7.28ksi occurred in the tail beam while the stress at the top gage location on the bascule girder was +1.22ksi. The FEM analysis did provide acceptable estimates of girder stresses at the top gage location. So the FEM is used to predict girder top stress at the gage under factored HL-93 and OSOW loads. The tail beam stress is then estimated by multiplying the stress under

the test load by the ratio of girder stress at the top gage location under the selected load divided by the top girder stress measured with the test load. As an example – the OSOW truck was predicted to create a stress at the gage location 9.38 times larger than the measured stress with the test load. The stress in the tail lock would also be expected to be 9.38 times larger. Since the dead weight of the bascule leaf is expected to be balanced by the counterweight – no dead load stresses are assumed in the tail lock.

With factored HL-93 loading in both lanes the tail lock stress would be near 66ksi . If the factored OSOW Dual500-2 truck crosses the bridge, the expected tail tension stress would reach 68ksi. These estimates indicate that the tail lock capacity may indeed control the load capacity of the entire bridge. While the suggested stresses in the steel material with a 36ksi yield stress limit are approximate, the values suggest that further close examination of the tail locks on bascule bridges is strongly warranted.

Stresses near the midspan joint between bascule leafs have not been discussed. This is another region where complex forces exist and the current finite element meshing and detail modelling was not sufficient to predict accurate stresses in that region. To allow movement in the joint, with an initial gap opening, a "hook" element was used in the model and it was attached to a node at the bearing point of the "tooth" in the joint as previously shown in Figure 4.2-14. The stress contours predicted by the analysis are shown in Figure 4.4-3, but these values are not reliable. The stresses in the midspan joint are not expected to be as high as suggested in the tail lock region, but further examination of the details of this joint may be desirable.

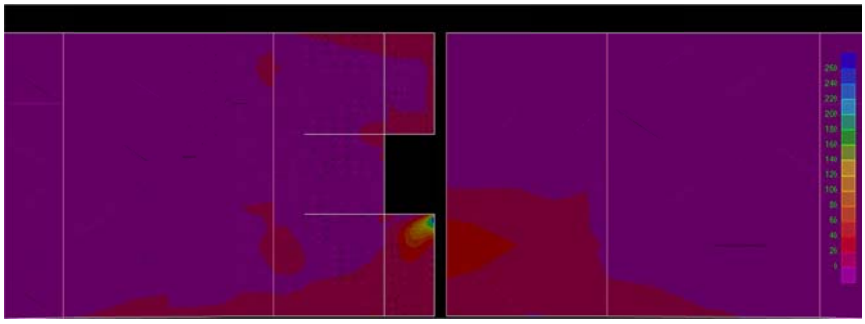

Figure 4.4-3. Stress contours in the midspan joint region with stress concentration at the bearing point.

5. WINNECONNE BRIDGE

5.1 Winneconne: Introduction and Structural Components

The Winneconne bascule bridge (B-70-913) is a twin-leaf bascule over the Wolf River in Winneconne, Winnebago County. It carries State Highway 116 (Main Street) in an East-West direction across the river. It was designed by the Wisconsin Highway Commission and built in 1934. It is classified as another Rolling Lift Trunnion bascule just like the Marinette Bridge with an underneath counterweight (see Figure 4.1-1 for the double leaf Rolling Bascule Bridge configuration).

The Winneconne Bridge has a total span length of 95 ft. Each lift span of the bridge extends 39.5 ft. Deck width is 30 ft. with two traffic lanes in opposite directions. Each lane is 15 ft. wide with a 6.75 ft. wide concrete sidewalk on both sides. The operator's house is located on the southwest side. A picture of the bascules and the approaching spans is shown in Fig. 5.1-1.

Figure 5.1-1. Winneconne Bridge (Wisconsin, HSI ID: B709130002, Bascule bridge, span = 95 ft.)

The bridge has two main bascule girders that vary in depth with a parabolic vary depth. Besides the two bascule girders, there are 11 stringers running in the longitudinal direction parallel to the girders on 3 transverse floor beams per leaf. The deck, originally designed as an asphalt plank, was replaced in 1975 with a 5-inch open grid. Other major work performed after first construction involved painting, overlay concrete work and cleaning of expansion joints. An elevation view, frame plan and cross-sectional view from 1975 deck replacement plans are shown in Fig. 5.1-2.

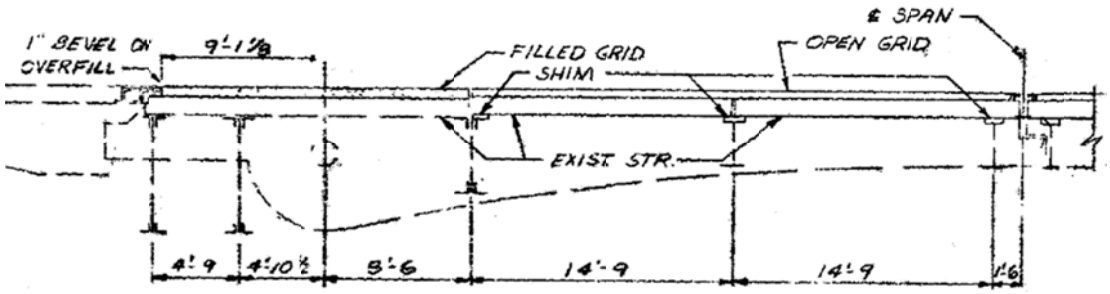

(a)

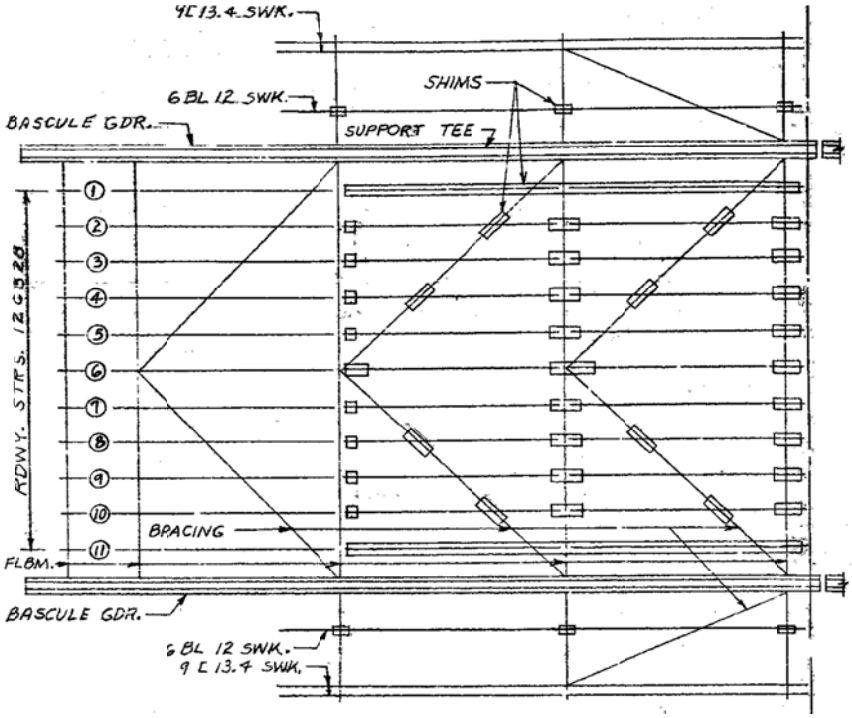

(b)

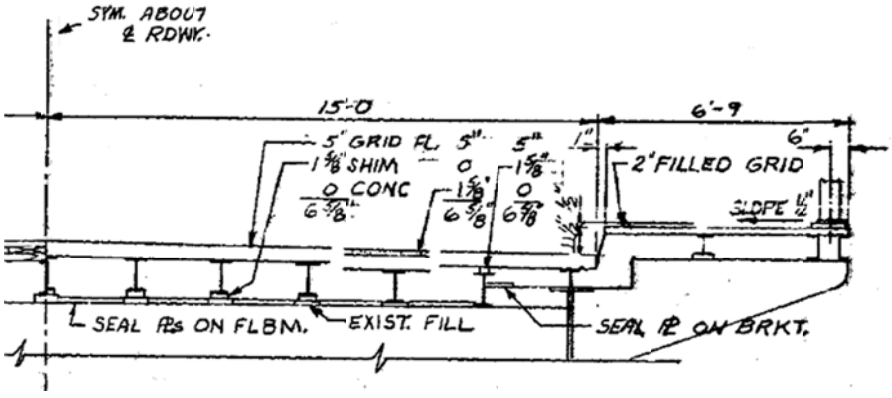

(c)

Figure 5.1-2. Winneconne Bridge plans. (a) Elevation view with East to right (b) Framing plan (half of bridge total span). (c) Cross sectional view (half of the bridge). Adapted from WisDOT HSI database [10].

Structural Components

The main structural members of the bridge are made of steel. The girders, floor beams, stringers, and bracing are all components made of grade 36 steel. A summary of the main steel structural members obtained from WisDOT design drawings [10] can be seen in Table 5.1-1.

The plate girders on the Winneconne Bridge were built up from angles and flange or cover plates riveted together to the web plate. To avoid local web buckling, vertical stiffeners (typically double angles, 2L 3½ x 5 x $^{5}/_{16}$) are provided approximately every 3.6 ft. along the girders as shown in the photo of Figure 5.1-3. Furthermore, additional cover plates typically 14 in. by 0.5 in. are bolted on top of the flanges in required zones. These plate girders have a variable section throughout their span, varying depth and thickness. The girder's depth varies from 48 in. at floor beam No. 3 to 126 in. at floor beam No. 1 (with 1 being closest to the pier).

Floor beams and stringers are common W-shape sections with constant section along their axis. Floor beams are connected to the plate girder by rivets (web area) and stub brackets (bottom flange). The stringers are not continuous between floor beam 1 and 3, being broken at stringer-floor beam connections. Their bottom flange is connected to the floor beam flanges by rivets.

Lateral bracing is provided by a V-shape bracing formed by structural angles along the bridge axis. Top lateral and bottom bracing are connected to the girders by rivets, both used to prevent lateral torsional buckling of the girders.

Table 5.1-1. Main structural elements description and dimensions.

Member Name	Type	Dimension
Girder	Plate girder with parabolic shape	Variable Section
Floor beams	Simple span W-shapes from cl to cl of girders, spaced at 14ft-9in	W30x108 (F.B. No. 2 & 3)
Stringers	Simple spans W-shape framed on top of the floor beams, spaced at 28.5in.	W12x28
Top Lateral bracing	V pattern structural angles connecting the two girders	L 3½ x 3½ x 5⁄16 L 4 x 3½ x 3⁄8 L 3½ x 3 x 3⁄8
Side Walk	C-shape channels connected to top of the bascule girder	12 C 30 15 C 33.9
Counter-Weight trusses	Combination of Tee sections and double angles supporting the concrete counter-weight	ST 4 WF 24 ST 5 WF 16.5 ST 6 WF 39 2L 7 x 4 x 5⁄8 2L 8 x 8 x 3⁄4 2L 4 x 3½ x 3⁄8

Figure 5.1-3. Bascule Girder view. Stiffeners every 3.6 ft. and a variable cross section along the bridge.

The 6.75-ft. wide concrete sidewalk is cantilevered on metal brackets connected to the sides of the plate girders by bolts visible in Figure 5.1-3. The current deck of each leaf is a galvanized 5-in. steel open welded grid flooring (ASTM A36). It is fastened to the stringers with stainless bolts approximated every 1 ft. A picture detailing the deck flooring is shown in Fig. 5.1-4.

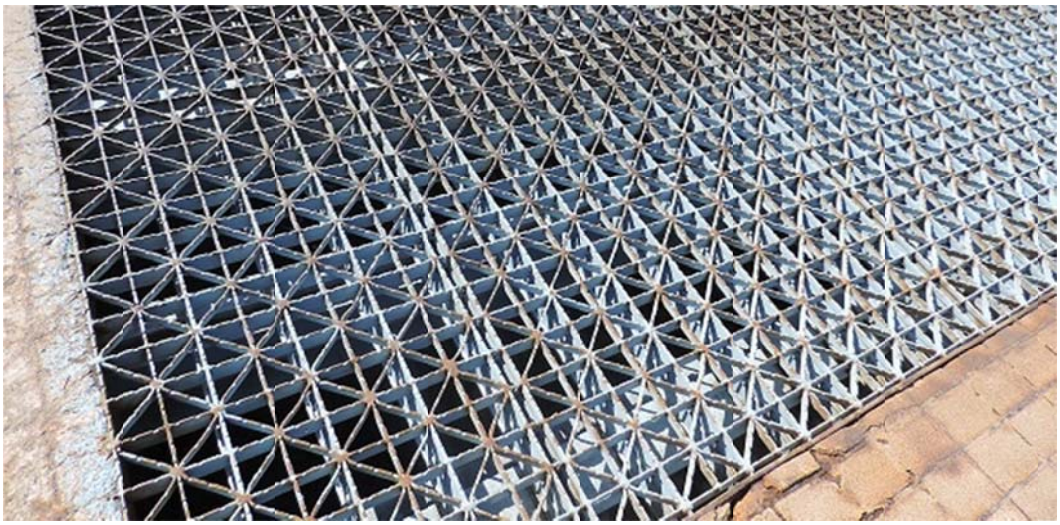

Figure 5.1-4. 5-Inch 4-Way modified open grid metal deck.

5.2 Winneconne: Development of Three Dimensional Finite Element Model.

Unlike the Mirror Lake and Marinette bridges, the Winneconne bascule bridge was not field tested. Therefore, the 3D FEM was created according to design plans, visual observations during an annual bridge inspection, and the experience obtained from the previous Marinette bascule bridge analysis process. The 3D FEM model of the bridge was created using the commercial CSiBridge software. OSOW loads were applied to the analytic model to evaluate the bridge performance. Then, critical members with high stress to capacity ratios were identified. Those will be recommended as the members to consider in the issuing of permits for future OSOW vehicles.

Model Development

The same types of elements used to model the Marinette Bridge were used in the Winneconne model. Floor beams, stringers, bracing elements and stiffeners, angles and flanges of the two girder sections were modeled using frame elements. The steel open grid deck, girder web and counterweight concrete area were modeled using shell elements. Connections were simulated by links with different directional stiffness since members like stringers and floor beams had their centroids at different locations. The links connected the centroid of a stringer, over the floor beam, to the centroid of the floor beam to resemble the actual geometry as accurately as possible. Bridge geometry was taken from WisDOT design and shop drawings [10].

In the model, the steel deck to stringer, stringer to floor beam and floor beam to girder connections were assumed to transfer only shear, no moment. The first two connections were modeled by using partially fixed linear links, rigidly linking displacement in the vertical direction. These links were defined from the centroid of each member. In the case of the floor beam to girder connection, a link element wasn't necessary since the floor beam ends (frame element) and the girder web (shell element) shared the same nodes. However, in order to obtain a shear-transfer connection, end releases were used at both ends of the floor beam element. Since the floor beams were connected to the girders through web bolts and stub brackets on the floor beam bottom flange, the actual connection may transfer shear and some moment. Here the connection was assumed to just transfer shear, and the effect of the stub bracket was ignored.

The bridge's mid-joint connection was assumed to only allow the transfer of vertical shear forces between the two leaves. The connection was modeled using partially fixed linear links transferring zero moment between leaves but fully transferring displacements. For this bridge two model analyses were conducted. In the first one, a tight mid-joint connection was modeled with a partially fixed linear link. In the second one, a gap of 0.125 inches at the mid-joint connection was modeled with a hook element to see the effects of having a gap in term of stresses in the structure.

Typically the joint is adjusted at least once per year to eliminate gaps, but with repeated loading the gaps in bearings do grow again.

The counterweight, a large concrete block with embedded steel truss members, was modeled in the same way as for the Marinette bridge model. Its rigid behavior was modeled by using very high stiffness values with the concrete shell areas connected rigidly to the truss elements and the girder web by sharing the same nodes. Again, the "Rigid Body constraint" tool was used to link all the nodes together so the counterweight acted as a unit.

Joint restraints used in the Marinette Bridge model were also applied to the bascule girders. The connection between the bascule girder and the pier was modeled assuming that the bascule girder can only rotate about the transverse axis of the bridge. Vertical and horizontal movement at the contact point between the "tread" and "track" (see Figure 4.1-1) was assumed to be zero (i.e. pinned). The contact between the tail beam and the approach span beam was modeled by using a roller connection like in the Marinette Bridge, this assumption preventing only vertical movement at that point. Diagrams of the model can be seen in Figure 5.2-1.

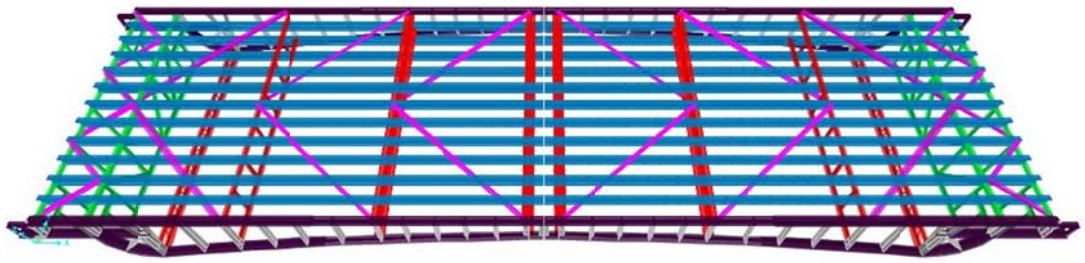

(a)

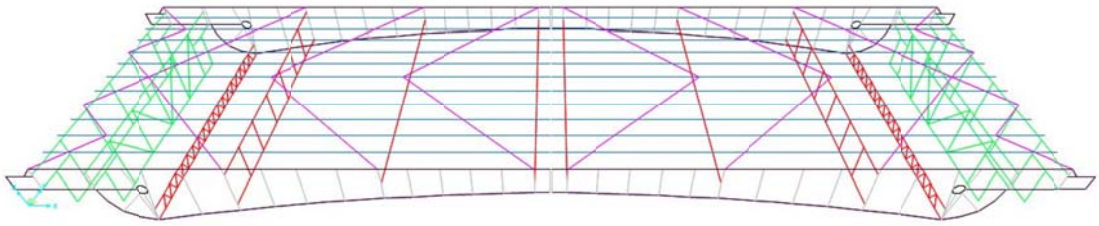

(b)

Figure 5.2-1. (a) Extruded model. (b) Analytic model.

The sidewalk was assumed to act as a cantilever on the main girder as seen in Figure 5.2-2. The cantilever, with small stringers, was assumed to resist none of the truck loading but to only create a

dead load on the girders. From the plan geometry, an equivalent moment-force and vertical force were applied to the top of the girder simulating the dead loading effect coming from the sidewalk.

Figure 5.2-2. Sidewalk cantilevered on brackets connected to girder web.

5.3 Winneconne: Impact of OSOW Vehicles.

For the Winneconne Bridge two different OSOW analyses were performed in order to quantify the effects of having a gap at the mid-joint connection. Therefore, two nearly identical models were tested under the same load combinations with the difference being that one model had a tight mid-joint and the other one had an initial gap of 0.125 inches. With the results, a comparison between the stresses seen in the main members and an evaluation of the mid-joint connection were achieved.

After running the described vehicles on the Winneconne bridge (six dual lane trailers, two single lane trailers and the HL-93 trucks), critical members where high stresses developed were identified. Dead load of the bridge was included in the analysis for all the load combinations. Again, only the response of principal members was considered in this report. For this bridge, floor beam No. 3 corresponded to the one closest to the mid-joint connection. The results obtained from the models are summarized in Tables 5.3-1 and 5.3-2. Load factors were: 1.25 (dead), 1.75 (HL-93), and 1.35 (OSOW). The truck type notation in those tables is explained in Section 4, Table 4.4-1 and is as follows:

- ***Single312*** represents the 312 kips gross weight single trailer,
- ***Single446*** represents the 446 kips gross weight single trailer,
- ***Dual486*** represents the 486-kip gross weight dual trailer,
- ***Dual500*** represents the 500-kip gross weight dual trailer.

Moment envelopes for different members under the moving load combinations with a closed mid-joint are shown in Figure 5.3-1. Figure 5.3-2 plots the axial force envelope for the girder flanges. Flanges of the girders carry mostly axial force in resisting girder moments. Top flanges are in tension while the bottom ones are in compression. The counterweight of the bridge is so stiff that girder deformation and stresses adjacent to the block are insignificant.

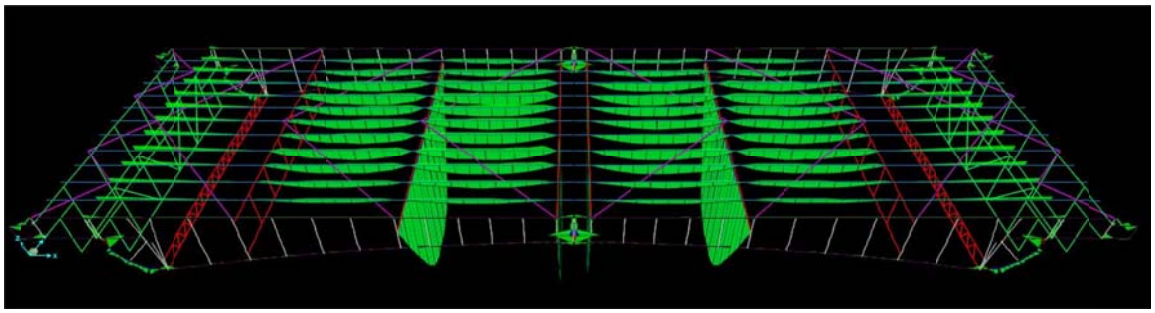

Figure 5.3-1. Moment envelope on critical members under OSOW/HL-93 truck combinations.

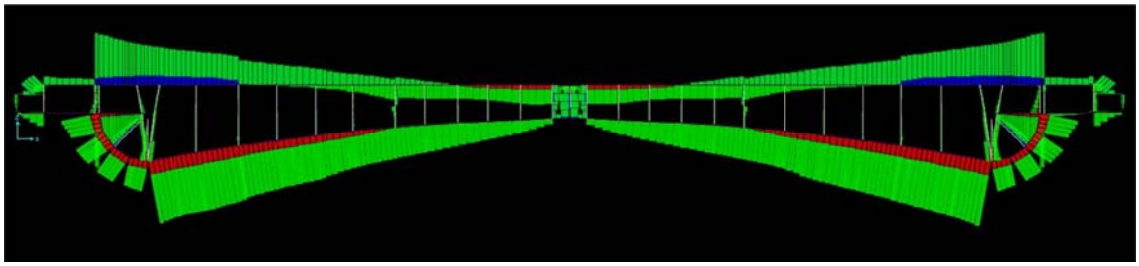

Figure 5.3-2. Axial force envelope on girder flanges under OSOW/HL-93 truck combinations.

With the axial and bending moment diagrams under each load combination, Tables 5.3-1 and 5.3-2 were developed. The first one results from a model with a closed mid-joint and the second one with an initial 0.125 in. gap. Only results for the members with high stress are listed. The stringer numbers relate to the analytic model element numbering (diagrammed in the Appendix). The highest loaded stringer, element 19, is the 4th stringer in from the girder and between floor beams 2 & 3, the span adjacent to the midspan joint.

Table 5.3-1. Max. stress in principal members under OSOW + HL93 truck loading. No gap at mid joint.

0'' gap	Controlling Member	Max. Moment (kip-in)	Max. Axial (kip)	Min. Axial (kip)	Max Tension (ksi)	Max Compression (ksi)
HL-93	F.B. No. 3	12594	-12	-15	42	-43
	Stringer No. 19	826	0	0	23	-23
	Flange	0	423	-600	14	-20
Dual500-2	F.B. No. 2	6394	-18	-19	21	-22
	Stringer No. 21	422	0	0	12	-12
	Flange	0	521	-756	17	-25
Dual500-6	F.B. No. 2	6705	-18	-19	22	-23
	Stringer No. 19	324	0	0	9	-9
	Flange	0	382	-550	12	-18
Dual500-10	F.B. No. 2	5288	-18	-19	17	-19
	Stringer No. 20	306	0	0	8	-8
	Flange	0	382	-551	12	-18
Dual486-2	F.B. No. 3	4679	-13	-14	16	-16
	Stringer No. 21	412	0	0	11	-11
	Flange	0	347	-532	11	-17
Dual486-6	F.B. No. 3	4963	-13	-14	16	-17
	Stringer No. 19	318	0	0	9	-9
	Flange	0	263	-402	9	-13
Dual486-10	F.B. No. 3	3928	-13	-14	13	-14
	Stringer No. 20	310	0	0	8	-8
	Flange	0	263	-402	9	-13
Single312	F.B. No. 2	5123	-18	-19	17	-18
	Stringer No. 20	361	0	0	10	-10
	Flange	0	372	-530	12	-17
Single446	F.B. No. 2	5084	-18	-19	17	-18
	Stringer No. 20	397	0	0	11	-11
	Flange	0	361	-517	12	-17

Axial load in the stringers is negligible since there is no composite action in the floor beam-to-stringer connection. Stresses in the stringers did not control, i.e. have the highest value, for any load case.

Floor beams developed the maximum stresses identified in any member under the truck combinations and should be considered the critical bridge member. Different truck combinations generated maximum stresses in different floor beams. The values for maximum stresses shown above represent the maximum value found among all the floor beams under a specific load combination. For example, load combinations HL-93, Dual486-2, 486-6 and 486-10 induced maximum stresses in floor beam No. 3 (beam nearest midpan joint), whereas load combinations Single312, Single446, Dual500-2, 500-6 and 500-10 induced maximum stresses in floor beam No. 2.

The maximum stress seen in the floor beams among all the truck combinations was under the HL-93 load combination reaching a value of 43 ksi in compression, causing yielding. Dual500-6 and Dual500-2 followed with stresses close to 23 ksi, a 47% decrease with respect to the stresses under the HL-93 truck. Dual500-10, Dual486-6, Single312 & 446 all showed a percentage of smaller of around 60% compare to the HL-93. Finally, Dual486-10 is the truck combination that created the lowest stress among all the trucks on the floor beams, with a 69% decrease with respect to the HL-93 value.

Again, the maximum overall stress occurred in a floor beam under the HL-93 truck combination and was not affected by the gap at midspan. Load combinations HL-93, Dual486-2, 486-6 and 486-10 induced maximum stresses in floor beam No. 3. Load combinations Single312, Single446, Dual500-2, 500-6 and 500-10 create maximum stresses in floor beam No. 2.

The HL-93 load combination induced the largest stress reaching a value of 43 ksi in compression, again causing yielding. Dual500-6 and 500-2 loadings followed with stresses close to 23 ksi, a 48% decrease with respect to the stress under the HL-93 truck. Dual500-10, Dual486-6, Single312 and Single446 showed a percentage of decrease around 61%. Finally, Dual486-10 was the truck combination that created the lowest beam stress among all investigated load cases, with a 69% decrease with respect to the HL-93 value. As shown here, the percentage of differences in floor beam stress stays the same when we have a gap.

The maximum girder flange stress increased by 1 ksi with the open initial gap, to 26ksi with the Dual500-2 loading. And from 25ksi to 26ksi when a initially open gap existed at the midspan joint, versus a tight joint. The gap allows the loaded leaf to deform and resist a portion of the load before the gap closes. Once the gap closes the adjacent leaf starts to pick up load, but loaded leaf already is carrying an initial part of the load independently.

Stringer stresses remained low and the open gap had little effect. The stringer stresses remained at 12ksi or lower under any of the truck loads.

Table 5.3-2. Max. stress in principal members under OSOW + HL93 truck loading. Gap at mid joint of 0.125''.

1/8'' gap	Controlling Member	Max. Moment (kip-in)	Max. Axial (kip)	Min. Axial (kip)	Max Tension (ksi)	Max Compression (ksi)
HL-93	F.B. No. 3	12488	-11	-15	42	-43
	Stringer No. 19	820	0	0	22	-22
	Flange	0	602	-708	20	-23
Dual500-2	F.B. No. 2	6408	-18	-20	21	-22
	Stringer No. 21	412	0	0	11	-11
	Flange	0	600	-795	20	-26
Dual500-6	F.B. No. 2	6718	-18	-20	22	-23
	Stringer No. 19	318	0	0	9	-9
	Flange	0	436	-575	14	-19
Dual500-10	F.B. No. 2	5303	-18	-20	17	-19
	Stringer No. 20	300	0	0	8	-8
	Flange	0	437	-575	14	-19
Dual486-2	F.B. No. 3	4641	-12	-14	15	-16
	Stringer No. 21	406	0	0	11	-11
	Flange	0	437	-582	14	-19
Dual486-6	F.B. No. 3	4915	-12	-14	16	-17
	Stringer No. 19	315	0	0	9	-9
	Flange	0	327	-434	11	-14
Dual486-10	F.B. No. 3	3890	-12	-14	13	-14
	Stringer No. 20	306	0	0	8	-8
	Flange	0	326	-434	11	-14
Single312	F.B. No. 2	5149	-18	-20	17	-18
	Stringer No. 20	356	0	0	10	-10
	Flange	0	464	-581	15	-19
Single446	F.B. No. 2	5144	-18	-20	17	-18
	Stringer No. 20	391	0	0	11	-11
	Flange	0	464	-562	15	-18

Summary of Results for Closed and Open Mid Joint - Winneconne's 3D FEM

From results seen in Tables 5.3-1 and 5.3-2, maximum stresses occurred in the floor beams under the HL-93 truck combination, reaching values past yield of 43 ksi, regardless of whether there is

an initial midspan gap or not. The HL-93 truck presented the critical load case which could be attributed to the high load factor of 1.7 and the 33% of dynamic allowance used. OSOW loads had a lower load factor and did not include dynamic effects. Two lanes were loaded simultaneously with the HL-93 load. When OSOW trucks were crossing the bridge it was assumed that traffic would be controlled and only one vehicle would be on the bridge at that time. For all investigated OSOW load combinations, stresses in members stay below the yield point, at a maximum of 67% yield capacity. If the bridge is designed for HL-93 loading it will be safe for the OSOW loads examined here.

The maximum observed stress was relatively similar among all floor beams for a single given truck load. The maximum variation between beams was spotted under the HL-93 load with a difference in moment values of 25% between floor beams No.2 and 3.

Small stress differences on the order of 1-4% were spotted when there was an initial gap at the center joint versus a closed mid-joint. Moment values in stringers when there is an initial gap of 0.125 inches are slightly higher, 1ksi, than the results with no gap. This could be happening since when there is a gap the girders of one leaf seem to react in a more flexible manner because the girders of the adjacent leaf are not initially helping resist load. The stringers act as if they are relatively stiffer elements, compared to the initially loaded girders, and pick up a bit more of the cantilever moment created by the truck loading. However, the percentage of increase in moment ranges between 1 and 2% suggesting that a small gap at the mid-joint doesn't vary the stringer results in a significant way and can be ignored.

Similarly, the same effect is seen in the axial force developed in the girder flanges. The maximum axial force and stress in the flanges are found when there is an initial gap in the center lock. The girders of one leaf have to carry the all the load as the truck starts to cross the bridge before loads starts being shared by the other leaf. The increase in girder flanges stress with a gap is only 4% and again might be ignored.

In the case of the floor beams, however, there is no trend when comparing results with gap and no gap at the center lock. Under four of the trucks the no-gap condition resulted in higher beam moments, in the other five cases the model with gap had higher moments. The difference in maximum moment with respect to the values with no gap at the mid-joint connection just ranged between -4% to 2% representing a small variation that again can be ignored.

6. CAMERON AVENUE BRIDGE

6.1 Cameron Avenue: Introduction and Structural Components

The Cameron Ave arch bridge (B-32-202), built in 2004, is one of the two long span bridges over the Mississippi River in the city of La Crosse, Wisconsin. Combined, the Cameron arch and the Cass St truss provide for easterly traffic and westerly traffic respectively across the river. The Cameron Avenue bridge is an x-braced steel tied-arch bridge with vertical double hangers. The tied-arch bridge has two arches, one on each side of the roadway, acting together with tie girders rigidly connected to each arch rib at the bottoms. The tie resists horizontal thrust from the arches and partially supports the deck system. The superstructure system is composed of a partial composite concrete deck over longitudinal stringers which in turn are supported by transverse floor beams that connect into the main girders. Vertical hangers, connecting the arch ribs and the tie girders, were placed at every other floor beam to aid in resisting vertical loading. The total span of the arch bridge is 475 ft. with six longitudinal stringers, twenty-one transverse floor beams along with the two main tie girders. The width between arch ribs is 50 ft. and consists of two vehicle lanes of 15 ft. and 18 ft. respectively and an 8 ft. wide sidewalk on the south side (Figure 6.1-2).

Figure 6.1-1. Cameron Ave Bridge

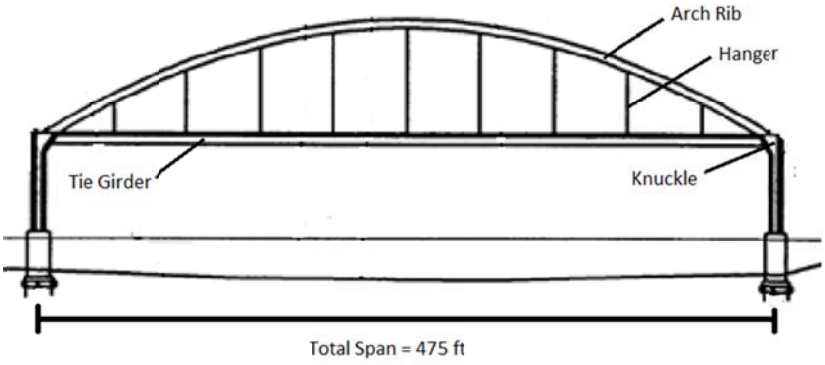

(a)

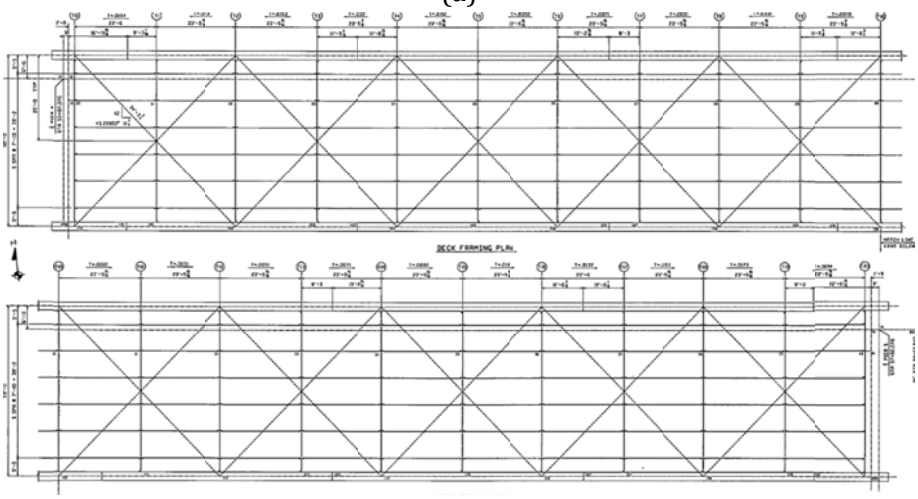

(b)

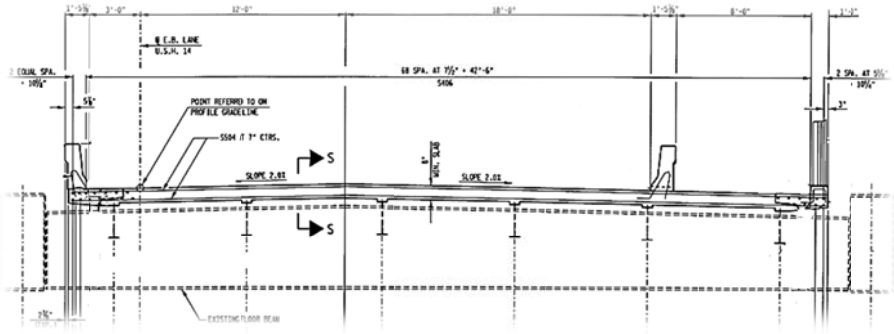

(c)

Figure 6.1-2. Plans of La Crosse Bridge structural components (a) Elevation view (b) Framing Plan (Upper is west half span, lower east half span) (c) Cross Section

Structural Components

Dimensions of the main members, shown in Table , were used for initial analysis purposes. All steel members are Fy = 50 ksi, except the rib bracings and the hangers, which are 46 ksi.

Table 6.1-1. Main Component dimensions

Member Name	Type	Dimension
Tie1	Main bolted box section with angles	69×30×1.5×0.75 (depth × width × flange thickness × web thickness)
Tie2	Heavier equivalent tie girder section used at the tie/arch knuckle	69×30×1.5×1.375 (depth × width × flange thickness × web thickness)
Arch1	Main arch rib welded box section	69×31.2×1.375×1.375 (depth × width × flange thickness × web thickness)
Floor beams	Simple span I-beam from cl to cl of tie girders	Cross section depth varies from 4.58ft to 5.2ft (Details see Fig. 6.1-3)
Stringers	Simple spans framed into the floor beams	W 24×55
Arch bracing	X pattern using structural tubing	TS 20×12×1/2
Lower Lateral	X pattern connecting at the hanger locations	W 12×58
Hangers	A set of bridge strands at each hanger location	Diameter 2-3/8in.

The tie girders consist of box sections with internal stiffener diaphragms (see Figure 6.1-3a) every 22.5 ft. These box sections are composed of webs and flange plates bolted together using angles. Spreadsheets were used to compute properties of equivalent HSS sections. In Table , Tie 1 is the tie section used for most of the length while Tie 2 is a section with heavier webs that represents the arch/tie knuckle joint. Bending stiffness of the tie girder is very important in a system such as the one used on this bridge, where only every other floor beam has a hanger, to distribute superstructure live loads evenly to the arch.

The arches, unlike the tie girders, are welded box sections. While the arches would preferably resist primarily axial compressive force, bending is also of concern particularly when the bridge is loaded with asymmetric concentrated loading. The arch shape is efficient for uniform loading, but asymmetric loading will introduce uneven tension forces in different hanger locations and create bending in the arch. X pattern rib bracing between the arches provides buckling stability to the arches when under compressive force.

Two bridge strands of 2-3/8in. diameter each are used to form a tension hanger set that suspends the tie girders from the arches at each tie location (Figure 6.1-3a). The two strands are spaced 16 inches apart and parallel to the bridge span, providing a total hanger area of 6.76 square inches. Each set of strands are held firmly into two grooved open strand sockets, which are rigidly bolted into the

diaphragms of both the arch and girder section via thick gusset plates. Seals are clamped to each strand outside the openings where the strands extend into the flanges of the box sections.

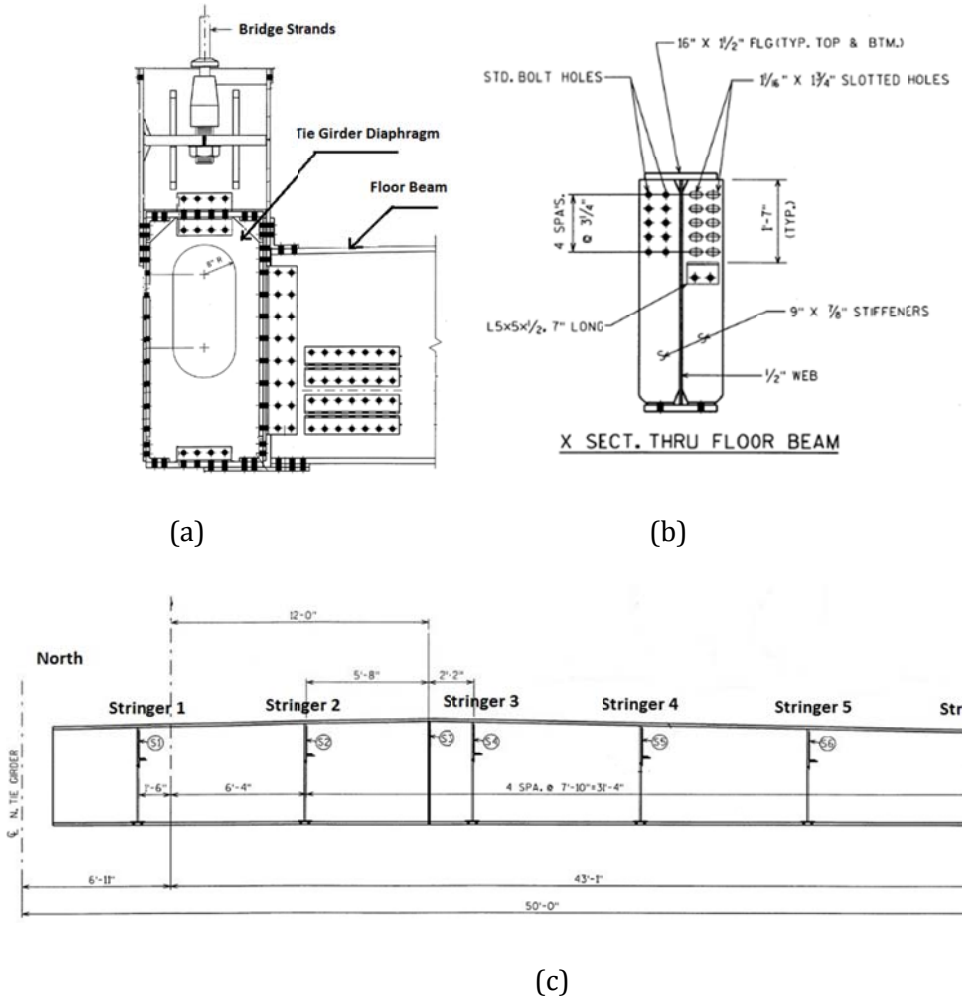

Figure 6.1-3. Non-prismatic floor beam configurations and connection details: (a)Floor beam and girder connection (elevation view) (b) Cross section through floor beam (c) Floor beam elevation.

Floor beams are non-prismatic I-beams with uniform web thickness and flange dimension but varied web depth across the width of the bridge to provide crown in the roadway surface. Both the web and flanges are bolted into the tie girder with angle plates as shown in Figure 6.1-3a&b.

Height considerations led to placement of the stringers with their top flanges at the height of the floor beam flanges. Rather than being supported on the floor beams, the stringers frame into the beams. Therefore the top flange was coped and the bottom flange was cut on one side to allow the stringer to be bolted into the stiffener of the floor beam as detailed in Figure 6.1-4. Deck shear

connectors are spaced on the stringer top flange at 6in. apart near the ends and increase to 8in. apart towards the center to provide composite action with the concrete deck.

The concrete deck is cast-in-place with uniform depth of 8 in. with reinforcing steel interspersed transversely and longitudinally through the slab. The total width of the deck is 44ft. and consists of a 33ft. roadway and an 8ft. wide sidewalk only on the southern side. The deck is haunched above the stringers and the floor beams about 1.25 in. and 5.875 in. respectively. As mentioned before, with shear connections (studs) provided, full composite action could be achieved between the stringer and the deck. Studs were not provided between the deck and floor beam, although haunches below the deck rested on the floor beams.

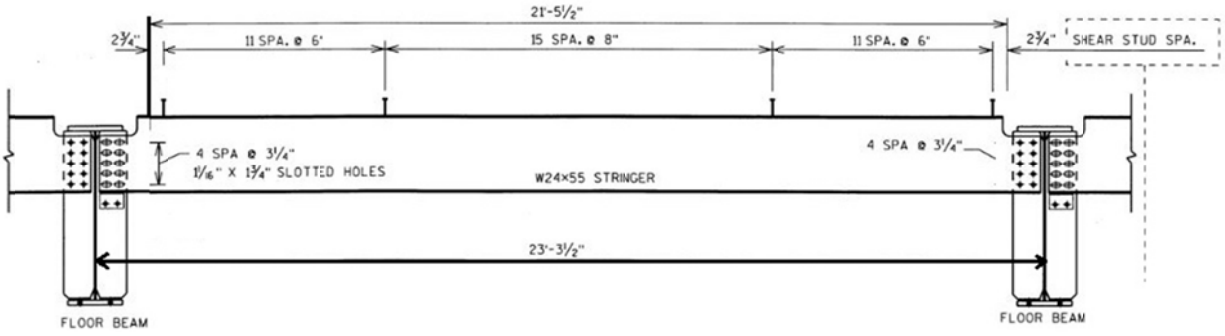

(a) Stringer dimension and shear connection (studs) spacing (elevation view)

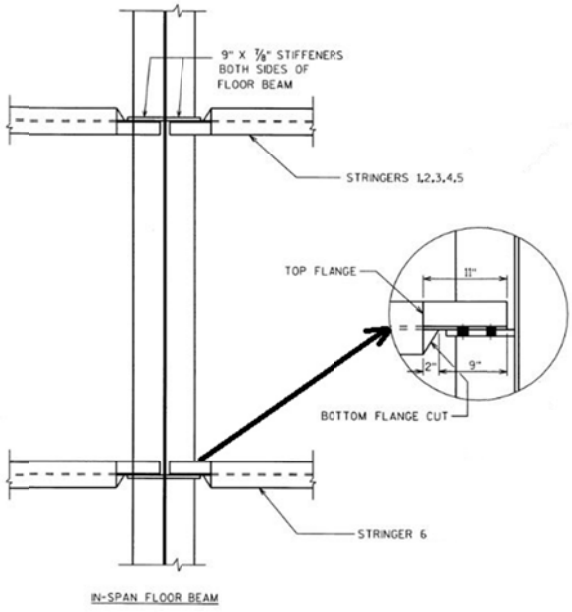

(b) Stringer and floor beam connection (plan view)

Figure 6.1-4. Stringer shear studs and floor beam connection details

6.2 Cameron Avenue: Field Load Testing

Three large-scale tied arch bridges were selected for examination as part of this study. Of those three, only the Cameron Ave bridge was chosen for field testing due to the critical rerouting-importance of this bridge location, i.e. over the Mississippi river. Field test results are intended to provide a basis for checking the accuracy of predicted internal component forces from initial software analyses.

Selection of Test Location

Although maximum axial force in the arch is generated when the whole span is loaded, maximum bending in the arch and tie girders occurs with just part of the span is loaded, i.e., asymmetric loading cases. Before the field load test was conducted, possible locations of truck load placement for maximum strain effects in certain bridge elements were analyzed using an initial analytic model. The preliminary analyses predicted that the second set of hangers, from the arch end, would experience the maximum strain. This strain would occur with stationary truck wheel loading right above the floor beam that connects to the tie girder at that hanger location. Using that position of truck loading, strains were measured in the floor beam, the hangers and the tie girder section near the hanger/floor beam location. Accurately measuring very low levels of strain in structural members is difficult in the field, so members that would likely have the largest strain values would be the best targets for instrumentation to measure strain. The following locations were instrumented (Figure 6.2-1):

- the second pair of hangers (H2) from the west end on the south side of the bridge,
- web of the fifth floor beam (FB5) from the west end that connects into the same girder location as the hanger H2,
- web of the two tie girder sections (T3 and T4) that were just west of the H2 hanger location.

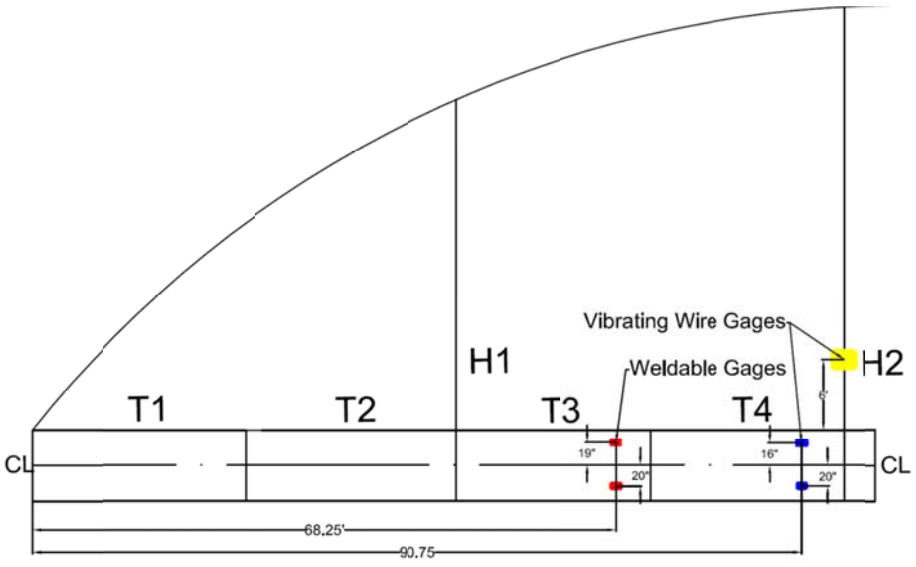

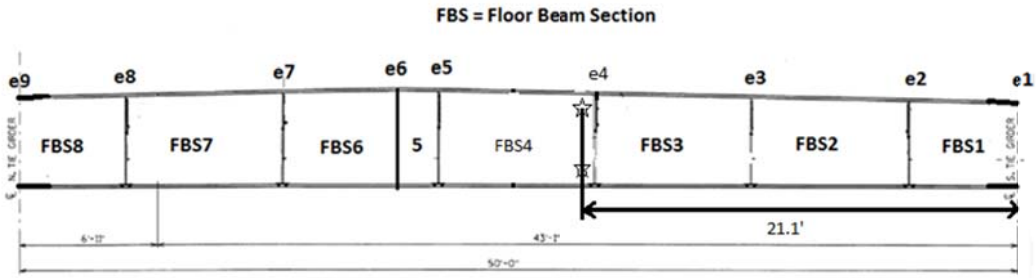

Figure 6.2-1. Instrumentation locations: (a) elevation view (South) with gage locations on H2 and T3, T4 tie girder sections (b) gage locations on No.5 floor beam (South is to the right).

Loading Regime

Two dump trucks of known weight and dimensions, along with the UB-60 snooper truck for bridge inspection, were used to impose stationary live loading. Each truck was weighed (front and back axles separately) before arriving at the bridge for testing.

The load regime was designed to achieve a high strain in the instrumented second set of hangers. First two dump trucks heading east were parked side by side and as close as possible to the south edge of the deck (wheels adjacent to the barrier) with the center of their back two axles right above the 5th floor beam (which connects to the instrumented second hanger set). Then the snooper truck drove backwards along the south edge (cab headed west) and parked with its rear bumper as close as possible to the dump truck adjacent to the barrier as shown in Figure 6.2-2a. The distances from the outer wheels to the barrier foot and that between each wheel were measured when the trucks were in position. Locations of each wheel load relative to the tie girder center were calculated to use later in analytic modeling. Truck locations are shown in Figure 6.2-2b.

(a)

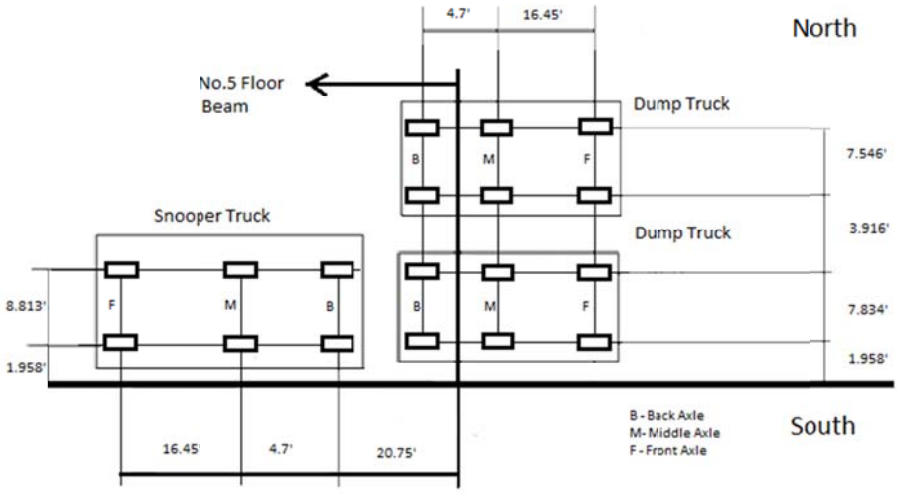

(b)

Figure 6.2-2. Instrumentation locations (a) trucks (South is to the right), (b) plan view location of trucks relative to south girder (bold line represents the center line of the south girder.

Gage Installation

Two Geokon 4000 vibrating wire (VW) gages with 6-in gage length, two Geokon 4100 weldable VW gages with a 1.75-in gage length, and four 0.25-in long weldable foil strain gages were used to measure the strain change during the load test.

Two foil gages were applied on the web of the fifth floor beam from the west end using a snooper truck at the location shown in Figure 6.2-3a. The beam gages were applied on the web, 20 inches up and down respectively from the center of the beam, oriented parallel to the length of the beam in order to measure axial and bending strains. After the location was sanded with electric grinders to remove paint, the metal was further cleaned by hand with sandpaper and alcohol. The gage then was spot welded on the cleaned patches directly using a Sunstone Pulse Tack Welder and finished with an anti-corrosion spray coating.

Two short VW gages and two foil gages were applied on the tie girder at locations shown in Figure 6.2-1 using a similar procedure. Though the gages were intended to be 20in. from the girder center, the actual positions were slightly varied as shown in Figure 6.2-1. Figure 6.2-3b shows a foil gage on the girder web and 6.2-3c&d show the VW gage application.

(a)

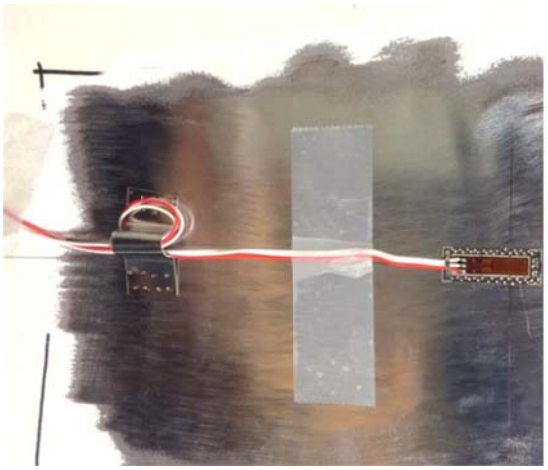

(b)

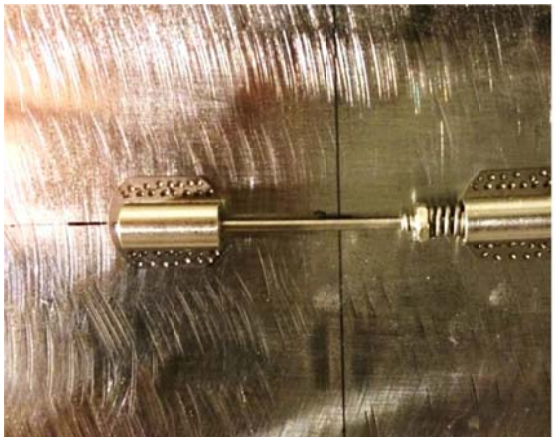

(c)

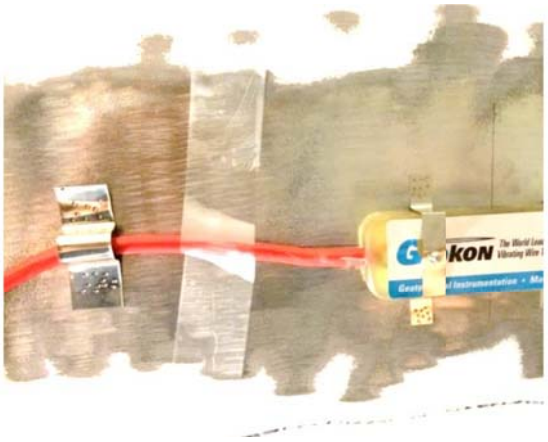

(d)

Figure 6.2-3. Gage installation - a) applying gages on the 5th floor beam with a snooper truck, b) weldable foil gage used on box girder web, c) VW gage welded on box girder web, and d) VW gage with cover and lead wire.

The Geokon 4000 VW strain gages and vibrating coils with wire leads were mounted using friction clamps on the two hangers as visible in Figure 6.2-4. Both gages were at approximately 6ft. from deck level to avoid local stress concentration near the hanger end connections.

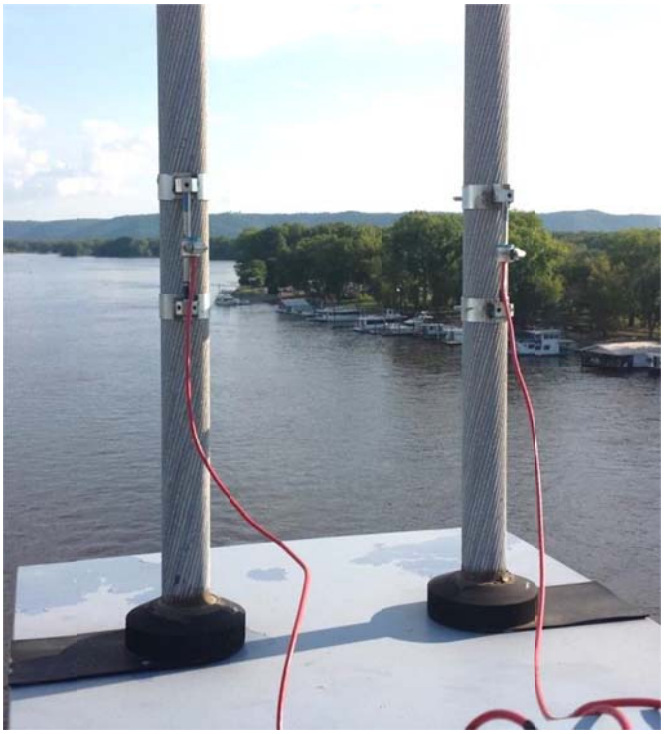

Figure 6.2-4. VW strain gages with vibrating coils on bridge hangers.

Data Collection Scheme and Results

To start the test, the City of La Crosse police blocked traffic to eliminate vehicles passing over the bridge. An initial reading of all the gages was taken with no vehicles on the bridge. Then the trucks were driven into their positions, the strains under stationary truck loading were collected. While taking the readings, the exact truck axle locations on the deck edge and relative to each other were recorded in order to repeat the same loading in the analytical model later. Finally after all the trucks were driven off the bridge, another reading was taken to see if any drift developed in the gage readings.

After the data was collected, the initial gage readings were subtracted from the readings with the trucks present. The resulting values, the strains created by the trucks, are listed in Table 6.2-1. Unfortunately the VW gages in the tie girder malfunctioned but the nearby foil gages provided good results.

Inspecting the two girder strains and the floor beam strains it is clear that there the top strain, a compression, is smaller in value than the bottom strain, a tension. That condition would be expected in the tie girder since it resists the horizontal thrust from the arch and should be carrying an axial tension force. It doesn't seem reasonable for the floor beam – which should not be carrying axial tension. The two floor beam strains can be used to define a neutral axis. With the high tension strain at the bottom

the neutral axis is above the steel beam centroid. The neutral axis would move upward if the floor beam combined with the deck and became a composite section.

Table 6.2-1. Micro-strain results from the field test.
(positive = tension, negative = compression)

Gage label/location	Field Result (micro-strain)
Hanger No.2	148.85
Girder T4 section – 19" above the center	-40.5
Girder T4 section – 20" below the center	90.5
Floor beam FB5 – 20" above the center	-59.5
Floor beam FB5– 20" below the center	106.5

6.3 Cameron Avenue: Development of Three Dimensional Finite Element Model.

An initial three-dimensional finite-element-model (3D FEM) was created using the original bridge design plans. This model was loaded to identify critical high stressed members and to select locations on the bridge where high strains were expected, locations to place test gages.

After the field tests were completed the identical truck loads were placed on the analytical model to evaluate the quality of the model's predictions by comparison with the measured strains. When deviations were found between the predicted and measured data, the analytical model was examined and assumptions compared with knowledge from visual inspection of the bridge to identify possible errors in modelling. Variations in the element type and size, boundary conditions, and connections were found to be influential in changing the accuracy of the model.

Some of the initial assumptions that were made in building the analytical model were reviewed. The model was slightly adjusted when possible errors were detected. Oversize-overload (OSOW) loads, simulating known OSOW vehicles, are then applied to the analytic model to evaluate the bridge performance with a goal of providing improved methods for WisDOT to employ in issuing load permits. All 3D FEM linear elastic simulation models of the bridge were created using the commercial CSiBridge analysis software.

Initial Model Development

Using the design plans from the WisDOT HSI (Highway Structures Information System), an initial model was prepared as illustrated in Figure 6.3-1.

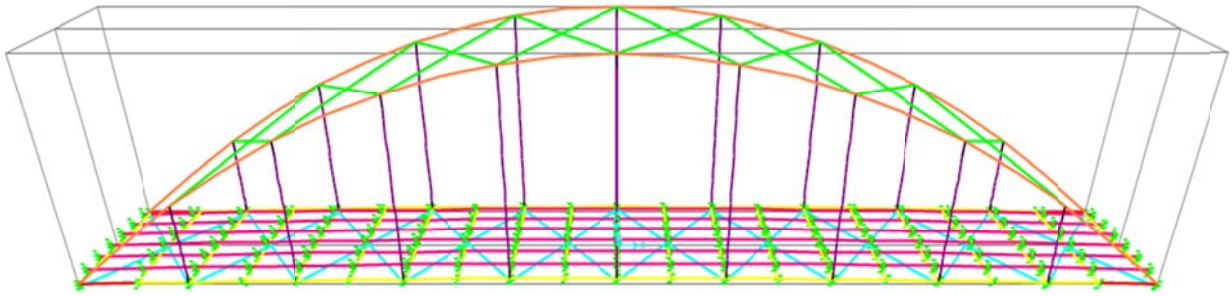

Figure 6.3-1. 3D FEM model of Cameron Ave Bridge

As suggested by Chung et al. (2005), when modeling beam sections using a single frame element defined with the exact shape can provide prediction of the same accuracy but with much less analytical calculation compared to modelling it with different shell elements for the web and flanges respectively. Therefore, the tied girder and arch were modelled with frame elements that had the properties of a box cross-section with the same stiffnesses as the complex ones on the bridge. This use of a simulated box section allowed correct modelling of the tie girder with inner diaphragms and corner angles. In the previous Table 6.1-1, Tie 1 represents the tie girder sections (divided length wise into 23.5 ft. each) that are used for most of the length of the girder. Tie 2 is a section (25.25 ft in length) with heavier webs representing the tie girder where it joins with the bottom of the arch. The girder is assumed to have a rigid connection with the arch. The bridge has a vertical curve and the varying elevation of each tie girder start and end nodes were calculated using spreadsheets to model the actual profile.

Similarly, the non-prismatic floor beams are I-shaped sections with varying depth. The model's floor beams are broken into three segments – each having a uniform cross section equal to the average of the bridge's varying section in that segment. The actual linear variation of the section is listed in Table 6.3-1, the section depth linearly increases from 4.52ft. to 4.82ft. along E1 through E4 and then linearly decreases to 4.58ft. at E9. At the ends of the floor beams, rigid connections that transfer force in all directions of translation and rotations into the tie girder were assumed for the model because both the web and the flanges of the floor beam are bolted (Figure 6.1-3a&b) to the tie girders, allowing moment transfer.

It was assumed that composite action developed between the floor beams and the deck even though shear connectors were not employed. The deck is haunched down to the top of the floor beam

so there is likely shear capacity existing due to bond and friction. This might best be considered as partially composite action. A fully composite action was assumed in the initial model.

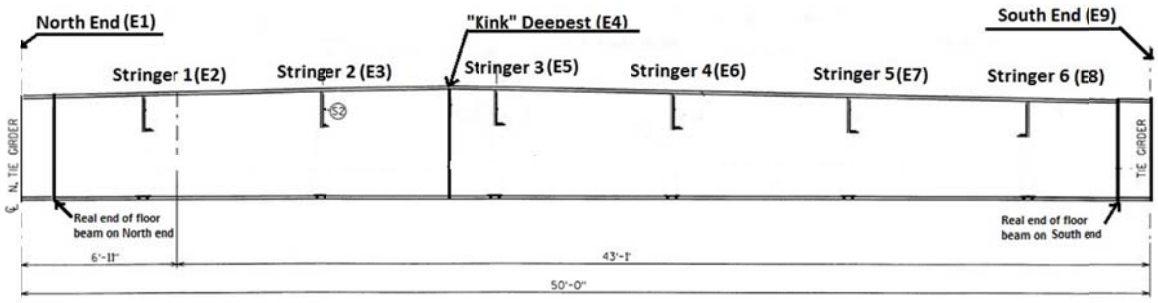

Figure 6.3-2. Floor beam frame element definition (Elevation view)

As shown in Figures 6.1-4 and 6.3-3, six longitudinal discontinuous stringers frame into the floor beams. While the normal interval between stringers is 84in., Stringer 1 and Stringer 6 are 65in. away from the centerline of the north and south tie girders, respectively. The lower flanges of the stringers are just sitting on an angle which is bolted to a floor beam web stiffener. This implies that the moments in the stringers are not transferred into the floor beams because there is no bottom flange or top flange connection (Figure6.1-4). In terms of the initial model, the connections between the stringers and the floor beams are modeled as hinged connections transferring no bending moment into the floor beams.

For simplicity only one cable is used in the model to represent a set of two hangers. The model cable element has a diameter of 2.933in. to provide an identical total cross section area as the sum of the two original bridge strands, 6.76 square inches. Anchorage connections between the hanger to the arch and hanger to tie girder are interpreted as straight rigid elements in the model.

The concrete deck has a uniform 8-in. depth. Haunches are provided above the stringers and floor beams. The slab and the stringers were considered as fully composite with the presence of shear connections on the top flange of the stringer spaced at 6in. near the ends and 8in. in between as detailed in Figure 6.3-3.

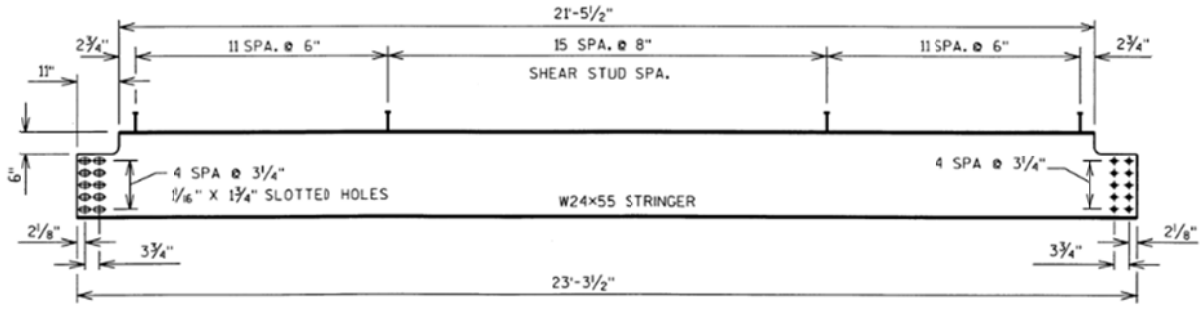

(a) Shear connection (studs) spacing on the stringers

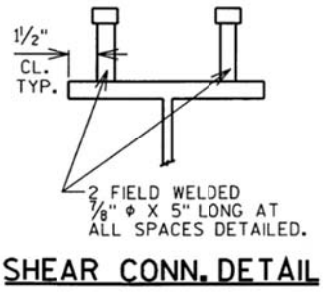

(b) Shear connection details

Figure 6.3-3. Shear connection provided on the stringers.

Different slab-beam system modeling techniques were reviewed in order to select an accurate and economical method for this bridge. As suggested by Chung et al. (2005) the eccentric beam modeling method essentially utilizes straight frame elements with the geometric properties of the beam sections and places shell elements at the centroid of the concrete slab. Then, vertical rigid link elements are inserted between the beam centroid and deck to ensure composite action. While this method is rather simple, it is proven to be accurate when predicting deflection, strain, and flexural behavior of the slab-beam interaction. The beam must be separated into short segments with links at the ends of each segment. In this model the stringer links to the deck were initially placed at 84in. intervals

Shell elements are widely used to idealize the bridge deck since behavior of this structural component is governed by flexure. More specifically, a thick shell element (Mindlin type) is generally recommended for an accurate analysis (compared to thin shell element a.k.a. Kirchoff type) because it accounts for transverse shear deformation, though this may not be significant in a bridge application. However, Mindlin shells are susceptible to "shear lock" which is caused by large aspect ratios. Therefore each shell element is further divided into approximately 1ft by 1ft sections. Then the stringers below were divided accordingly, changed from the initial 84in. sections, to create nodes that connect with shell element corners with straight vertical links. Given that studs are 6-in apart near the ends of the stringers and 8-in apart elsewhere, a fully-composite action is assumed in the initial model. A 28in. spaced connection between the shell elements and the stringers was used to assure the fully composite action. Details of the finite element modelling are summarized in Table 6.3-1.

Table 6.3-1. Details of model finite element modelling.

Element Name	ASTM Material	Element type	Cross-section Dimension (inches)	Segment length	Number of elements used
Tie1	A709 HPS50W	Box/Tube Section	69×30×1.5×0.75 depth × width × thickness flange × web	23.5ft	18 in one girder
Tie2	A709 HPS50W	Box/Tube Section	69×30×1.5×1.375	25.25ft	2 in one girder

Arch	A709 HPS50W	Box/Tube Section	69×31.2×1.375×1.375	Projected horizontal distance same as each girder sections	20 in one arch
Floor Beams	A709 HPS50W	I/Wide Flange Section	16×1.5×0.5 flange width × thickness × web thickness various section depths	North end to "kink": 23.1ft Depth: 4.82ft to 5.2ft "Kink" to South end: 31.1ft Depth: 5.2ft to 4.58ft	1 each floor beam
Stringers	A709 HPS50W	I/Wide Flange Section	W 24×55	23.5ft	6 longitudinally partitioned into 20 separated segments by the floor beams
Rib Bracing	500 Grade B (46 ksi)	Box/Tube Section	TS 20×12×1/2	Approx. 68.6ft	16 used to brace the two arches
Lower Lateral	A709 Grade HPS50W	I/Wide Flange Section	W 12×58	Approx. 68.6ft	20 used to brace the two ties and resist wind loads
Hangers	586 Class C (100 ksi)	Cable Section	Diameter 3.588 in Equivalent to dual strands	Between the hanger connections	9 between tie and arch on same side
Hanger Connections	A709 Grade HPS50W	Custom general section	High moment and shear resistance	5ft down from arch center and 3.5ft up from tie center	2 for each hanger
Concrete Slab	$f'_c = 4000$ psi	Thick shell	8in thick	23.5ft × 7ft 10in (length × width)	Total width 44ft × 475ft

In the analytic model, the connections between different elements and element types are where oversimplified assumptions could be made and therefore induce modeling errors that could accumulate and affect the overall accuracy of the model significantly. Link elements are used in joints and different degrees of freedom are defined according to the real connection cases. Hinged joints only transfer translations in x-, y- and z- translations whereas the rigid joints transfer both translations and rotations in three directions between the connected elements. The locations of each joint type in this bridge are shown in Table 6.3-2.

Table 6.3-2. Joint modeling details

Joint Location	Joint Type
Stringer to floor beam	Hinged joint
Floor beam to tie girder	Rigid joint
Tie girder to arch	Rigid joint
Hanger to Tie girder	Hinged joint

Appropriate idealizations and simplifications based on engineering judgement were done when developing the initial finite element model. Assumptions were made regarding the connections and support condition. Stringers are assumed as pinned-pinned connections at the ends to the floor beams, which in turn are rigidly connected with the girders box sections. Splices between girder sections are ignored. Link elements that only have freedom in vertical and horizontal directions, but are rigid in those directions, were used to model the interaction between the concrete deck and the stringers it sat on. Knuckle sections at the arch and girder joint are not modeled with exact details but by simply joining them with with a rigid connection. Boundary conditions of the superstructure were idealized as simple roller and pin supports, such that all translations were constrained at one end while only vertical and transverse translations were constrained at the other end.

Truck loadings on the model simulated the condition shown previously in Figure 6.2-2. The loads from the two dump trucks and the UB-60 snooper, as applied on the FEM model, are listed in Table 6.3-3. The x-y axes origin in the model was taken at the middle of the entire bridge, with x and y in the plan of the bridge. The truck wheel loads were applied as point loads. The total load on the bridge was 210.2 kips (thousands of lbs.).

Comparison with Field Measurements

Field strain results collected while all three trucks (two dump trucks and the snooper truck) were on the bridge are compared with strain predictions from the initial analytic model under the same loading in Table 6.3-4 with wheel effects applied as point loads at each wheel location in Table 6.3-3.

Table 6.3-3. Truck wheel loads and coordinate input for the model.
("DT" refers to dump truck, truck "A" is close to barrier, UB-60 is the snooper, N and S refer to north or south wheel line [south is near barrier], F-M-R refer to front – middle – or rear axle.)

	Wheel	Location-X (in)	Location-Y (in)	Load (kips)
DT-A	F-N	1464	-47	11.6
	F-S	1464	-129.25	11.6
	M-N	1662	-47	12.02
	M-S	1662	-129.25	12.02
	R-N	1722	-47	12.02
	R-S	1722	-129.25	12.02
DT-B	F-N	1464	105.75	12.5
	F-S	1464	23.5	12.5
	M-N	1662	105.75	11.455
	M-S	1662	23.5	11.455
	R-N	1722	105.75	11.455
	R-S	1722	23.5	11.455
UB-60	F-S	2190	-129.25	9.15
	F-N	2190	-35.25	9.15
	M-S	1992	-129.25	12.43
	M-N	1992	-35.25	12.43
	R-S	1938	-129.25	12.43
	R-N	1938	-35.25	12.43

Table 6.3-4. Micro-strain result comparison between the field test and the initial FEM

Gage label	Field Result (micro-strain)	Initial Model Result (micro-strain)
Hanger No.2	149	135
Girder T4 section – 19" above the center	-41	-43
Girder T4 section – 20" below the center	91	73
Floor beam FB5 – 20" above the center	-59	-43
Floor beam FB5– 20" below the center	106	115

Adjustment to the Model Based on Closer Examination of Design Details

Though the strains compared in Table 6.3-4 showed that the model was working quite well, improvement might be obtained. In construction of the initial model the floor beams were assumed to be composite with the deck, even though no connectors were specifically provided between the floor beam and deck. The concrete bond and possible friction forces were thought to be sufficient to create composite action.

Figure 6.3-4 shows the strain diagrams consistent with the measured floor beam and girder strains, if the strain variation was linear. The initial analytic model gives slightly higher tension at the beam center of gravity than shown by the field measurement. The neutral axis with the model strains is also higher than the neutral axis with the measured strains. Both of these observations are consistent with a model cross section that has composite action – since adding the deck to the beam would bring the neutral axis higher and increase tension strains in the beam. The measured strains indicate that less composite action is actually occurring in the floor beams. From the neutral axis location for the measured data, however, some composite action is obviously present since the neutral axis is not at the centroid of the beam (and no axial force would be expected in the floor beams).

A modification of the initial model was performed to create partially composite behavior between the concrete deck and the floor beam. It is possible near midspan of the beam, where vertical and horizontal shear values are lower, that the beam does develop composite action from concrete bond or friction. At the beam ends the higher shear forces may break the bond, allowing slip, and eliminating composite action.

Each floor beam element was initially modeled with 9 nodes, E1 through E9 as shown in Figure 6.3-2. A revised model then released the composite action at both ends of the beam, allowing relative transverse displacement between the deck and beam. The result of this modification is also shown in Figure 6.3-4 with the strain diagram labelled “Modified”. The model simulation of beam strains was improved, particularly at the beam bottom. Unfortunately this type of modification can only be achieved if the actual strain condition in the beam is known. A logical approach to the beam modelling would normally assume no composite action since there were no studs. With no composite action in the model, the strain diagram for the beam passed through the beam centroid. The actual measured tension strain at the center of gravity, clear in the Figure, obviously indicated that a non-composite modelling assumption did not simulate the actual bridge condition.

Looking further at the field measurement results In Figure 6.3-4, one could observe that in the tie girder section the strain at the girder center of gravity is not zero, due to the tension force in the member created by the arch thrust. The predicted strains from the initial model are smaller than the field result. This indicates that modeled girder section should be resisting more axial tension force. No

modifications were made to the analytic model to improve girder behavior because there was no member or geometric indication that the initial modelling was in error.

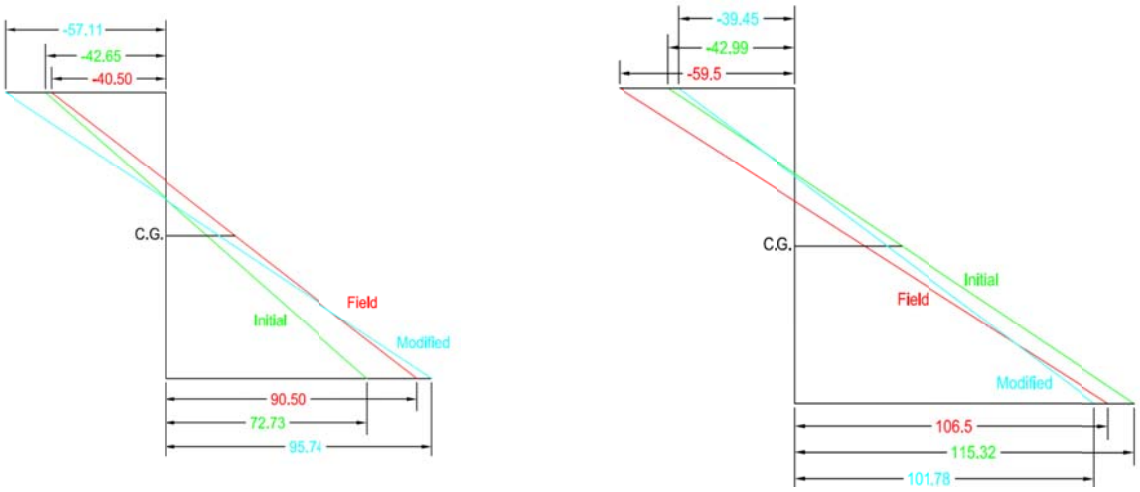

Figure 6.3-4. Linear strain diagrams: left = linear strain diagram over the depth of the tie girder, and right = linear strain diagram over the depth of the floor beam.

The Cameron Avenue analytic model is considered to be successful in simulating the actual bridge test load effects. Table 6.3-5 shows that the error in predicted hanger strains is negligible. The error in predicted floor beam strain is 20με near the beam top, equivalent to 600psi in stress. Tie girder strain is 16με in error, or 480psi. The adjusted model will be used in predicting the bridge response under OSOW vehicle loads.

Table 6.3-5. Comparison of final strains from test load.

Gage label	Field Result (micro-strain)	Adjusted Model Result (micro-strain)
Hanger No.2	149	150
Girder T4 section – 19” above the center	-41.	-57
Girder T4 section – 20” below the center	91	96
Floor beam FB5 – 20” above the center	-59	--39
Floor beam FB5– 20” below the center	106	102

6.4 Cameron Avenue: Impact of OSOW Vehicles.

Three types of vehicular loads, i.e. AASHTO the standard HL-93 notional truck loading and two types of OSOW vehicles, as described in Chapter 2, were employed in the OSOW bridge response analyses.

The total road width of the Cameron Ave bridge between parapet walls is 33ft. and consists of two lanes of 16.5ft. each. Based on their dimensions relative to the lane, two single-trailers and double trailers with 2ft. and 6ft. spacing at the center are driven along the center of each lane in this bridge (because of the asymmetry of the floor beams) and the double trailers with 10ft. between are driven along the middle of the bridge to generate the practical worst case scenario. An LRFD load factor of 1.75 is applied to the HL-93 truck; the multi-presence and dynamic factors were included. Under the OSOW trucks a single lane was loaded, the LRFD 1.35 load factor is applied and no dynamic effects were included. Notation for the trucks loads is the same as used in the previous bridge analyses and may be summarized as:

- ***Single312*** represents the 312 kips gross weight single trailer,
- ***Single446*** represents the 446 kips gross weight single trailer,
- ***Dual486*** represents the 486-kip gross weight dual trailer,
- ***Dual500*** represents the 500-kip gross weight dual trailer.

Peak forces and stresses induced in critical members, as predicted by the Cameron Ave analytic model, by the series of OSOW vehicles are listed in Table 6.4-1. Table 6.4-2 lists forces in individual components with the loading that caused the force. The forces shown for beams and stringers include the bending moment in the beam alone and added axial force from composite action. Since members have both axial and bending, and peak values of those forces occur at different locations, two values of peak stress are calculated for each: based on peak moment or on peak axial. All of the values shown are 2015 AASHTO LRFD Strength 1 or 2 factored results.

Table 6.4-1. Max stress results in each structural group under factored Dead+HL-93 loading.
*(moments are ft*k, forces are kip, stress is ksi, compression is negative)*

Girder	Max Moment 6447	Axial Force 1901	Stress (ksi) 29.3
	Max Axial Force 2518	Moment @same location 706	Stress 15.4
Arch	Max Moment 6449	Axial Force -2339	Stress -24.9
	Max Axial Force -3083	Moment @same location 1667	Stress -15.7
Floor Beam	Max Moment 2148	Axial Force 119	Stress 18.1
	Max Axial Force 547	Moment @same location 912	Stress 14.9
Stringer	Max Moment 171	Axial Force 300.8	Stress 36.3
	Max Axial Force 484	Moment @same location 51.6	Stress 35.1
Hanger	Max Axial Tension 348		Stress 39.2

Table 6.4-2. Maximum member stresses from factored Dead+OSOW truck loads.
*(moments are ft*k, forces are kip, stress is ksi, compression is negative)*

Girder	Max Moment 7030	Axial Force 2034	Stress 31.8	Load Case: Dual500-2
	Max Axial Force 2408	Moment @same location 540	Stress 14.4	Dual500-2
Arch	Max Moment 7104	Axial Force -2551	Stress -27.4	Dual500-2
	Max Axial Force -2925	Moment @same location 1427	Stress -14.5	Dual500-2
Floor Beam	Max Moment 1903	Axial Force 97	Stress 16.9	Dual500-2
	Max Axial Force 553	Moment @same location 929	Stress 15.1	Dual500-2
Stringer	Max Moment 154	Axial Force 298	Stress 34.4	Dual500-2
	Max Axial Force 472	Moment @same location 50	Stress 34.2	Dual500-2
Hanger	Max Axial Tension 364		Stress 41.0	Dual500-2

The highest predicted stress under OSOW loading, listed in Table 6.4-2, occurs in the bridge's hanger cable at midspan with a peak of 41ksi in tension, well below the minimum specified yield stress. Amongst the flexural members the highest stress, 34.2ksi, occurs in the north side stringer 4ft from the east end of the bridge. The tie girder develops a stress of 31.8ksi in the north girder at 176ft east of the bridge center. The arch itself developed a compression stress of 27.4ksi in a section just east of the second from the east end. All of the maximum stresses occurred under the 500kip dual lane OSOW truck with trailers spaced at 2ft.

The HL-93 truck max stresses in the stringer and floor were higher than the stress created by any of the OSOW vehicles by 5%and 24% respectively. In the arch, tie girder and hanger the HL93 stresses were 4% to 9% lower than OSOW stresses. The single trailer OSOW vehicles did not impact the bridge members as much as the HL-93 or Dual500 trucks.

7. Chippewa River Memorial Bridge

7.1 Chippewa: Introduction and Structural Components

The Chippewa River Memorial Bridge (B-09-087) was built in 1971 spanning 485ft. over the Chippewa River at Cornell, Wisconsin. The structural type is an arch truss bridge, as shown in Figure 7.1-1, with inclined structural tubing as diagonals between the arch and tie girder. Plans for a reconstruction in 2006 showed the 50.5ft. wide concrete deck was temporarily re-configured with a 3ft. walkway on the north side separated from a 14ft. westbound lane by a 2ft. barrier wall. A second 2ft. barrier wall separated the 16ft. eastbound lane from the original 4ft. sidewalk on the south. The two lanes were separated by additional barriers near the center of the deck with a 3ft gap between as laid out in Figure 7.1-2c. After repairs the deck had a new concrete overlay and was returned to the original layout with a 4ft. sidewalk on the south side and barrier walls removed. The roadway width is 44ft. allowing 3 lanes of possible traffic. Photos taken during a bridge inspection in 2013, as in Figure 7.1-3, show the current geometry. The two main steel trusses are spaced at 54.5ft. with lower chord tie girders supporting and stiffening the deck system, which consists of seven longitudinal stringers, twenty one transverse floor beams and twenty sets of x-pattern lower lateral bracing. The girders and arches are rigidly connected to each other at the ends where they meet. The diagonal hangers are rigidly connected to the arch and girder.

Figure 7.1-1. **Chippewa River Memorial Bridge (Wisconsin, HSI ID: B-09-087)**

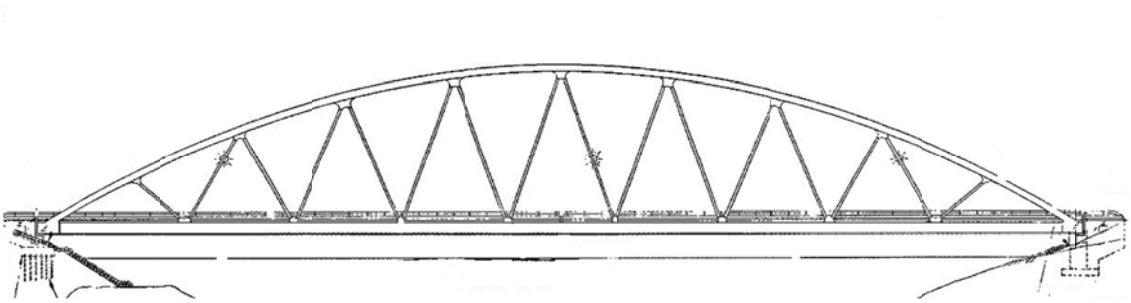

(a) Elevation view

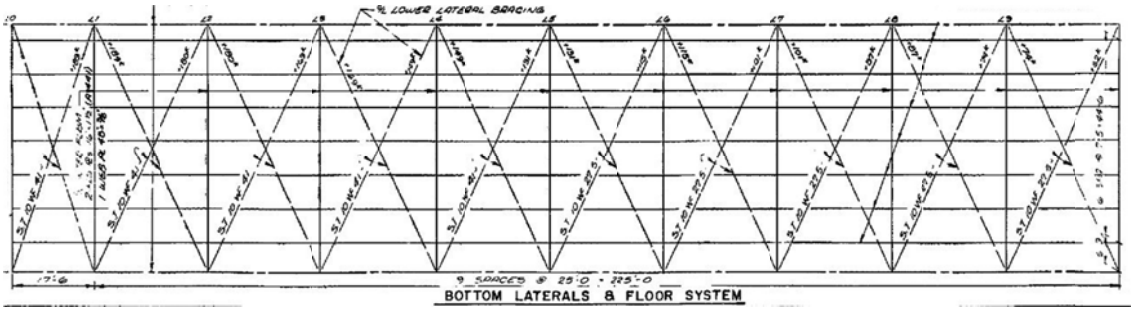

(b) Framing plan

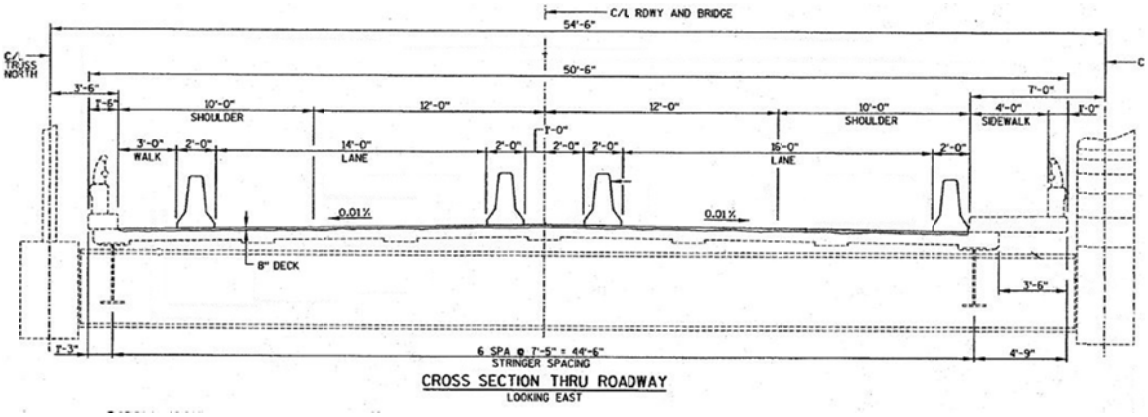

(c) Cross-section view during 2006 re-construction

Figure 7.1-2. Elevation framing and cross section view for Chippewa River Memorial Bridge.

Figure 7.1-3. Chippewa bridge deck during inspection in 2013.

Structural Components

The characteristics of the main structural members in the bridge are summarized from the HSI data and tabulated in Table 7.1-1. Structural carbon steel was used for most main members Fy = 50 ksi yield stress, and structural low alloy steel for built-up steel plate floor beams Fy = 36 ksi.

The most notable aspect about this bridge is in utilizing the inclined structural tubing as hangers. These tubing members generally span between every other transverse floor beam location except near the ends (Figure 7.1-4). The arrangement (spacing and inclination) of the hangers is an important parameter to be considered for a tied arch bridge. Inclined hangers with an oblique angle can distribute the vertical traffic loads more uniformly to the arch. This can result in a reduction of arch bending moments under concentrated floor loads. The design axial force, flexural and torsional moments in the arch and tie girders may decrease, allowing the section sizes to decrease

Table 7.1-1. Structural Components.

Member Name	Type	Dimension
Tie	Built-up box section	63×36 7/8×1.5×7/16 (depth × width × flange thickness × web thickness)
Arch	Built-up box section	38.5×38.5×1.25×1.25
Floor Beam	End floor beams	50×3/8×16×1 (depth × web thickness × flange width × flange thickness)
	Interior floor beams	50×3/8×16×1.5
	Bridge center floor beam	50×3/8×16×1.5
Stringers	Simple spans framed into the floor beams	W 21×55
Arch Bracing	X pattern using structural tubing	TS 12×12×5/16

Lower Lateral Bracing	Deeper section used near the ends	W 10×41
	Shallower section used in between	W 10×27.5
Hangers	Structural tubing	TS 12×12×3/8

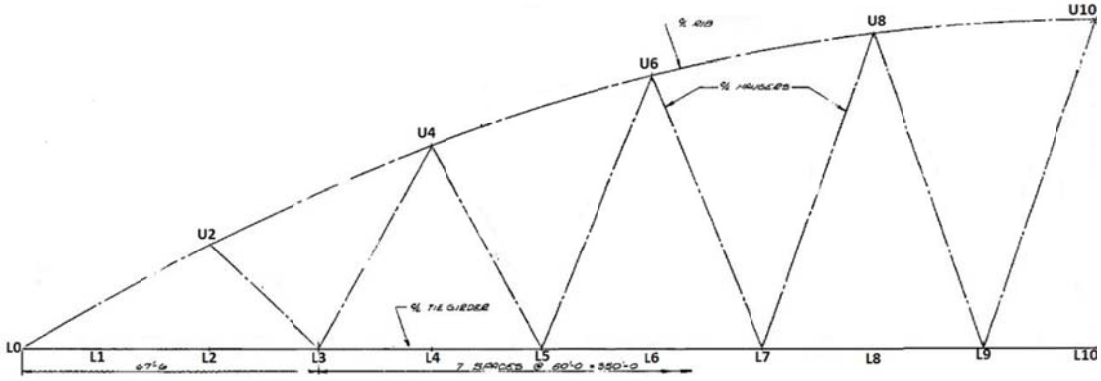

Figure 7.1-4. Hangers, tie girder and arch rib section (elevation view)

All of the hanger tubing is bolted to parallel gusset plates, which are rigidly connected with the diaphragm of the arch ribs and tie girders on the top and bottom respectively (Figures 7.1-5&6).

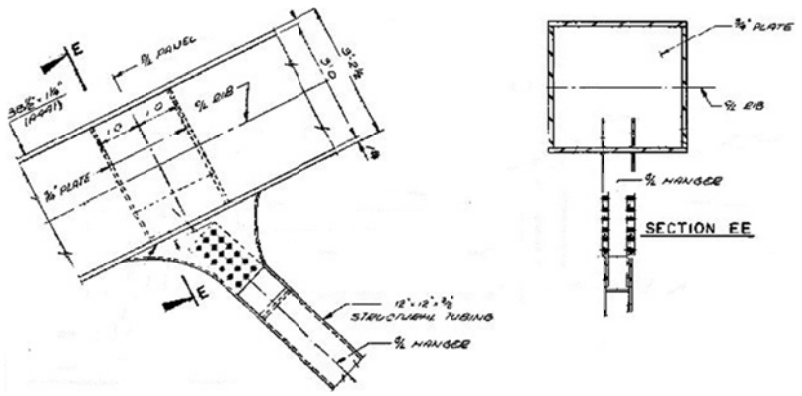

Figure 7.1-5. Hanger top and arch rib connection (elevation & cross section).

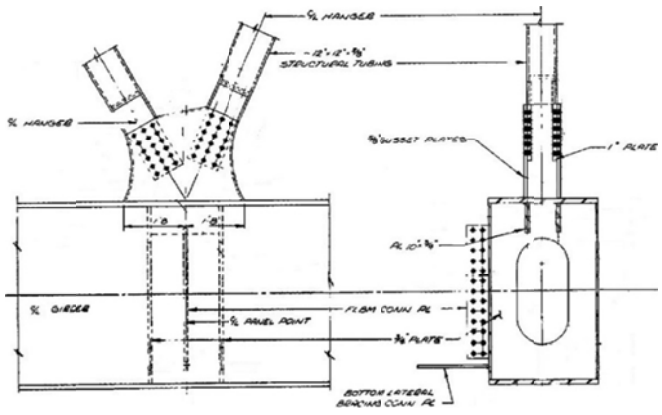

Figure 7.1-6. Hanger bottom and tie girder connection (elevation & cross section).

As shown in Table 7.1-1, eighteen floor beams are typical interior floor beam size. The section dimensions of the two end floor beams, however, are distinct. The floor beam spacing also varies along the bridge span. The first interior floor beams at both ends are placed 17ft. 6in. from the end floor beams whereas the other interior beams are all spaced 25ft. apart. The upper and lower flanges and webs of the floor beams are bolted rigidly into the tie girder. No concrete or studs are present on the top flange of the floor beams.

All interior stringers are spaced at 7ft.- 5in., but the edge stringers are 6ft.- 9in. and 3ft.- 3in. away from the centerline of the north and south girders respectively. Part of the stringer bottom flange near the ends is cut for construction clearance with the floor beams as illustrated in Figure 7.1-7. Only the web is bolted into the web stiffeners of the floor beam, indicating a pinned connection. Shear connections with the concrete deck are inclined steel angles (L 4×4×3/8), are spaced at 9in. near the ends of the stringers and 1ft. in the center region as noted in Figure 7.1-7.

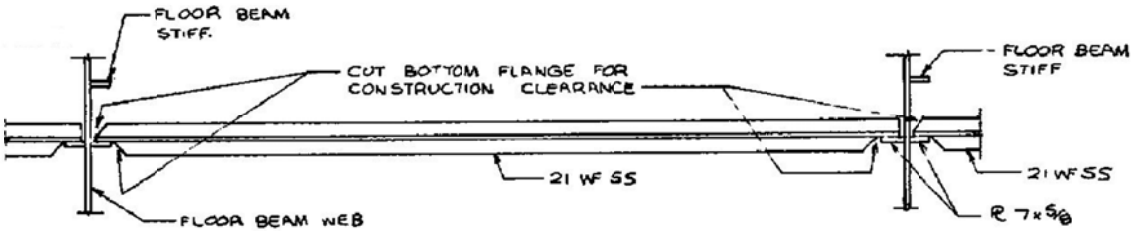

(a) Stringer-floor beam connection plan view

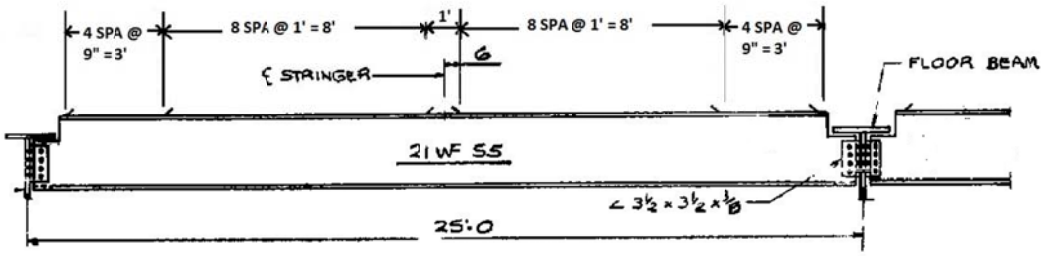

(b) Stringer-floor beam connection elevation view and shear connector spacing

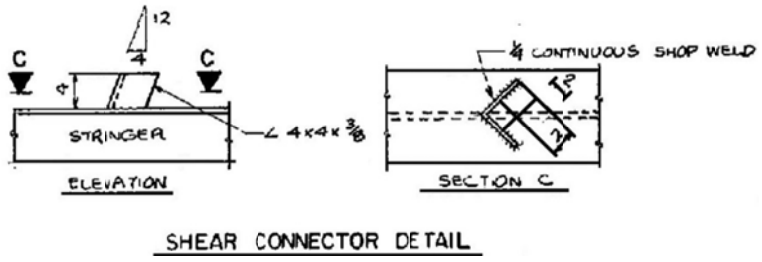

(c) Angle connector details (elevation and plan views)

Figure 7.1-7. Details of the stringers, connections, and composite shear connectors.

Both the arch rib and arch bracings are structural tube sections. The lateral bracings brace the two arch ribs together at projected floor beam locations between the hanger locations. The one X-pattern on each half of the arch in Figure 7.1-8 provides for lateral wind load resistance.

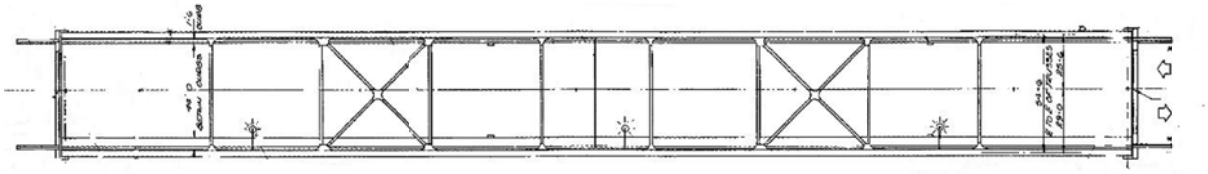

Figure 7.1-7. Arch bracing pattern - plan view.

7.2 Chippewa: Development of Three Dimensional Finite Element Model.

Model Development

The Chippewa bridge was not load tested, but a close inspection of the structure was completed during the annual bridge inspection. Based on the bridge design plans and field observations, the finite element analysis model was assembled. The assumed properties of each of the structural elements used in the model are listed in Table 7.2-1.

Table 7.2-1. Finite element member properties.

Element Name	ASTM Material	Element type	Cross-section Dimension (inches)	Segment length	Number of element divisions used
Tie	A572 Grade 50	Box/Tube Section	63×36 7/8×1.5×7/16 (depth × width × flange thickness	17.6ft at the ends 25ft in between	20 in one tie

Element Name	ASTM Material	Element type	Cross-section Dimension (inches)	Segment length	Number of element divisions used
			× web thickness)		
Arch	A709 HPS50W	Box/Tube Section	38.5×38.5×1.25×1.25	Projected horizontal distance same as each girder sections	20 in one arch
Floor beams	Grade 36A	Built-up I-Shape Section	50×3/8×16 (depth × web thickness × flange width) Flange thickness 1”	54.5ft	Interior floor beams have thicker 1.5” flanges
Stringers	A572 Grade 50	I/Wide Flange Section	W 21×55	17.6ft at the ends 25ft in between	7 in total, each partitioned into 20 segments by the floor beams
Rib bracing	A572 Grade 50	Box/Tube Section	TS 12×12×5/16	Horizontally 54.5ft X-pattern approx. 74ft	8 horizontal ones 4 x-pattern ones
Lower Lateral	A572 Grade 50	I/Wide Flange Section	W 10×41 W 10×27.5	Approx. 60ft except for the end girder section 57.4ft	20 deeper ones near the ends 20 lighter ones in between
Hangers	A572 Grade 50	Box/Tube Section	TS 12×12×3/8	Every other interior floor beams caries from 34.5 ft to 79 ft	16 inclined
Concrete Sab	$f'_c = 4000$ psi	Thick shell	8in thick	25ft × 6ft 9in (length × width)	Total width 54.5ft × 450ft

Appropriate idealization and simplification based on engineering judgement were done when developing the finite element models. While the main bridge structural sections were modelled with

their real dimensions, assumptions were necessary regarding the connections between members and support conditions.

Since both the upper flange and web of the floor beams are fully bolted with the tie girder, axial, shear and moment forces can be transferred through their connections. Floor beam to girder connections are assumed as rigid in the analysis model. At the same time, concrete haunches filled the space between the slab and the floor beams with maximum 3.5in thick near the centerline of the deck. Partially composite action was modeled over the floor beams, similar to the La Crosse Bridge, with two composite links at beam ends that are free in translation in the floor beam direction and do not add to composite action.

The stringers, in contrast, can only transfer shear loads with their web connection to the floor beams. Stringers were assumed as pin-pin connections at the ends to the floor beams. Due to the presence of steel angle shear connectors on the top of the stringers, the concrete deck is modelled as fully composite with the stringers below. Link elements constraining vertical and horizontal translation were used to model the interaction between the concrete deck and the stringers it sat on.

Splices between girder sections were ignored and the girder was assumed continuous. The knuckle sections at the arch and girder joints were not modeled with exact details but by simply rigidly connecting the members when they met.

The boundary condition of the superstructure was idealized as simple roller and pinned support, i.e. one end constraining all direction translations and the other end free in the longitudinal translation. Figure 7.2-1 shows the 3D FEM of the Chippewa bridge built in CSiBridge (with the deck not shown), which will be used for OSOW analysis.

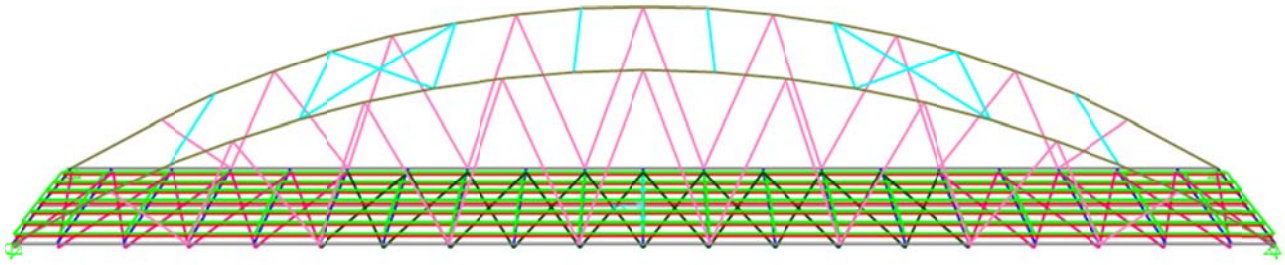

Figure 7.2-1. 3D finite-element-model of the Chippewa River Memorial Bridge.

7.3 Chippewa: Impact of OSOW Vehicles.

The finite element model of the bridge, shown in Figure 7.2-1, was loaded by moving the HL-93 notional load and the OSOW vehicles along the length. The AASHTO assumed lane width is 12ft.. Since the roadway width is 44ft. and there is a 4ft. walkway on the south side, not separated from the roadway by a barrier, analyses were run assuming both three loaded lanes and four loaded lanes (over the walkway) with the HL-93 loading. Load notation used for the loads is:

Single312 represents the 312 kips gross weight single trailer,
Single446 represents the 446 kips gross weight single trailer,
Dual486 represents the 486-kip gross weight dual trailer,
Dual500 represents the 500-kip gross weight dual trailer.

Analysis results from the model for stress in the max force resisting members for each structural group under the HL-93 and limited OSOW vehicles are listed in Tables 7.3-1 & 2 respectively. The results all reflect 2015 AASHTO LRFD Strength 1 or 2 factored loading.

Table 7.3-1. Max stress results in each structural group under factored Dead and HL-93 loading.
*(moments are ft*k, forces are kip, stress is ksi, compression is negative)*

Girder *Frame 362*	Max Moment(kip-in) 5106	Axial Force (kip-in) 1998	Stress (ksi) 29.4
Frame 360	Max Axial Force 2801	Moment @same location 2591	26.1
Arch *Frame 468*	Max e Moment 1564	Axial Force -3517	-28.7
Frame 467	Max Axial Force -3717	Moment @same location 1136	-27.3
Floor Beam *Frame 16*	Max Moment 1364	Axial Force -138	-15.1
Frame 109	Max Axial Force 710	Moment @same location 1130	21.6
Stringer *Frame 240*	Max Moment 159	Axial Force 106	14.3
Frame 250	Max Axial Force 138	Moment @same location 84	18.0
Diag Hanger *Frame 225*	Max Moment 102	Axial Force 96	24.1
Frame 228	Max Axial Force 468	Moment @same location -5.9	27.8

Table 7.3-2. Maximum member forces from factored Dead and OSOW truck loads.
*(moments are ft*k, forces are kip, stress is ksi, compression is negative)*

Girder *Frame 362*	Max Moment 4624	Axial Force 1769	Stress 26.4	Dead +Dual500-2 In north lane
Frame 360	Max Axial Force 2508	Moment @same location 2203	Stress 22.9	Dead +Dual500-2 In north lane
Arch *Frame 468*	Max Moment 1432	Axial Force -3068	Stress -25.4	Dead +Dual500-2 In north lane
Frame 467	Max Axial Force -3324	Moment @same location 1011	Stress -24.4	Dead +Dual500-2 In north lane
Floor Beam *Frame 16*	Max Moment 1311	Axial Force -119	Stress -14.3	Dead +Dual500-2 In south lane
Frame 109	Max Axial Force 589	Moment @same location 931	Stress 17.8	Dead +Dual500-10 centered
Stringer *Frame 241*	Max Moment 126	Axial Force 93.4	Stress 19.8	Dead +Dual500-2 In north lane
Frame 250	Max Axial Force 123	Moment @same location 83.2	Stress 16.9	Dead +Dual500-2 In north lane
Diag Hanger *Frame 224*	Max Moment 26.8	Axial Force 236	Stress 18.4	Dead +Dual500-2 In north lane
Frame 228	Max Axial Force 479	Moment @same location -6.4	Stress 28.5	Dead +Dual500-2 In north lane

All member stress results, except for the diagonals, are largest under the strength factored HL-93 notional truck loading rather than the OSOW vehicles. The maximum stress reached by any member is 29.4ksi of tension, 59% of the yield, in the tie girder with the HL-93 load. The OSOW stress in the arch reaches 25.4ksi compression, equaling 51% of the yield stress and 88% of the HL-93 induced stress. Floor beams see a stress of 17.8ksi with OSOW vehicles, 49% of the yield and 82% of the HL-93 stress. Stringer stresses under the OSOW trucks reached a maximum of 19.8ksi, 40% of the yield and 81% of the HL-93 stress. The diagonal hangers were the only members where the OSOW trucks had higher stress effects

than the HL-93 loading. A peak hanger stress of 28.5ksi, 57% of yield, occurred with the Dual500-2 truck in the north lane of the bridge. The hanger OSOW stress was just 3% larger than the HL-93 induced stress.

8. LEO FRIGO MEMORIAL BRIDGE

8.1 Frigo: Introduction and Structural Components

The Leo Frigo Memorial Bridge (B-05-158-010) was built in 1979 spanning 450ft. over the Fox River at Green Bay, Wisconsin. Figure 8.1-1 shows the structural type as a steel tied arch bridge with vertical hangers. Supporting two separate longitudinal concrete decks, the bridge is designed to carry two lanes of traffic in both directions. The major structure consists of two steel tie girders and arch ribs. The girders and arches are rigidly connected to each other at the ends where they meet. The hangers are double straight steel strands used to transfer vertical loads from the tie girders, at each floor beam location, to the arch. Both concrete decks are 43.5ft. wide composing a total 80ft. of roadway width. Underneath there are ten longitudinal stringers along with eleven transverse floor beams. The plans for the bridge are shown in Figure 8.1-2.

Figure 8.1-1. **Leo Frigo Memorial bridge in Green Bay.**

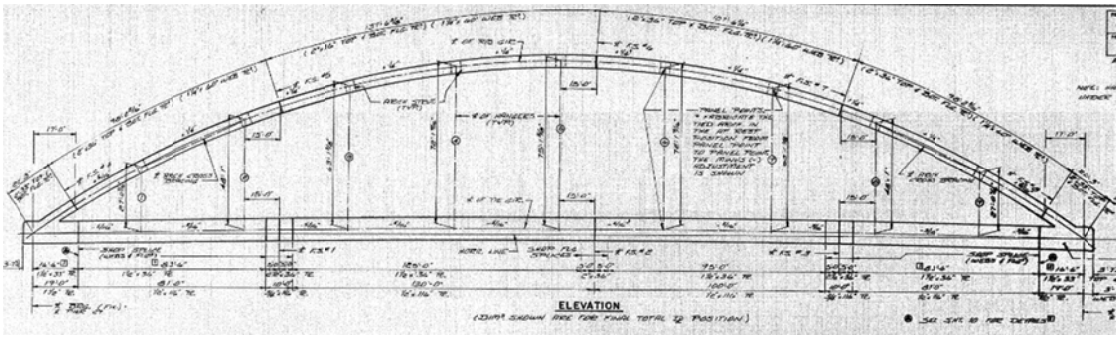

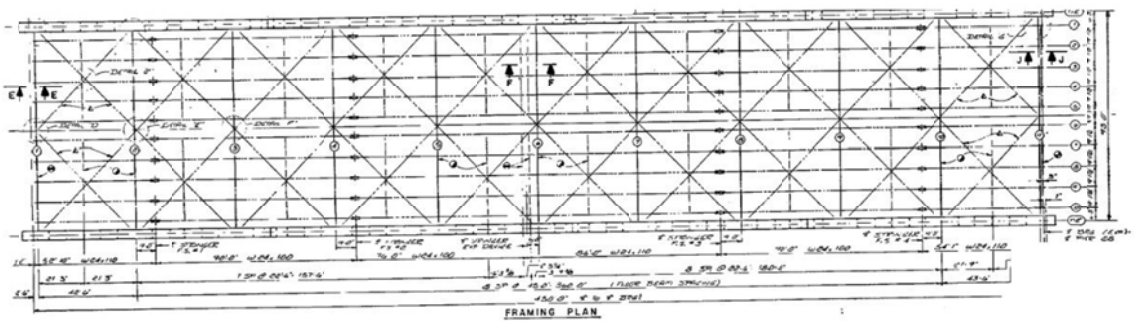

Figure 8.1-2. Plans for Leo Frigo Memorial Bridge, elevation & floor plan.

Structural Components

The dimensions of the main members in the Frigo bridge are summarized in Table 8.1-1. All steel is structural carbon steel (ASTM A588) with yield stress Fy = 50 ksi.

The tie girder box sections are composed of web and flange plates welded together. Spreadsheets were used to compute properties of equivalent HSS sections when the structure was modelled in the analysis software. In Table 8.1-1, the first tie section with thicker web plate was used till 26.125ft. from the knuckle joints with the arch. The second section was used along most of the length. The arches, like the tie girders, were welded box sections.

Two bridge strands of 2.25in. diameter were used to form one set of tension hangers at each floor beam location. The two strands were spaced 1ft apart and parallel along the longitudinal direction, providing an area of 6.08 square inches at each hanger locations with a total 610 kip capacity (100ksi strength). Each set of strands terminated inside the arch and girder, anchoring into a strand socket as detailed in Figure 8.1-3. These anchors and sockets were bolted into the diaphragm in the box sections. Strands were sealed on the flange plate of the box with cast covers.

Floor beams are plate girders with an I-beam cross-section and used various flange plate thicknesses (1.5in., 2in. and then 3in.) as shown in Figure 8.1-4 (though difficult to read). Floor beams 1 through 10, counting inward from the knuckle, have a uniform web thickness of 9/16in. Floor beam No.11 (near the center) has a 3/4in. web near its ends and 9/16in. elsewhere. The floor beams were spaced at 45ft., except the two end spans were 42ft.-6in. (west) and 43ft.-6in. (east). Both the web and flange of the floor beams are bolted into the tie girder with angle plates forming a rigid connection. Since the stringers crossed over the top of the girders (Figure 8.1-5) there was no concrete haunch or direct connection between the floor beams and the concrete deck.

The stringers are steel wide flange sections supported above the floor beams. Channel sections are bolted between the webs of the stringers as diaphragms as shown in Figure 8.1-5. There are three sizes of channel sections and their locations are tabulated in Table 8.1-1. Shear connectors are provided

on top of the stringers with varied spacings as detailed in Figure 8.1-6. No shear connectors are placed within 5ft. of the floor beams, the region in which the stringer is experiencing negative moment.

The stringers were continuous over the tops of all floor beams. Near midspan, however, a deck joint was created and the stringers were discontinuous. Approximately 53in. to the west of the center floor beam, FB#6, the stringer was discontinuous with a shiplap joint. A stub stringer cantilevered out from FB6 and the stringer extending from FB5, to the west, was simply supported on the stub.

There are two concrete decks in this bridge side by side, both cast-in-place 8in. concrete slabs. The width of each deck is 43.5ft. and is composed of a 40 ft. roadway and parapet walls on each side. The deck is haunched above the stringers about 3in. With shear connections provided over the middle region of each stringer span, there is partially composite action between the stringer and the deck.

Table 8.1-1. Dimensions of major structural members.

Member Name	Type	Dimension
Tie Girder	Built-up box section	119×36×1.5×1.5 (At the joint) (depth × width × flange thickness × web thickness) 119×36×1.5×0.5 (At the middle)
Arch	Built-up box section	64×36×2×1.25 (depth × width × flange thickness × web thickness)
Floor Beam	End floor beam	50×3/8×16×1 (depth × web thickness × flange width × flange thickness)
	Interior floor beam	50×3/8×16×1.5
	Bridge center floor beam	50×3/8×16×1.5
Stringers	Framed into the floor beams	W 24×110
Diaphragm	Channel section	C 12×20.7 (Typical at floor beams 2 through 10) C 15×33.9 (At end floor beam 1) C 16×36 (At end floor beam 11)
Arch Bracing	Strut	60×36×1.125×0.5
	Cross Bracing	48×36×1.125×0.5
Lower Lateral Bracing	Deeper section used near the ends	W 10×41
	Shallower section used in between	W 10×27.5
Hangers	A set of bridge strands at each hanger location	Double 2.25in diameter A586 Class B bridge strand

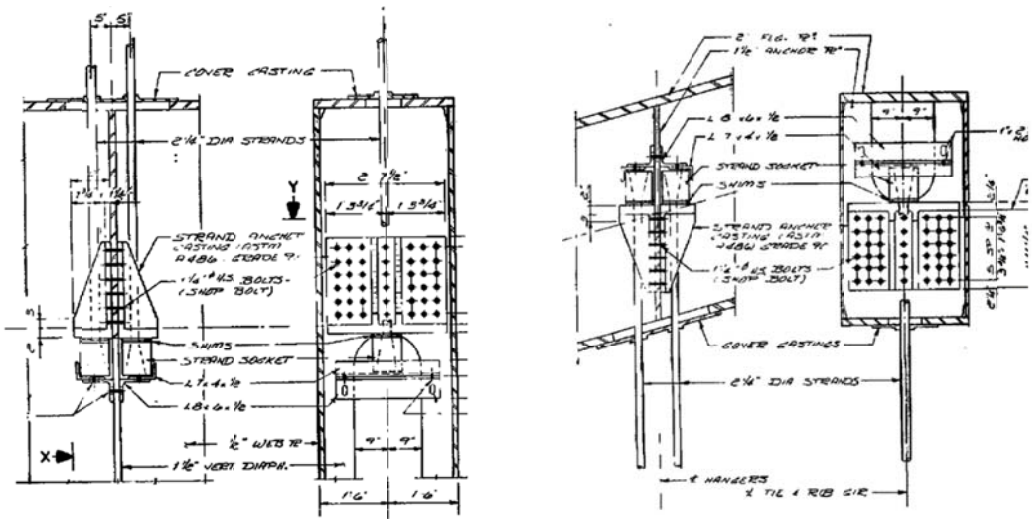

Figure 8.1-3. Connection details between hanger and girder (left), and arch (right).

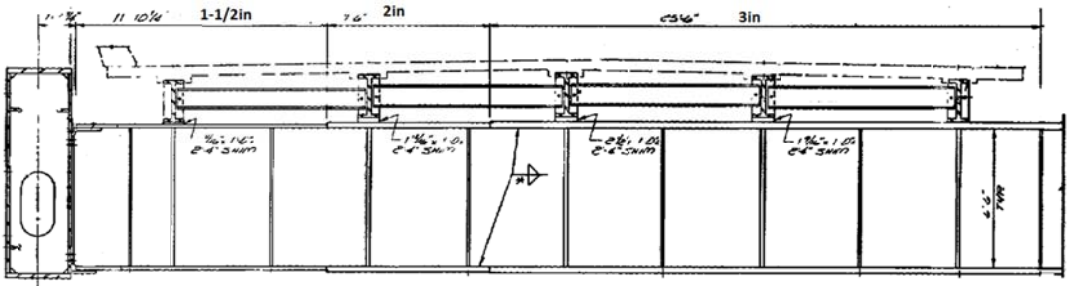

Figure 8.1-4. Typical Floor Beam Elevation View, ½ span.
(flange thicknesses are dimensioned at top: 1-1/2", 2", and 3")

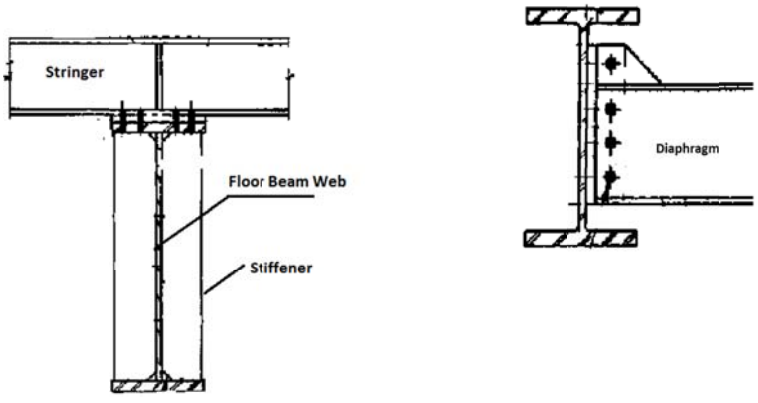

Figure 8.1-5. Floor beam and stringer, stringer and diaphragm connection details.

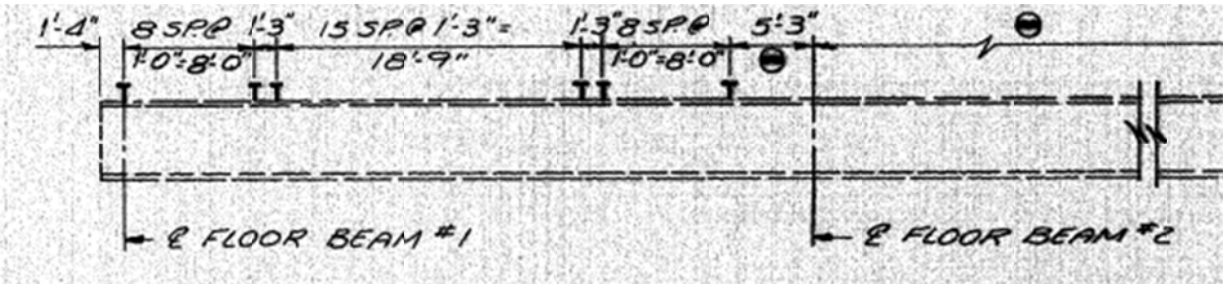

Figure 8.1-6. Shear connector spacings above stringers.

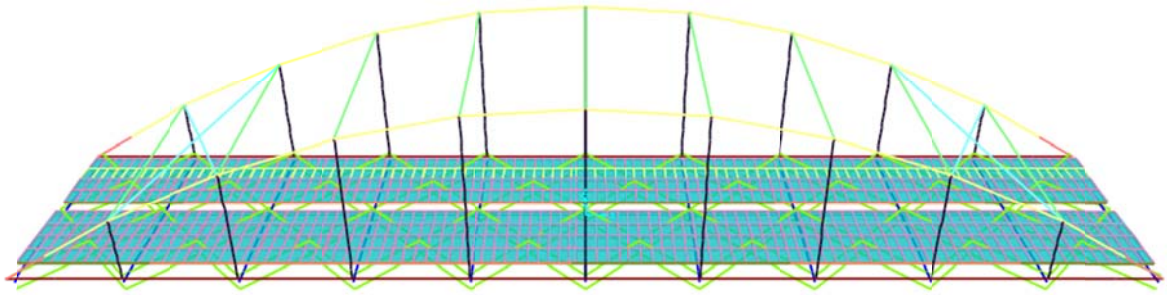

Figure 8.2-1. 3D FEM of Leo Frigo Memorial Bridge.

8.2 Frigo: Development of Three Dimensional Finite Element Model.

The Frigo bridge was not load tested. Idealizations and simplifications based on engineering judgment were made in modelling the Frigo bridge just as in the other two arch bridges. While the main bridge structural sections are modelled exactly, assumptions are made regarding the connections and support condition. The complete model of the bridge is diagrammed in Figure 8.2-1.

Floor beams are assumed rigidly connected with the tie girder box sections. Splices between girder sections are ignored and the section is assumed continuous. The concrete deck was assumed composite with the stringers including the region over floor beams. Link elements constraining vertical and horizontal translation are used to model the interaction between the concrete deck and the stringers it sat on. The knuckle joint section at the arch and girder joints are not modeled with exact details but simply by assuming the arch is rigidly connected with the tie girder. The boundary condition of the superstructure is idealized as simple roller-pinned supported, i.e. one end constraining all direction translations and the other end free in longitudinal translation.

8.3 Frigo: Impact of OSOW Vehicles.

Analysis results from the bridge model for the critical members with max stress levels for each structural group under are listed in Table 8.3-1 for the HL-93 notional loading and in Table 8.3-2 for the OSOW vehicles. With a 40ft. wide roadway in each direction, six lanes of HL-93 loading could be applied. Only one OSOW truck was assumed on the bridge at any time. The OSOW vehicle notation is as used previously:

Single312 represents the 312 kips gross weight single trailer,
Single446 represents the 446 kips gross weight single trailer,
Dual486 represents the 486-kip gross weight dual trailer,
Dual500 represents the 500-kip gross weight dual trailer.

The frame numbers listed in the tables are element numbers in the analytic model. A key to the member locations is shown in Figure 8.3-1.

Table 8.3-1. Max stress results in each structural group under factored Dead+ HL-93 loading.
*(moments are ft*k, forces are kip, stress is ksi, compression is negative)*

Girder *Frame 280*	Max Moment(kip-ft) 16,481	Axial Force (kip) -3029	Stress (ksi) 36.9
Frame 720	Max Axial Force 3870	Moment @same location 2933	21.4
Arch *Frame 662*	Max Moment 4206	Axial Force -3944	-23.5
Frame 701	Min Axial Force -4988	Moment @same location 1678	-21.4
Floor Beam *Frame 115*	Max Moment 13,685	Axial Force -117	-24.7
Frame 131	Max Axial Force 564	Moment @same location 7735	16.3
Stringer *Frame 1720*	Min Moment -1020	Axial Force 263	52.4
Frame 1771	Min Axial Force 274	Moment @same location 565	33.0
Hanger *893*	Max Axial 517		85

Table 8.3-2. Maximum stresses from factored Dead+OSOW truck loads.
*(moments are ft*k, forces are kip, stress is ksi, compression is negative)*

Girder *Frame 280*	Max Moment 13,648	Axial Force 2849	Stress 32.1	Dual500-2
Frame 718	Max Axial Force 3432	Moment @same location 1611	17.6	Dual500-2
Arch *Frame 677*	Max Moment 3325	Axial Force -3839	-21.1	Dual500-2
Frame 711	Max Axial Force -4466	Moment @same location 1391	-18.9	Dual500-2
Floor Beam *Frame 115*	Max Moment 12,247	Axial Force -153	-22.3	Dual500-2
Frame 131	Max Axial Force 337	Moment @same location 5978	12.2	Dual500-2
Stringer *Frame 1720*	Min Moment -1156	Axial Force -302	-59.6	Dual500-2
Frame 1720	Min Axial Force -316	Moment @same location -1132	-58.9	Dual500-2
Hanger *883*	Max Axial Force 466		76.6	Dual500-2

The stringers are actually predicted to reach the yield stress (>50ksi) under the factored loads from both the HL-93 trucks (52.4ksi) and the Dual550 OSOW vehicle (-59.6ksi). These high stringer stresses occur at the stringer support over the first interior floor beam from the east end of the bridge. Stringer yielding (-53ksi), under OSOW loads, is also predicted at the stringer support over the 2nd interior floor beam from the west end.

From the tables, one can observe that the maximum stresses are always created by the AASHTO HL-93 factored loading, except in the stringer case where the factored OSOW Dual500 truck caused the largest stress. Highest stress in the arch occurs due to a combination of bending and axial load, at the ¼ point of the arch. The highly loaded hanger is at midspan with HL-93 loading and just west of midspan under the OSOW vehicle. Locations of the highly stressed members are shown in Figure 8.3-1.

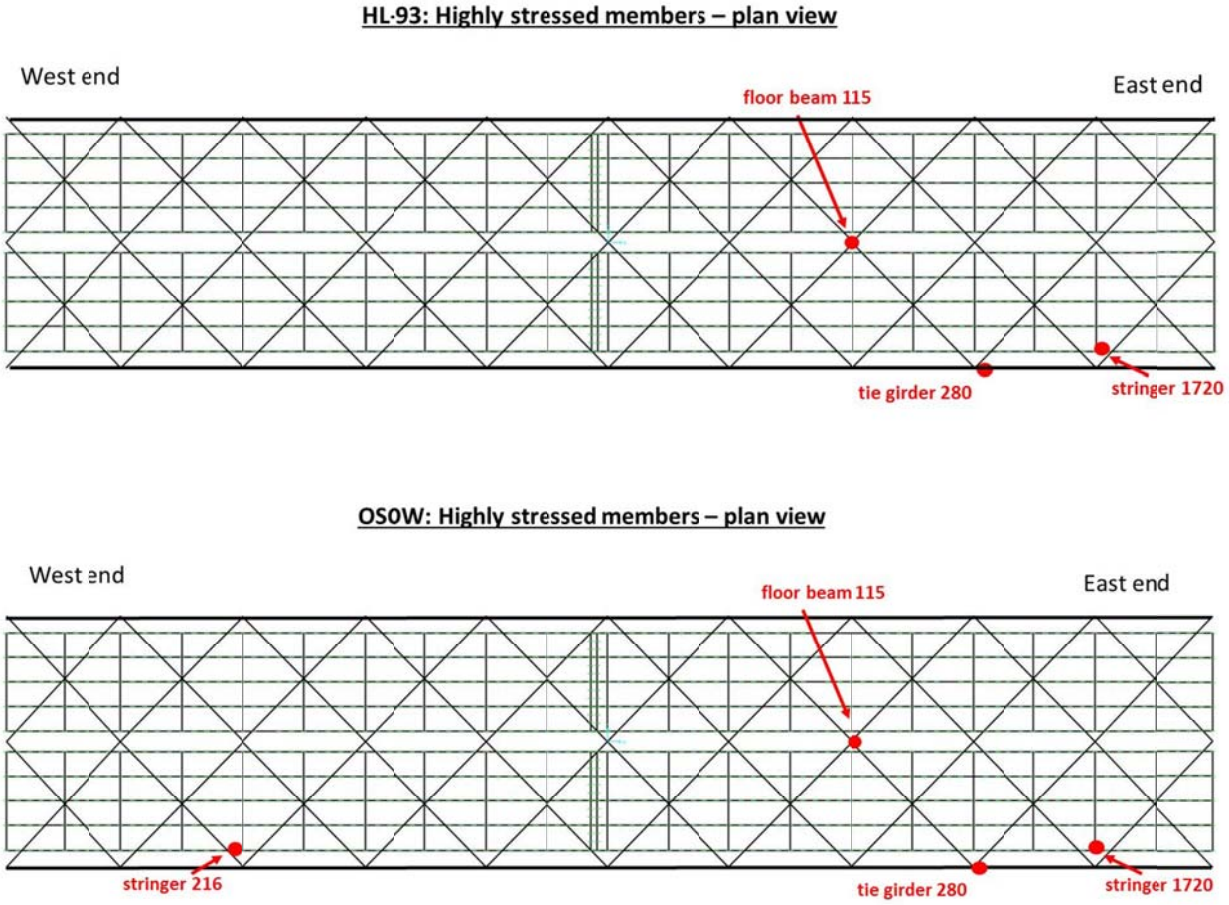

Figure 8.3-1. Plan views of Frigo bridge showing locations of highly stressed members.

9. SIMPLIFIED ANALYSIS METHODS FOR MEMBERS IN COMPLEX BRIDGES

The comprehensive calibrated 3D FEMs are generally thought to be accurate in the estimation of the behavior of the complete structure as well as that of each individual component. Building and running full scale 3D bridge FEMs, however, is time-consuming and error-prone due to the complexity of many structures. Since critical information (e.g., required floor beam or stringer strength under certain super loads) may not be available to bridge authorities when needed to support decisions regarding allowing permit loads to cross a bridge, simplified methods for checking the force impact on members are of interest.

The development of simplified analysis methods is included in this section to allow quick estimation of future OSOW loading effects on critical bridge members. The focus here is on the development of simple 2D models that can replicate the force estimates found in complicated 3D FEM analysis.

As a first step – the results of the FEM analyses are reviewed to identify members that may be critical for controlling the size or geometry of permit loads that can be carried by the complex arch and bascule bridge structures examined earlier. Then the development of simplified 2D models will be described in detail.

9.1: Critical Elements in Arch and Bascule Bridges.

The bridge elements that exhibited the highest stresses under factored HL-93 and OSOW vehicles are listed in Tables 9.1-1&2. Under HL-93 loading the capacity in all of the bridges is controlled by either the stringer peak stress or the floor beam peak stress. The stringer controlled in the Marinette bascule, Cameron tied arch and Frigo tied arch. The girders, arches or hangers did not control in any bridge.

With loading from the selected OSOW vehicles the controlling member is not as consistent. For both bascule bridges, however, the main bascule girder capacity controlled the bridge's capacity. The floor stringer is still the controlling member in the two tied arches: Cameron and Frigo. The OSOW capacity of the Chippewa arch truss is limited by the capacity of the diagonal hangers.

Based on these results, developing a simplified method for estimating permit vehicle effects on the bridge stringers and floor beams appears to be most critical since they control capacity in seven of the 10 cases for the bridges with HL-93 and OSOW loading. While OSOW loading is of prime interest, the HL-93 design loading provides a familiar basis for comparison. The following sections will look at simplified methods to work with each of the bridges as a step in developing an overall method that may apply to multiple bridge types.

Table 9.1-1. Comparison of element peak stresses in members, shown as % of yield for HL-93 loads.

HL-93 induced member stress given as % of the yield stress:					
member type:	Marinette bascule	Winneconne bascule	Cameron tied arch	Chippewa truss arch	Frigo tied arch
floor stringer	81%	64%	72%	36%	104%
floor beam	64%	119%	36%	61%	50%
girder	61%	56%	58%	58%	74%
arch	na	na	50%	58%	48%
hanger	na	na	51%	56%	85%
(Shaded cells indicate element that controls capacity of that bridge.)					

Table 9.1-2. Comparison of element peak stresses in members, shown as % of yield for OSOW loads.

OSOW induced member stress given as % of the yield stress:					
member type:	Marinette bascule	Winneconne bascule	Cameron tied arch	Chippewa truss arch	Frigo tied arch
floor stringer	44%	33%	68%	40%	120%
floor beam	47%	64%	34%	50%	44%
girder	78%	69%	64%	52%	64%
arch	na	na	54%	50%	42%
hanger	na	na	54%	57%	77%
(Shaded cells indicate element that controls capacity of that bridge.)					

9.2: Marinette Bascule Bridge - Simplified 2D Methods.

The nature of the bascule bridge and the joint between the two opening leafs of the bascule creates complexity. These joints need to be considered as “hinges” that can transfer vertical shear force from one leaf to the other, but no moment. Most simplified bridge analysis methods do not accommodate placement of a hinge in a span. A further complication comes if the joint is not tight and some displacement of one leaf is required before shear transfer occurs. In this condition the bridge is a non-linear structural system.

The bascule bridge commonly contains three main members to be examined: the bascule girder, floor beams, and stringers. Generally there are only two bascule girders, one on either side of the roadway. The capacity of these girders controlled the bridge capacity in the two bridges examined here when loaded with OSOW trucks. In the 3D FEM analyses, the HL93 and OSOW Dual500-2 trailer (500kip) were the two trucks that induced the highest stresses in the Marinette girders. The same trucks are used

in the 2D girder analyses here. Stringers controlled the bridge capacity under HL-93 load and stringer behavior will be examined first.

Stringer Analysis

Wheel loads are carried on the metal bridge deck and transferred to the longitudinal stringers. Stringers in the Marinette Bridge span 171 inches (14.25ft) between floor beams and are alternately continuous (i.e. each stringer is continuous over 2 spans on 3 floor beams, but the simple supported ends are alternated between adjacent stringers). Some of the Marinette bridge stringers between floor beams 4 and 5 (close to the mid joint) are non-continuous – are just simply supported with a 171inch span. These are the critical stringers for positive moment since there is no continuity, and negative end moment, at either end.

The first step in the analysis is to select the position along the length of the selected stringer to position the truck load to induce the largest bending moment. This can easily be done using simple software such as PCBridge[6] or QConBridge[7]. Alternately the simple rule that the resultant total load vector and the nearest wheel should be equidistant from the center of span can be used if a single simple span stringer is investigated. The locations are as follow.

HL93 Truck: Maximum truck moment is found when the back wheel is located at midspan of a non-continuous stringer, 7.125 ft. from left support. The moment is 57ft-k.

Dual500-2 Trailer: The wheel line moment, a negative moment, was found over an interior 2 span floor beam support. As described earlier, the axle spacing of the trailer for the Dual500-2 truck is constant at 5ft. along the last 60ft. of the truck, the heavier part with 32k per axle set, 8k per wheel, on two adjacent trailers. The two trailers are only 2ft. apart. The maximum positive span moment is 35.2ft-k and minimum negative moment is -42.9ft-k.

To estimate the total truck moment carried by any stringer an attempt was made to use a wheel load distribution factor. The AASHTO Standard Specifications Section [9] 3.23.2.3.1.5 factor to use for cases with concrete flooring supported by 4 or more steel stringers was tried as a method to estimate the portion of the wheel load that goes into the stringer. The older value was used because the 7th Ed. AASHTO LRFD Bridge Design Specifications [2] does not include a similar equation. The Standard Spec. equations for the distribution factor are as follows:

$$\frac{S}{5.5}$$

$$\frac{S}{(4 + 0.25 * S)}$$

Where, S is the distance in feet between outside and adjacent interior stringers. The first equation is used when S is 6ft. or less, the second for over 6ft. The truck wheel line load moment is multiplied by this factor to estimate the portion of a wheel line resisted by a single stringer. The spacing

between stringers is 48 inches in the Marinette bridge, which gives a distribution factor of 0.73 using the AASHTO equation.

An alternate method for estimating the wheel load on a stringer uses an assumption regarding the decking behavior and a simple calculation. The deck is assumed to be simply supported on the stringers with a span equal to the stringer spacing (4ft.). An axle of the OSOW Dual500-2 truck is placed on the decking, with all four wheels, and the reactions of the deck on the stringer provides a distribution factor. In the Marinette case one of the center trailer wheel lines is placed directly over a stringer. The close wheel on the adjacent trailer is 2ft. away, or at the middle of the adjacent deck span. The reaction on the stringer below the wheel line is the combination from the two wheels – 1.5 wheel loads. As a distribution factor a stringer resists 1.5 wheel lines

The maximum moment values, obtained with the simplified method by multiplying the truck moments by the load factor, are shown in Figure 9.2-1 for the HL-93 truck and Figure 9.2-2 for the Dual500-2 truck and trailers. The HL-93 truck wheel load is the 16k and the Dual500-2 wheel load is 8k. The HL-93 wheel line creates a peak moment of 57ft-k and the OSOW wheel line creates -42 ft-k on a continuous 2 span stringer or +45.5ft-k on an end simple span stringer.

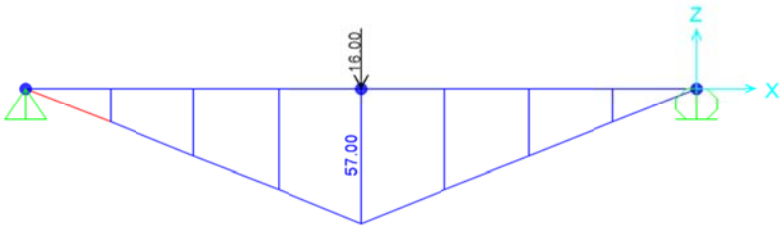

Figure 9.2-1. HL93 Wheel line moment diagram. Stringer moment is 57ft*k multiplied by the AASHTO factor 0.73 = 42ft*k.

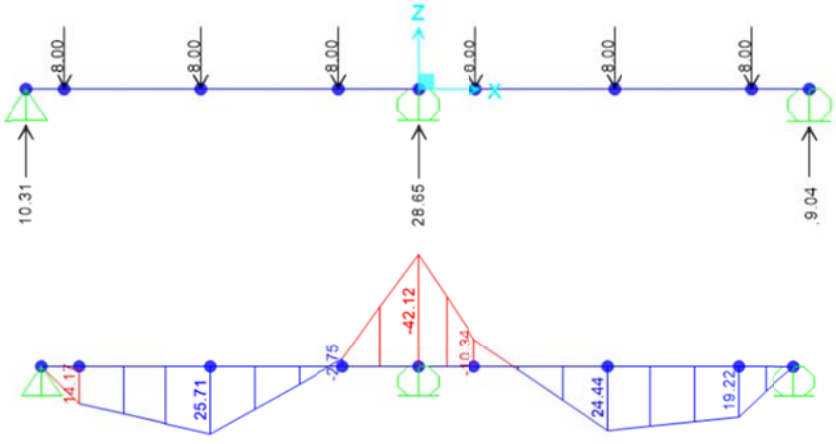

Figure 9.2-2. Dual500-2 Wheel line moment diagram with min negative moment over support. Stringer moment predicted as -42ft*k multiplied by 0.74 factor = -31.2ft*k. Alternate distribution factor of 1.5 would give -63ft-k.

Note that the 0.73 distribution was used. That AASHTO factor was originally defined based on truck loadings with wheels spaced at 6ft. on center on the axles. The dual trailer actually has wheels closer together, spaced at 4ft. on an axle and 2ft. between wheels on two trailers. It is expected that using the AASHTO factor with the OSOW truck would underestimate the total wheel load resisted by a single stringer. A comparison of the simply estimated stringer moments and results from an accurate 3D FEM analysis are listed in Table 9.2-1.

Table 9.2- 1. Comparison of Marinette stringer moments - accurate vs. approximate.

Bridge	Truck	Max. Moment 3D Model (kip-ft.)	Max. Moment 2D Analysis (kip-ft.)	% change vs. 3D Model
Marinette	HL93	42	42	0%
	Dual500-2, AASHTO df	-51	-31	-39%
	alternate df		-63	+23%

(df = distribution factor for portion of wheel line resisted by a stringer.)

Load and dynamic allowance factors as well as dead load are not included in Table 9.2-1 values. Moment values found in the 2D analysis for the HL93 trucks correlate very well with the 3D model. This means that the simplified analysis may be used for predicting stringer forces when trucks having an axle spacing similar to the HL-93 truck (6ft.) are being considered. For the OSOW trucks, values found in the AASHTO simplified analysis are up to a 40% smaller than the 3D Model. This shows that the AASHTO equation used here does not work for the special axle configuration of the OSOW trucks on these bridges. A simple alternate distribution, based on simple span deck calculations, overestimates the negative moment by 23%. More data from other bridges and load configurations is needed in order to create a general modification of the AASHTO equation for such trucks.

Floor Beam Analysis

For the floor beam analysis, reaction values estimated from the stringer analysis are used as point loads applied directly to the floor beam. The maximum moment in the floor beam is calculated. This is an approximate method because the reactions on the stringer are calculated with the same span location of the truck as used for the stringer moment analysis. The true maximum reaction would occur with a different truck position, usually with one axle directly above the floor beam. This approximation will underestimate the reactions on the floor beam. Floor beams in the Marinette Bridge are 408 inches (34ft.) long. The floor beam is assumed to be simply supported at its ends based on the web only connection detailed in the bridge plans.

The maximum HL-93 reaction from a stringer will occur at the stringer's midspan floor beam support, with a 2 span continuous stringer. The mid and back axles of the HL93 truck are located with one axle on each span as shown in Figure 9.2-3a for a single wheel line. On the adjacent stringer the maximum reaction is obtained by adding the reactions at the support when the two non-continuous stringers meet as shown in Figure 9.2-3b.

One simplifying assumption made here is that the truck wheel lines are directly above stringers. Further – the two wheel lines shown in Figure 9.2-3 are from two separate trucks in different positions. In reality the truck wheel position relative to the stringers would depend on stringer spacing and the wheel spacing on the truck axle. Assuming that 4 wheel lines are directly above stringers near the center of the floor beam span should provide a conservative (overestimate) of the floor beam moments.

The floor beam loads visible in Figure 9.2-4 (21.92 and 12.67 kips) are from the combination of the reactions at the mid support (floor beam) shown in Figure 9.2-3. Now, applying those reactions as loads to the floor beam creates the moment diagram, with peak of 452ft*k, shown in Figure 9.2-4.

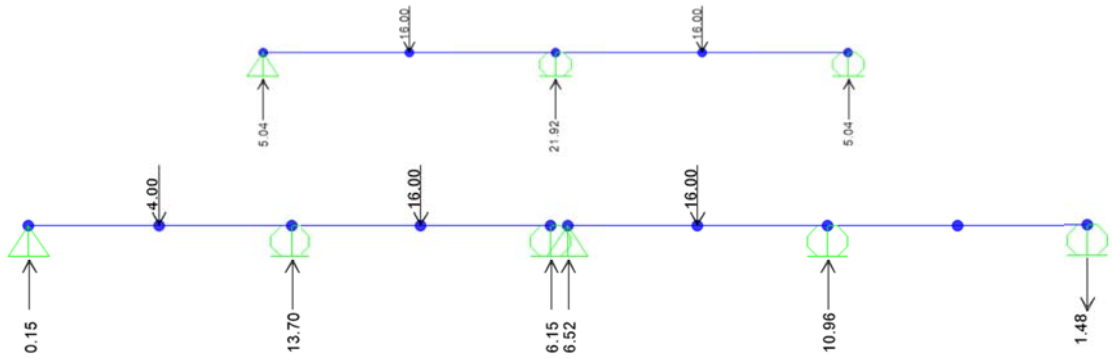

Figure 9.2-3. HL93 Wheel loads applied to two stringer lines: top-a) back and mid axle on spans of a two span stringer, bottom-b) front, mid and back axles on two sequential stringers.

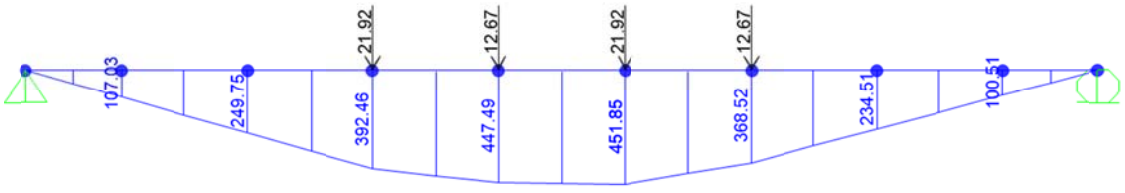

Figure 9.2-4. HL93 Floor beam moment diagram – assuming that four truck wheel lines are applied above the four interior stringers.

Reactions from a Dual500-6 trailer set are found in a similar manner. Reactions are found from a set of stringer analyses (same procedure as for the HL93 truck), assuming the 4 trailer wheel lines are directly above four stringers near midspan of the floor beam. Since wheels are spaced at 4ft. on the dual trailer axles and the trailers are at 6ft. spacing, this may be an acceptable representation of the 4ft spaced stringer loading on the floor beam, though in reality some of the truck loads would also be resisted by stringers other than the center four and the loads on the floor beam should be more widely distributed. The OSOW loading moment diagram, with peak of 642.4ft*k, for the floor beam is shown in Figure 9.2-5. Combining both moments with the LRFD impact factor and load factor would produce:

HL-93: 1052ft*k

Dula500-5: 867ft*k

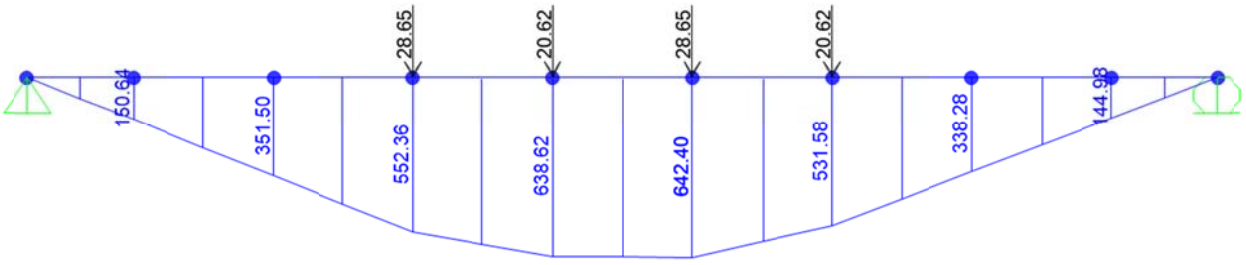

Figure 9.2-5. OSOW Dual500-6 Floor beam moment diagram – assuming that four wheel lines from the two trailers are applied above four stringers.

Table 9.2- 2. Comparison of Marinette floor beam moments - accurate vs. approximate.

Bridge	Truck	Max. Moment 3D Model (kip-ft.)	Max. Moment 2D Analysis (kip-ft.)	% change vs. 3D Model
Marinette	HL93	394	452	+15%
	Dual Trailer 1-6	587	642	+9%

Table 9.2-2 compares floor beam estimated moments. Again load and dynamic allowance factors as well as dead load are not included in the table values. Moment values from the 2D analysis are up to 15% greater than the 3D values, a conservative result. The simplified analysis seems to be a good tool to estimate the truck induced forces in floor beams. The error in simplified results could be due to the approximate distribution of the load on the floor beams from the stringers. In our analysis, the full truck loads were transferred by just the four stringers near midspan of the floor beam. The true load coming from the stringers will be distributed along the entire floor beam and not only in the assumed limited locations.

Girder Analysis

Girder force analysis might be simplified by modeling a girder as a 2D uniform prismatic beam with a fixed support at each end and connected in the middle by a link element only capable of transferring vertical loads as diagrammed in Figure 9.2-6. Three important assumptions are made in this analysis approach. First, most bascule bridge girders are not uniform prismatic beams; their cross section varies along the length. Since this is a symmetric model and nearly determinate, the girder section variation has little impact. An "exact" analysis, assuming the girder depth varied linearly along its length was performed, but results proved that there was a change of less than 1% with respect to the average moment of inertia analysis. Secondly, the joint between leafs may have an initial gap that allows one leaf to move relative to the other. If a gap exists, then the varying girder stiffness becomes more important and the structure is indeterminate. The simplified model assumes no gap exists. And finally, in doing 2D modeling an assumption must be made regarding the portion of truck loading that is transferred to each of the two bridge girders.

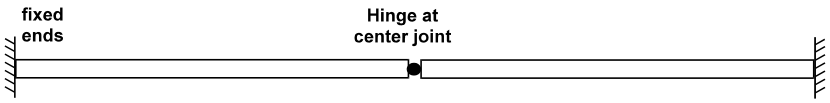

Figure 9.2-6. Simple 2D model of bascule bridge with hinged joint at center.

The length of each girder in the Marinette Bridge was taken from the plans as 791 inches (65.9ft). A girder is modelled with uniform stiffness, fixed at the abutment and with a hinge to the adjacent leaf's girder at midspan exactly as laid out in Figure 9.2-6.

In the HL93 analysis two trucks are assumed to be on the bridge simultaneously in symmetric transverse positioning. Both trucks are placed on one leaf. With the symmetric layout, one girder would collect the full load from one truck.

For the Dual500-2 truck, only one truck is assumed to be allowed on the bridge and it is placed adjacent to one edge of the roadway. To determine the portion of truck load that would be collected by a single girder, a supplementary hand calculation with the floor beam as a simply supported span is conducted. The Dual500-2 wheels of one axle line are placed on a transverse floor beam and the reactions from the floor beam on the girder are calculated by hand. In the Marinette bridge the girder closer to the dual trailer received 64% of the total axle weight, while the furthest girder received only 36%. This same distribution is then assumed to exist for all the truck axles.

Once the portion of truck loading (HL-93 or Dual500-2) carried by each girder was determined, the portion of the truck axles loads were applied directly on the girder in the model described earlier as

point loads at each axle location. As a simplification, the loads were applied at the axle locations rather than attempting to find how much load goes on each floor beam and then applying the loads on the girder at the floor beam locations. The maximum moments in the girder can then be calculated, but due to the indeterminacy created by the hinge, an analysis software such as SAP200 or CSiBridge is best used. In this case the calculated moments are:

HL93:	-2118ft*k	or as a factored load:	-4930ft*k
Dual500-2:	-7044ft*k	or as a factored load:	-9509ft*k

The girder moments from the simplified method are compared with those obtained during the accurate 3-D FEM analysis in Table 9.2-3. Load and dynamic allowance factors as well as dead load are not included in the table results. The values in parenthesis for the 2D analysis column are results from a model that considered a linear variation of the cross section between support and mid joint, rather than a constant cross section. So, in order to simplify the analysis, the results using an average cross sections are used for reference when comparing the 2D versus the 3D data.

Results from the simplified analysis are very accurate for the HL93 trucks, with a variation of only 3 percent. For the OSOW trucks, the simplified values are 21 percent greater than the values from the complex 3D models. These conservative estimates for OSOW trucks may be good when rating these complex bridges for permit loads. The difference in values might be explained by the simple idealized method of estimating what portion of a truck load is carried to each girder in the bascule bridge.

Table 9.2-3 . Comparison of Marinette girder moments accurate vs. approximate.

Bridge	Truck	Max. Moment 3D Model (kip-ft.)	Max. Moment 2D Analysis (kip-ft.)	% change vs. 3D Model
Marinette	HL93	-2185	-2118 (-2139)	-3%
	Dual500-2	-5811	-7044 (-7036)	+21%

9.3: Winneconne Bascule Bridge - Simplified 2D Methods

The Winneconne Bridge is the second of two bascule bridges examined during this study. It is similar in overall design to the Marinette bascule with the same unique complexity that exists in most bascule bridges.

This bridge again is composed of two main girders per leaf, one on either side of the roadway. The girders support transverse floor beams which in turn support longitudinal stringers. The floor system is composed of steel grating.

Stringer Analysis

Stringers in the Winneconne Bridge are all discontinuous (simply supported on floor beams) and 177 inches (14.75ft.) long. The stringer spacing is close at 28.5 inches (2-3/8ft.). The AASHTO equation for a wheel distribution factor, as described for the Marinette bascule, results in a value of 0.43, or each stringer is assumed to resist 43% of a wheel line.

With the HL-93 truck, the maximum stringer moment due to a wheel line is calculated by placing an axle at midspan of the simply supported stringer. The load and resulting moment is plotted in Figure 9.3-1. After applying the distribution factor, the moment resisted by the stringer is predicted as 25.4ft*k.

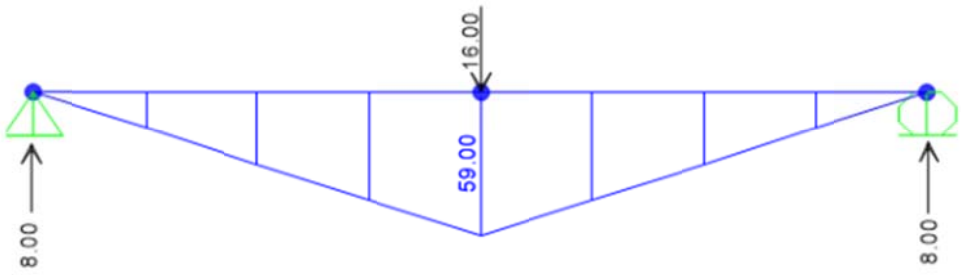

Figure 9.3-1. Moment with HL-93 wheel line load on a stringer span.

For the Dual500-2 truck and trailers the maximum stringer moment is found by using a simple program, such as QConBridge [7], or simply placing the resultant load and the nearest wheel equidistant from the span centerline to find the truck position along the span to induce a maximum moment. With the Dual500 loading, and axles at 5ft., one axle is placed at center of span with a leading and trailing axle 5ft. away. When the truck is located with wheel line loads placed as shown in Figure 9.3-2. the maximum moment develops. The same AASHTO distribution factor was used to estimate the portion of a wheel line carried by a single stringer. As noted for the Marinette Bridge, using the AASHTO factor should result in an underestimate of the stringer loads and resulting moment because the wheels are closer together on the OSOW truck than on an HS-93 truck. The maximum wheel line moment of 48.5ft-k is multiplied by the distribution factor (S/5.5 = 0.431) to predict a stringer moment of 20.9ft-k.

An alternate method would be to look at the axle loads of the OSOW vehicle supported on the grating floor and assume that the grating acts as a simple span between stringers. Placing one of the trailer middle wheels over the stringer, the wheel on the second trailer is 2ft. away while the grating span is 2.37ft. From simple calculations, the second wheel on the span adds 0.156 of its weight to the reaction where the other wheel line is located. The stringer then would resist 1.165 wheel lines. The moment would be 48.5ft-k multiplied by 1.156 = 56.1ft-k.

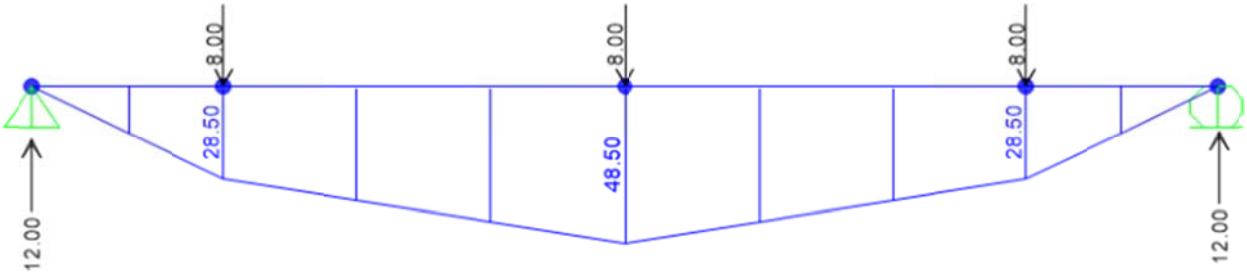

Figure 9.3-2. Dual500-2 wheel line moment on a stringer span.

Again the simple AASHTO analysis for stringer moments underestimates the true moment as illustrated in Table 9.3-1. HL-93 results are good since the assumed distribution factor was developed for that type of loading with a 6ft. axle spacing. The stringer moment is underestimated by 16% when the OSOW loading occurs, better than was seen with the Marinette bridge. The closer spacing of stringers in the Winneconne vs. the trailer wheel spacing makes the assumed AASHTO distribution factor somewhat better, but unconservative for evaluating permit truck effects.

The alternate method, looking at wheel loads on the grating floor and the floor reaction on the stringers, overestimates the moment by 124%. With the close stringer spacing (2.37ft.) of this bridge the deck is apparently distributing the load more efficiently than assumed using the simple span deck analysis for a distribution factor in the alternate method. Clearly an improved method for estimating OSOW truck wheel line distribution to stringers is needed.

Table 9.3-1 . Comparison of Winneconne stringer moments - accurate vs. approximate.

Bridge	Truck	Max. Moment 3D Model (kip-ft.)	Max. Moment 2D Analysis (kip-ft.)	% change vs. 3D Model
Winneconne	HL93	26	25	-4%
	Dual500-2 AASHTO df	25	21	-16%
	Dual500-2 alternate df		56	+124%

(df = distribution factor for portion of wheel line resisted by a stringer.)

Floor Beam Analysis

Floor beams in the Winneconne Bridge are 342 inches (28.5ft.) long. The beams are again assumed to be simply supported because the sole connection to the girder is through the beam web. Analysis of the floor beam moment follows the procedure described for the Marinette bascule.

For the analysis with two HL93 trucks on the bridge, assume that the trucks are placed symmetrically in the transverse direction and near the center of the floor beam span. The truck loads come to the floor beams through the stringer reactions. Again it is assumed that a truck wheel line always falls directly above a stringer. So the HL93 truck wheels are assumed to be spaced at 4.75ft apart,

rather than the AASHTO HL93 wheel spacing of 6ft, to sit over every other stringer as illustrated in Figure 9.3-3. In a similar fashion the Dual500-2 wheel lines are assumed to occur directly above a floor beam. This simplifying assumption conservatively places the truck loading close to the center of the floor beam and should again overestimate the floor beam moment.

The HL-93 analysis also assumes that one truck axle is placed directly above the floor beam and the other two axles are 14ft. away on the stringers, or near the end of the stringer's 14.75ft. span, so the effect of the other two truck axles is ignored. The reactions from the stringer on the floor beam and resulting moments for an HL-93 axle set are shown in Figure 9.3-3. The maximum floor beam moment is 304ft*k.

With the Dual500-6 truck and trailers the axles are spaced closer than the 14.75ft floor beam spacing so the stringer reactions on the floor beam are calculated by first analyzing the stringers with the Dual500 wheel line loading in a manner similar to the Figure 9.2-3 illustration but as simple supported. The resulting floor beam loading and beam moment diagram for the OSOW truck is shown in Figure 9.3-4. The maximum floor beam moment is predicted as 456ft*k without impact or load factors.

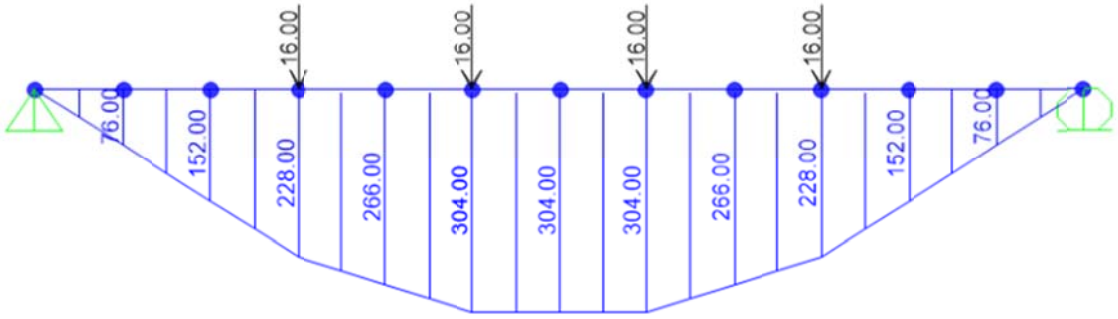

Figure 9.3-3. HL93 predicted floor beam moment diagram.

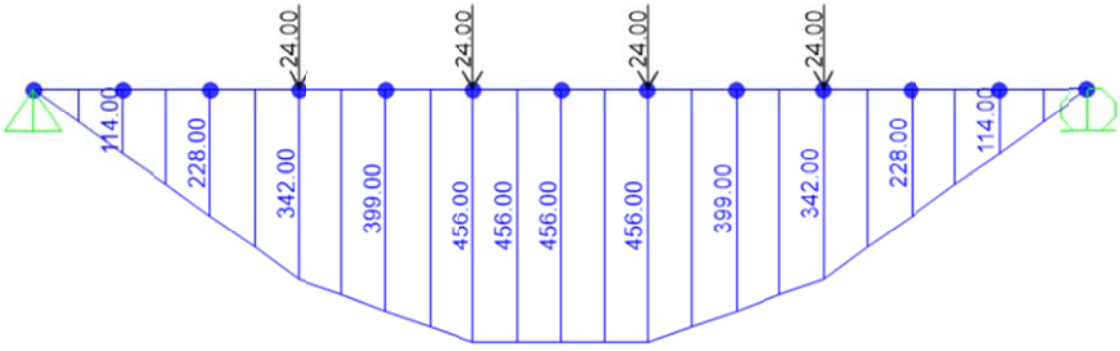

Figure 9.3-4. Predicted Dual500-6 induced floor beam moment diagram.

A comparison of the approximate predicted floor beam moments with the more accurate values from a 3D FEM analysis are listed in Table 9.3-2. Contrary to the results for the Marinette bridge, the HL-93 moment was underestimated this time by 13%. The Marinette moment was 15% high. It is not

clear why the HL-93 moment is underestimated in this case. The HL-93 wheel lines were assumed to be at double the stringer spacing, 4.75ft., rather than the actual 6ft. in the truck. This places all the wheel lines close together and should still overestimate the floor beam moment. Apparently more geometric configurations should be considered before adopting a simple method such as suggested here.

Table 9.3-2 . Comparison of Winneconne floor beam moments - accurate vs. approximate.

Bridge	Truck	Max. Moment 3D Model (kip-ft.)	Max. Moment 2D Analysis (kip-ft.)	% change vs. 3D Model
Winneconne	HL93	348	304	-13%
	Dual500-6	397	456	+15%

Girder Analysis

The Winneconne bascule girders are 474 inches (39.5ft.) long. The same procedure for simple analysis described for the Marinette Bridge is used again. The girder distribution factor calculated for the HL93 truck, by hand calculation on a simply supported floor beam, is again 1.0 with two HL-93 trucks and 0.75 for the Dual500-2 OSOW vehicle. The maximum moments at the support for both trucks are listed in Table 9.3-3. The values in parenthesis are results estimated using a linear variation of cross section for the girder along its length rather than a constant cross section.

The moment comparison in Table 9.3-3 shows HL-93 results nearly identical to those of the Marinette girder when looking at the errors in values from the simple prediction method. The method is quite accurate for HL-93 double truck loading with a symmetrical placement. The approximate method, however, overestimates the portion of an OSOW truck load transferred to a single girder when the truck is placed toward one side of the bridge.

Table 9.3-3 . Comparison of Winneconne bascule girder moments - accurate vs. approximate.

Bridge	Truck	Max. Moment 3D Model (kip-ft.)	Max. Moment 2D Analysis (kip-ft.)	% change vs. 3D Model
Winneconne	HL93	-1192	-1155 (-1166)	-3%
	Dual Trailer 1-2	-2700	-3481 (-3482)	+29%

9.4: Cameron Avenue Arch Bridge - Simplified 2D Analysis Methods

In the Cameron Avenue arch bridge, all stringers are 7'10" apart and simply supported on floor beams. While most are 23.25ft. long, the end spans are 25.25ft. long and therefore control for the max bending moment due to the extra length.

Stringer Analysis

The PCBridge software is used to find where the HL-93 and OSOW trucks should be placed along the stringer span to create the maximum stringer moment. This could also be easily found using the simple hand calculation method described with the Marinette and Winneconne bridge. The critical HL-93 location is with the truck driving from west to east with its back axle 9.25ft. from the west end of the stringer and middle axle 2ft. from the east end. The front axle is off the stringer. The maximum truck bending moment for a wheel line can be calculated by hand from the diagram in Figure 9.4-1 and is 105.5ft-kips. The AASHTO distribution factor, calculated as described previously, is 1.31 with spacing greater than 6ft. The OSOW truck position is determined in a similar manner and the resulting moments from a wheel line hand calculated. The same AASHTO distribution factor is used

If the alternate method is used for finding load distribution to a stringer, considering the deck as simple spans with axle wheel loads applied, the factor for the Dual500-2 truck would be 2.47 wheel lines per stringer. It is calculate with one inner trailer wheel line over the stringer, the other wheel of that axle 4ft. away on the deck to one side and the two wheel lines of the other trailer on the deck span to the other side.

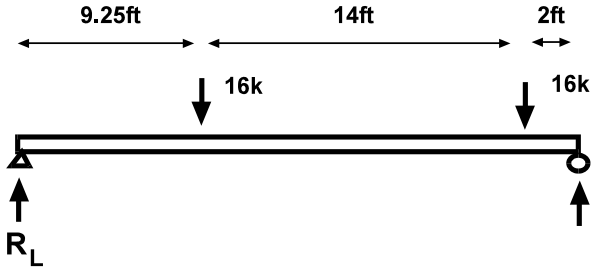

Figure 9.4-1. HL-93 truck position to cause max moment in stringer.

Predicted moment estimates, without load or impact factors, are listed in Table 9.4-1. The AASHTO distribution coefficient works well for the HL-93 truck but results in a 37% overestimate of moment for the OSOW truck when using the AASHTO load distribution factor. The alternate distribution factor, hand calculated looking at the deck as simple spans with an axle set of loads applied, would have overestimated the moment by 158%.

Table 9.4- 1. Comparison of Cameron stringer moments - accurate vs. approximate.

Bridge	Truck	Max. Moment 3D Model (kip-ft.)	Max. Moment 2D Analysis (kip-ft.)	% change vs. 3D Model
Cameron	HL93	138	138	0%
	Dual500-2	125	171	+37%

Floor Beam Analysis

In order to induce maximum bending moment in the floor beam, again assume that vehicle wheel lines are over stringers close to the center of the floor beam. This is a practical assumption for the LaCrosse bridge as well as the other arch bridges. The stringer spacings in these bridges are near 7.5ft., while the actual distance between the two wheel lines of an HL-93 truck is 6ft. so the match is good.

Figure 9.4-2 shows the HL-93 wheel line loading position on stringers to induce a large reaction at a floor beam. The calculated reaction on the stringer is 23.7k per wheel line.

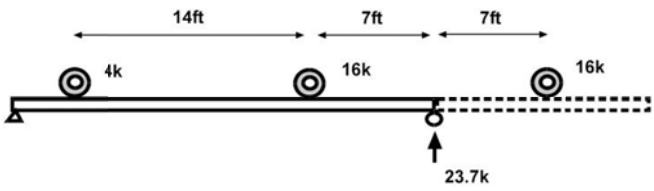

Figure 9.4-2. HL-93 truck position on stringers to create max reaction.

The reactions of the HL-93 (23.7k each) assumed to come from four of the stringers near the beam midspan are shown in Figure 9.4-3. With a uniform cross section and fixed ends, the beam moments are +294ft-k and -520ft-k.

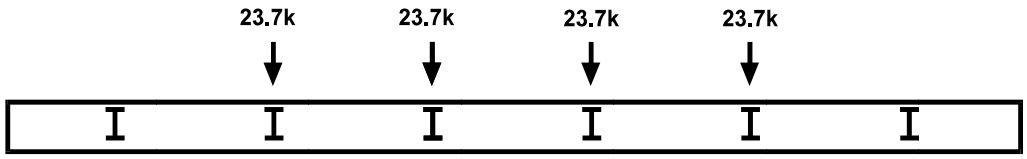

Figure 9.4-3. HL-93 stringer reactions as loads on floor beam.

A comparison of reaction forces at the stringer ends for the OSOW trucks, computed for a single wheel line with each of the four OSOW truck types, indicates that the Dual500-2 is the controlling case. With the Dual500 loading the stringer reaction is again calculated by analyzing the simple supported stringer with the 8k wheel loads at 5ft. spacing. The Dual500-2 end reaction is 23.2k per wheel line. Only one OSOW truck is assumed on the bridge. A more condensed loading pattern (closer wheel line spacing) exists for the Dual OSOW trucks so the loading is applied near to the center of the floor beam.

A new method of estimating floor beam forces will be used here for the OSOW trucks. The wheel line loading distribution to stringers will be approximated, since the AASHTO distribution equation used for the HL-93 truck is inaccurate for the OSOW wheel spacings. With this in mind, the four 23.2k reactions with 2ft. spacing between the two trailers are applied on the slab at the center of the bridge, as shown in Figure 9.4-4. The slab is a continuous beam across the six supports from the stringers. In this simplified method we assumed that each slab section between two stringers is a simply supported beam.

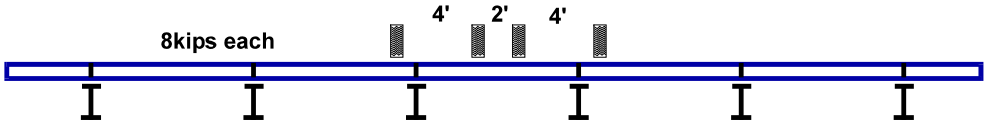

Figure 9.4-4. Lateral location of wheel lines of Dual500-2.

Because OSOW vehicles are much longer than stringers (a total of 60ft. with 32k axle loads spaced at 5ft. for Dual500) the reactions from a single stringer on the floor beam are doubled. This assumes that stringers on either side of the floor beam will be loaded. The truck placement shown in Figure 9.4-4 applies 93k of stringer reaction load to the floor beam at the two middle stringers as diagrammed in Figure 9.4-5.

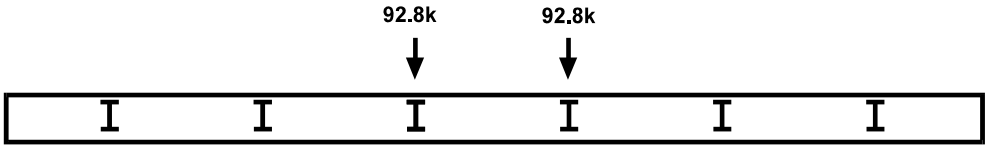

Figure 9.4-5. OSOW stringer reactions as loads on floor beam.

The floor beam is assumed to have a rigid connection to the tie girders so the moment from the 93k stringer reactions is calculated for a fixed ended beam. Though the depth of the beam varies, a constant section is assumed. But in addition to the variable beam depth, as described earlier – these floor beams act partially composite with the floor creating a highly varying stiffness. Since the fixed

ended structure is indeterminate, the internal moments will depend on stiffness. In the simplified calculation the beam is assumed to have uniform stiffness as well as fixed ends. This gives moments of +825ft-k and -1131ft-k. The approximate moment estimates are compared with accurate results in Table 9.4-2. Note that the approximate 2D results have large negative moments due to the fixed end condition assumed in the beam and the assumed uniform cross section.

Table 9.4- 2. Comparison of Cameron floor beam moments (fixed) - accurate vs. approximate.

Bridge	Truck	Max. Moment 3D Model (kip-ft.)	Max. Moment 2D Analysis (kip-ft.)	+M % change vs. 3D Model
Cameron	HL93	-117 & 822	-520 & 294	-64%
	Dual500-2	-77 & 1369	-1131 & +825	-40%

The results of Table 9.4-2 clearly show that the fixed end condition assumed for the floor beam in the simplified calculation was incorrect. The negative moments are very high. In the 3D model the floor beams are rigidly attached to the tie girders, but the small negative moments indicate that the girder does not provide serious restraint due to its torsional flexibility, certainly not like a fixed condition.

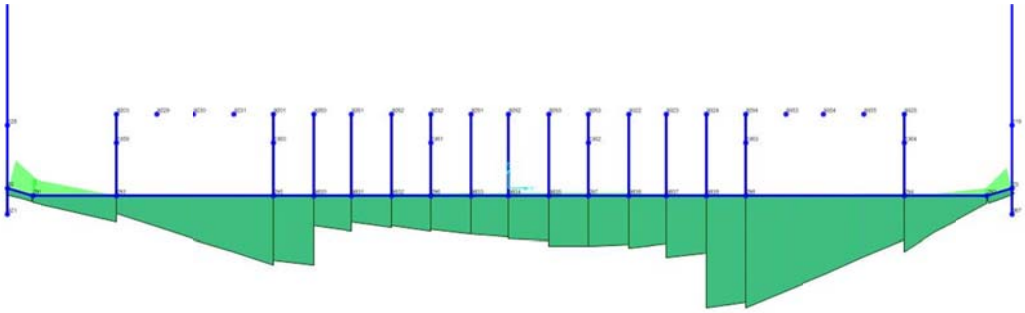

Figure 9.4-6. Moment diagram for partly composite floor beam of Cameron Avenue bridge.

The actual moment diagram for a floor beam, from the 3D analysis, is shown in Figure 9.4-6. The effect of the composite action is reflected in the abrupt reduction in the beam moments near the third points. Rather than being resisted by bending in the beam, the moment is now partially resisted by compression in the deck and tension in the beam. Simulating this varying stiffness effect from composite action is unreasonable in a "simplified" model. A second approximate analysis was made assuming that the floor beam was pinned at the ends but still with uniform section – now determinate and possible to calculate by hand. A simply supported beam moment calculation for the OSOW load of Figure 9.4-5 estimates a maximum moment of 1956ft-k. A similar calculation for HL-93 moment under the loads of Figure 9.4-4 gives 814ft-k. Table 9.4-3 provides a new comparison of the floor beam moments.

Table 9.4- 3. Second comparison of Cameron floor beam moments (pinned) - accurate vs. approximate.

Bridge	Truck	Max. +Moment 3D Model (kip-ft.)	Max. +Moment 2D Analysis (kip-ft.)	+M % change vs.3D Model
Cameron	HL93	822	814	-1%
	Dual500-2	1369	1956	+43%

Examining the results in Table 9.4-3 it is apparent that the simplified estimate of floor beam moments caused by an OSOW truck are inadequate with a 43% excess. This is attributed to the inability of the simple model to capture the effect of partial composite action, changing the beam stiffness, and the partial rigidity of the end support as influenced by the torsional rigidity of the tie girder.

9.5: Chippewa Arch Bridge - Simplified 2D Analysis Methods

Stringer Analysis

The stringer configuration of the Chippewa River arch bridge is nearly the same as the Cameron Avenue Bridge (spacing 7'-5" vs 7'-10" and span 25' vs 23.25' for Chippewa vs Cameron). The same results for maximum moment due to a wheel line can be assumed. The final stringer maximum moment is different, however, because the stringers are 7'-5" apart slightly changing the distribution factor. Stringer moment estimation results are shown in Table 9.5-1.

Table 9.5- 1. Comparison of Chippewa stringer moments - accurate vs. approximate.

Bridge	Truck	Max. Moment 3D Model (kip-ft.)	Max. Moment 2D Analysis (kip-ft.)	% change vs. 3D Model
Chippewa	HL93	131	134	+2%
	Dual500-2	142	165	+16%

Again, it can be seen that the use of the distribution factor works for the HL-93 loading configuration, but is conservative for the OSOW configuration.

Floor Beam Analysis

Following a procedure similar to that used in the Cameron Avenue bridge analysis – peak wheel line reactions from the stringers were calculated, slab transfer of wheel lines to stringers, and stringer reaction on floor beams from wheel lines were estimated. In the Dual500 loading case the four trailer wheels were placed with each trailer to one side of the stringer near midspan of the floor beam. Then assuming that the deck was simple spans, the distribution of the Dual500 load to the supporting stringers was hand calculated. The idealization in this calculation is shown in Figure 9.5-1 with the adjacent deck span to be superimposed with the shown span. The middle stringer received 2.38 wheel lines and the two adjacent stringers received 0.81 wheel lines each.

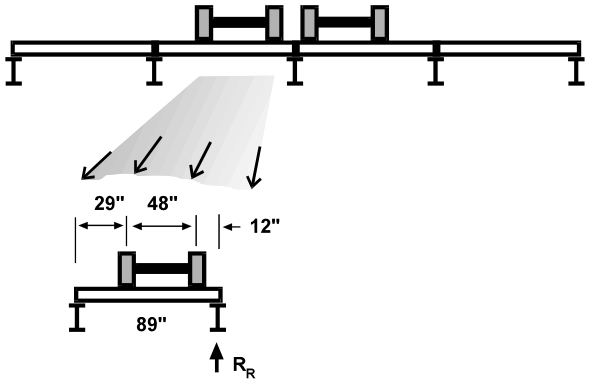

$$R_R = \frac{29}{89} + \frac{(29+48)}{89} = 1.19$$

$$R_L = 2 - R_R = 0.81$$

Figure 9.5-1. Model for distribution of Dual500 wheel line loads to stringers.

The Dual500 8k wheels spaced at 5ft. were assumed to extend over two stringer spans, with one axle directly above the floor beam. The model for this is detailed in Figure 9.5-2. A hand calculation of the reaction at the floor beam gave a force of 24k per such wheel line. A second stringer, to the right of the one shown, would contribute another 16k to the reaction for a total of 40k.The previous factors, 2.38 and 0.81, were applied to the wheel line 40k reaction to calculate the loads applied to a floor beam by the stringers.

Figure 9.5-3 shows the stringer loads applied to the floor beam of the Chippewa Bridge for the HL-93 and OSOW Dual500-2 loadings. The HL-93 includes three lanes loaded and a multi-presence factor of 0.85 with equal distribution to all stringers. One OSOW truck is assumed with no multi-presence factor and the distribution factors calculated above. Results for maximum moments by performing a floor beam analysis assuming fixed ends are shown in Table 9.5-2.

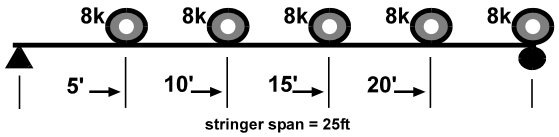

$$R_R = 8k * \left({}^{5}/_{25} + {}^{10}/_{25} + {}^{15}/_{25} + {}^{20}/_{25} + 1\right) = 8k * 3 = 24k$$

Figure 9.5-2. Dual500 stringer reaction on floor beam support.

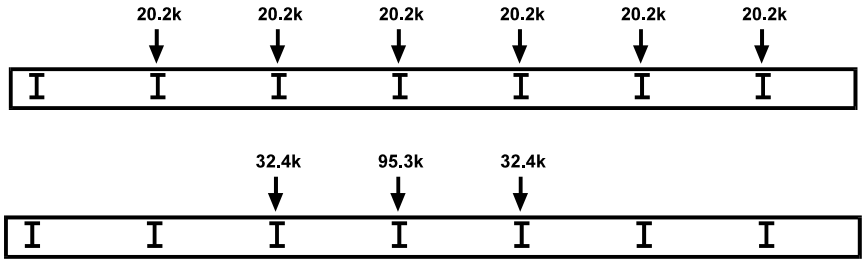

Figure 9.5-3. Stringer reactions on floor beams for the HL-93 loading (at top) and the OSOW Dual500-2 loading (bottom) looking toward East at a Chippewa cross section.

Table 9.5- 2. Comparison of Chippewa floor beam moments - accurate vs. fix end approximate.

Bridge	Truck	Max. Moment 3D Model (kip-ft.)	Max. Moment 2D Analysis (kip-ft.)	+M % change vs.3D Model
Chippewa	HL93	--244, +446	-601, +308	-30%
	Dual500-2	-225, +592	-1052, +815	+38%

The results of the simple analysis in Table 9.5-2 look quite poor compared to the 3D analysis results. As in the previous Cameron Avenue bridge analysis, the assumption of fixed ends in the simple floor beam analysis overestimates the size of the negative end moments. This is again attributable to the torsional stiffness of the tie girders providing less than a fixed end condition. In the cast of the Dual500 OSOW loading, however, the simplified method appears to overestimate both positive and negative moments. Apparently the actual loads applied near the center of the floor beam in this case are reduced and loads must be redistributed to adjacent stringers and floor beams. This distribution is a function of the relative stiffnesses of each of those members and is not represented in the simplified model. Figure 9.5-4 shows the 3D moment diagram for a floor beam under Dual500-2 loading along with the predicted simplified fixed end moment diagram.

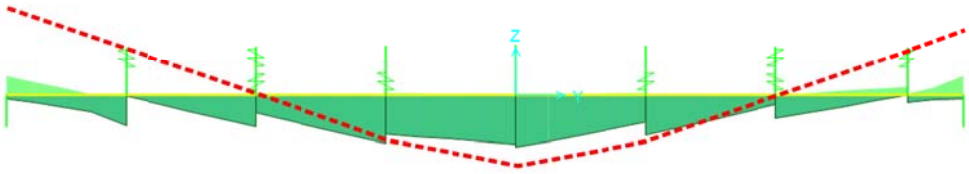

Figure 9.5-4. Comparison of 3D FEM predicted floor beam moment diagram (solid green) with a moment diagram from the fixed end simplified analysis (red dash) for the Dual500-2 OSOW truck loading.

The 3D analysis moment diagram of Figure 9.5-4 displays smaller moments along the full length of the floor beam compared to the results from the simplified analysis. But it additionally shows that at each stringer, where the deck is composite with the stringer, some composite deck action is also developing with the floor beam – reducing the floor beam moments as seen previously in the Cameron Avenue bridge. In an attempt to improve the simplified model prediction a second set of analyses were conducted with the floor beam end pinned instead of fixed. The positive moment increases substantially as shown in Figure 9.5-5 and Table 9.5-3.

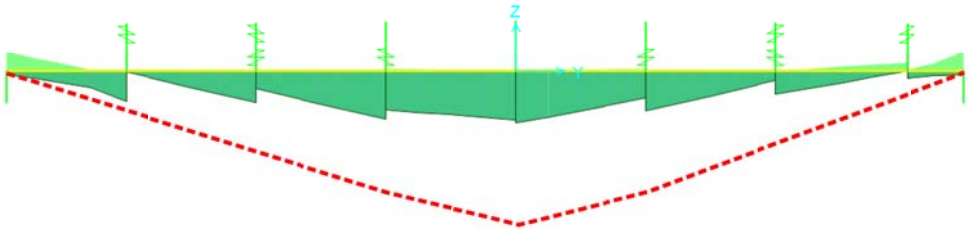

Figure 9.5-5. Comparison of 3D FEM predicted floor beam moment diagram (solid green) with a moment diagram from the pin ended simplified analysis (red dash) for the Dual500-2 OSOW truck loading.

Table 9.5- 3. Comparison of Chippewa floor beam moments - accurate vs. pinned approximate.

Bridge	Truck	Max. Moment 3D Model (kip-ft.)	Max. Moment 2D Analysis (kip-ft.)	+M % change vs.3D Model
Chippewa	HL93	--244, +446	+892	+100%
	Dual500-2	-225, +592	+1809	+205%

Neither of the simplified floor beam models for the Chippewa bridge are satisfactory for predicting effects of HL-93 loading or the Dual500-2 OSOW truck loading. The best model, assuming the beam has fixed ends, underestimated positive moments by 30% for the HL-93 truck and overestimated positive moments by 38% for the Dual500 load. In both loadings the negative end moments were overestimated. It is clear from inspecting the accurate 3D FEM response results that the floor beam is only partially restrained in bending at its ends, due the torsional flexibility of the tie girder, acts partially composite with the concrete deck and likely resists less load with more load distribution through the bridge structural system than assumed in the simplified model. An accurate estimate of floor beam moments appears to be difficult using a simplified approach without considerable further study of the behavior of these complex bridge systems.

9.6: Leo Frigo Memorial Bridge - Simplified 2D Analysis Methods

An immediate added complexity in predicting forces in the Frigo bridge comes from the unusual stringer system employed while providing an expansion joint near midspan of the bridge deck. The stringers run continuously over the top of the floor beams in this bridge. But, there are two separate continuous stringer sections coming from each end of the bridge with a special joint near the middle of the bridge. The joint is basically a shiplap support with a stub cantilever stringer extending out from the floor beam near midspan and the long stringer in the span simply supported on this stub.

Stringer Analysis:

In developing a simplified model of this stringer system the first step was to model one whole stringer, using the CSiBridge software, with the stringer simply supported (but continuous) over each floor beam but with a pin joint at the stub cantilever. An HL-93 truck wheel line was run along the stringer to find the truck position causing a maximum moment. The stringers are spaced at 9.12ft., wider than the HL-93 wheel spacing of 6ft. With 3 loaded lanes and 5 stringers, it might be reasonable to assume that each stringer carries an equal portion of the six HL-93 wheel lines – or 1.2 wheel lines each.

From the resulting moment envelope it was clear that the 6th full stringer span from the west end, the first full span beyond the overhang joint, developed the largest positive bending moment. The loading and moment envelope from the analyses are shown in Figures 9.6-1. The maximum wheel line induced moment is 210ft-k. Multiplied by the 1.2distribution factor and a 0.85 multi presence factor would give 214ft-k. A minimum factored negative moment of -138ft-k occurs at the end of the same span. The small cantilever stub is to the left of span 6 and the red dot indicates where the pinned joint is located in Figure 9.6-1.

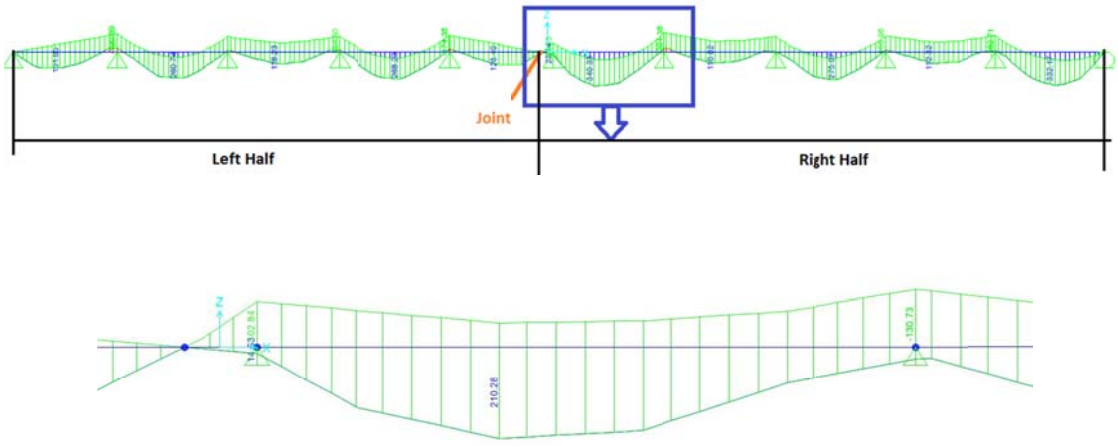

Figure 9.6-1. Moment envelope from HL-93 wheel line on continuous stringers and variation in 6th span with maximum positive moment.

When the Dual500-2 OSOW truck loading is applied, a similar analysis with a wheel line load on one stringer is completed. The maximum positive moment again occurs in the full span to the east of the joint with a value 312ft-k. At the east end of that span a -330ft-k negative moment develops. To determine how the Dual500 trailer's wheel line loads distribute to stringers an analysis similar to that described in Figure 9.5-1, for the Chippewa bridge, was used again. From the analysis with deck assumed as simple spans, but now spanning 9.12ft., the values of R_L and R_R of Figure 9.5-1 would be 1.34 and 0.66. The middle stringer would receive 2.68 wheel lines of load so the resulting positive stringer moment would be 836ft-k and negative moment -884ft-k. Alternatively, using the AASHTO distribution factor (1.46) based on the stringer spacing. That would give moments of 456ft-k and -482ft-k. A comparison of these values with the 3D analysis results is listed in Table 9.6-1.

Table 9.6- 1. Comparison of Frigo stringer moments - accurate vs. approximate.

Bridge	Truck	Max. Moment 3D Model (kip-ft.)	Max. Moment 2D Analysis (kip-ft.)	+M % change vs.3D Model
Frigo	HL93	147 & -194	214 & -135	+45%
	Dual500-2	298 & -496	456 & -482	+53%

Table 9.6-1 shows that the simplified analysis overestimates that stringer moment by 45% for the HL-93. While the simple analysis found the peak moment in the span adjacent to the joint, the 3D analysis showed the maximum positive moment to occur in the first stringer span in from the bridge's east end, the middle stringer of the deck. The simplified analysis assumes that all floor beams act like rigid vertical supports. In reality the floor beams deflect, changing the moment distribution.

Floor Beam Analysis

Estimation of the Frigo floor beam loading was attempted using the same process as described for the Chippewa bridge. The Frigo stringers have a 45ft. span and are continuous over floor beams. The Chippewa bridge had a 25ft. stringer span with simply supported stringers. To determine the stringer reaction on a floor beam a 2-span continuous stringer model was analyzed with truck wheel line loads applied as diagrammed in Figure 9.6-2 for the Dual500 truck. The HL-93 wheel line produces a reaction of 24.8k and the Dual500 produces 79.3k.

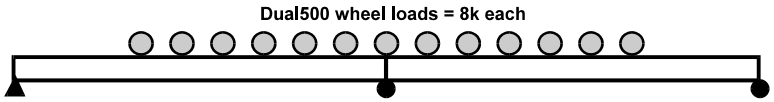

Figure 9.6-2. Multiple 8k Dual500 wheel loads applied to 2 span stringer model.

Since the AASHTO distribution factor produced a reasonable estimate of the Dual500 wheel load distribution causing stringer moments (compared to the factors from the simple slab span analysis), a similar distribution method was assumed for the portion of a wheel line load causing a reaction on a floor beam. The factor used above was 1.46 wheel lines per stringer. The Dual500 has 4 wheel lines and the two center wheels are spaced at 2 feet. Three stringers will be assumed to resist the Dual500 load – the two outside stringers are assumed to receive one wheel line, the middle stringer will resist 2 wheel lines. Only one OSOW truck is assumed on the bridge. This loading is shown in Figure 9.6-3.

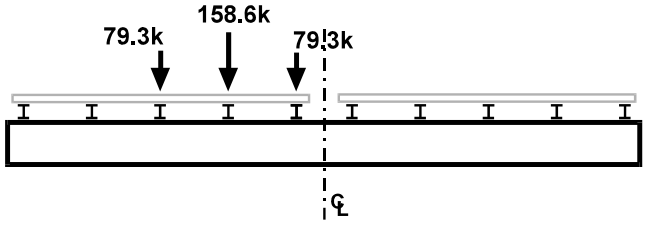

Figure 9.6-3. Simulated Dual500-2 loading on a Frigo floor beam.

With double roadway widths of 40ft., the bridge could be loaded with six adjacent HL-93 trucks or twelve wheel lines. Each of the ten stringers will be assumed to equally resist $12/10^{ths}$ of a wheel line. Five reactions of 1.2*24.8kips = 29.8k will be applied, adjusted by the multi presence factor of 0.65 to 19.3k each.

As noted in previous analyses, even though the floor beam is rigidly attached to the tie girders, the girder stiffness is insufficient to produce a fixed end condition. The floor beams will be analyzed for

moments assuming both fixed and pinned end conditions. The simplified predictions with the accurate 3D analysis results are listed in Table 9.6-2.

Table 9.6- 2. Comparison of Frigo floor beam moments - accurate vs. approximate.

Bridge	Truck	Max. Moment 3D Model (kip-ft.)	Max. Moment 2D Analysis (kip-ft.)	+M % change vs.3D Model
Frigo	HL93	2178 & -679	1978 pinned	-9%
			666 & -1312 fixed	-69%
	Dual500-2	4206 & -802	5398 pinned	+28%
			2156 & -3839 fixed	-49%

In estimating the floor beam moments the approximate method appears successful, though it overestimates the effect of the Dual500 OSOW load by 28% (conservative). The two methods used in obtaining these simplified results differ for the HL-93 and Dual500 loads.

In the case of the HL-93 all of the stringers are assumed to equally carry the load when all lanes are loaded. The reaction of the stringer on the floor beam is determined by first looking at a two span continuous stringer loaded with an HL-93 truck wheel line. Then the total reaction from all wheel lines is equally distributed to all the stringers and the beam moment analysis is done assuming pinned ends.

For the Dual500-2 OSOW vehicle loading, two trailers with 4ft. wheel spacing on an axle and a 2ft. trailer separation, the two closely spaced wheel lines are assumed to be carried on a single stringer. The two outer wheel lines are assumed to be carried by the two adjacent stringers. The reaction from any stringer on the floor beam, due to a wheel line, is calculated by applying the Dual500 wheel line on a two span continuous stringer.

9.7: Simplified Analysis for Stringer Moments

Before looking at forces in individual members – consider the bridge system. The force distribution in each of these bridges depends on the geometry and the type of support systems existing. Table 9.7-1 lists these various characteristics. A load placed on the deck of any of these bridges will be distributed to resisting elements depending on their spacing, stiffnesses and end support conditions. The stringer condition in the two bascule bridges differs significantly from that in the arch bridges, particularly in stringer spacing. The decks above the stringers also vary – with open steel gratings on the bascules and concrete slabs on the arch bridges. With the concrete slabs there may or may not be composite action between the deck and supporting members.

Table 9.7- 1. Bridge geometry and support characteristics.

Bridge	stringers			floor beams		
	spacing ft.	span ft.	span type	spacing ft.	span ft.	span type
Marinette bascule	4	14.25	2 span non-comp.	14.25	34	pinned non-comp.
Winneconne bascule	2.37	14.75	1 span non-comp.	14.75	28.5	pinned non-comp.
Cameron arch	7.83	25.25	1 span composite	25.25	47.5	rigid ends non-comp.
Chippewa arch	7.42	25	1 span composite	25	51.4	rigid ends non-comp.
Frigo arch	9.12	47	continuous composite	47	85	rigid ends non-comp.

Examining all of the simple analysis results for stringer forces described previously, it is apparent that a completely satisfactory analysis approach was not available for general application. The unique geometry, connections, and existence of composite affects the stringer behavior. The stringer moment prediction result for each of the bridges is summarized in Table 9.7-1.

Table 9.7- 1. Stringer simple moment prediction error – vs. accurate 3D analysis.

Bridge	Error in simplified method	
	HL-92 load	OSOW dual trailer
Marinette bascule	0%	-39%
Winneconne bascule	-4%	-16%
Cameron arch	0%	+37%
Chippewa arch	+2%	+16%
Frigo arch	+45%	+53%

The simplified prediction of stringer forces in all the bridges, except Frigo, was very satisfactory under the HL-93 load. From a geometry view all of the satisfactory bridges were similar in having short stringer spans and a lack of continuity. The Frigo stands alone with a stringer span nearly double the

other bridges, continuity over supports, though still having a similar stringer spacing. Clearly these changes affect the quality of a simple force estimate.

It is interesting, however, that in comparing the non-composite bascule bridges with steel grating and the first two arch bridges with composite concrete decks – the predicted simplified HL-93 forces developed in the stringers are accurate in all. This would not be expected. Composite action changes the ratio of relative stiffness between the bridge deck and the stringer and should produce a different load distribution. The Frigo arch is a unique case where the simplified method did not work for HL-93 loading. Looking at the at the very different geometry of that bridge, shown in Table 9.7-1, and the continuity in the stringers combined with composite action there is a clear change in relative member stiffness and a change in load distribution.

When under OSOW vehicle loading, with unusual wheel spacings on axles and axle spacings, the simplified methods of stringer force prediction produce very variable results. In the bascule bridges, where the AASHTO distribution factor from the previous Standard Specifications was used, the stringer moment with OSOW trucks was underestimated by 16 to 39%. This is a non-conservative result. The AASHTO equation for load distribution depends on the stringer spacing and was developed for HL-93 trucks with 6ft. wheel spacing on axles and widely spaced axles. The OSOW trucks, particularly the dual trailers, had a 4ft. wheel spacing on an axial and wheels on adjacent trailers were 2ft. apart, much closer together than used in the HL-93 truck. This may explain the poor results with the bascule bridges.

The three bridges with concrete decks had composite action between the stringer and deck. Though using the AASHTO distribution factor (as in the Cameron bridge) should under again underestimate the stringer force, the error was a 37% over-estimate. In the Chippewa and Frigo alternate distribution methods were used for the OSOW vehicles, and the stringer moments were over-estimated by 16% and 53% respectively. It is suspected that this overestimate occurs because the composite action reduces the bending moment carried in the steel stringer alone. While the simplified analyses ignored the composite action, it was explicitly included in the 3D FEM modelling.

Based on these results it could be suggested that the AASHTO distribution factors not be used with bascule bridges under OSOW loads and trucks with special wheel spacing/axle configurations. As a rough approximation of load effects on stringers in bridges with concrete decks, the composite action could be ignored and the truck load resisted by a stringer could be estimated using the AASHTO equations or by assuming the deck is fully loaded and all the stringers equally share the induced moments. The results from the analyses here indicate that these methods will over-estimate (conservatively) stringer moments by as much as 50%.

9.8: Simplified Analysis for Floor Beam Moments

Floor beam moment estimates obtained by the attempted simplified analysis methods appear to be as inaccurate as the stringer results. Table 9.8-1 shows the errors in predicting moment produced by the simplified methods compared to a full 3D FEM analysis of the bridge. It is noticeable that in all OSOW truck load cases the simplified estimate of floor beams was safely conservative.

Table 9.8- 1. Floor beam simple moment prediction error – vs. accurate 3D analysis.

	Error in simplified method	
Bridge	HL-92 load	OSOW dual trailer
Marinette bascule	+15%	+9%
Winneconne bascule	-13%	+15%
Cameron arch	-1%	+43%
Chippewa arch	+100%	+205%
Frigo arch	-9%	+28%

Various methods were employed to simply predict the floor beam moments. Each of the methods first depended on how the vehicle wheel line loads were distributed to the stringers. Then the reactions of the stringers on the floor beams needed to be calculated. Finally assumptions need to be made regarding the end support conditions for the floor beams. These were made by examining how the beams were connected to the supporting girders.

The first approach taken (Marinette and Winneconne), for the HL-93 load, was to calculate the reaction of the simply supported stringers on the floor beam if they were loaded by a single wheel line of the vehicle. Four stringers were then assumed to resist the load. Since the stringers were spaced at 4ft. and the truck wheels were spaced at 6ft. – adjacent stringers were assumed to have one of the four wheel lines. The floor beam moment was calculated as a simple span beam. This approach errored by 15% or less on the two bridges for HL-93 trucks. The same method was used for the OSOW truck with 6ft. spacing between trailers and four adjacent stringers were assumed to be loaded by one wheel line each – so the reactions were applied 4ft. apart on the floor beam. This resulted in a 9% to 15% over-estimate error. It may be that the simplified method used too close a load spacing on the floor beam, assuming that the 14ft. wide truck load was carried by a set of stringers 12ft. wide. The load on the floor beam may have been concentrated to closely to the center of the floor beam. The small error of 15% for floor beam force in these two bridges appears quite acceptable.

A second approach was used in the Cameron bridge because of the different geometry with 7.83ft. stringer spacing. The OSOW loading effects were estimated by first taking the axle and wheel configuration and placing it transversely near the center of the deck. The portion of load going to each stringer was calculated by assuming that the slab was a simple span beam strip between stringers. This provided simple distribution factors for the stringers. When the slabs were loaded, their reactions on the stringers were easily calculated. Then the reaction from a stringer line on the floor beam was calculated by applying a full wheel line of the OSOW vehicle on the stringer. Finally the load on the floor beam was taken as the distribution factor times the wheel line reaction. For the HL-93 loading, since the stringer spacing was close to the wheel line spacing, one wheel line was applied per stringer and the reaction on the floor beam calculated. These reactions were then taken as loads on the floor beam.

With the Cameron bridge the first significant problem in the floor beam analysis was recognized. While the bridge design insured that the flanges and webs of the floor were secured to the girders, creating a rigid moment resisting connection, analyzing the beams as if their ends were “fixed” was unsatisfactory. The negative end moments developed in the simple analysis were far above those found in the 3D analysis and the positive moments were smaller. It became apparent that a simple analysis with fixed ends was inappropriate. In the real bridge the tie girder torsional stiffness was insufficient to completely restrain the floor beam rotation. A pinned end analysis was an improvement, but the error in positive moment prediction in the girder was +43%.

Comparing the simplified predicted floor beam moment diagram with the moment diagram from a 3D analysis clearly exhibited the impact of partial composite action that was developed in the more accurate 3D analysis. Acting compositely with the deck, the composite beam resisted a good portion of moment through a couple consisting of compression in the deck and axial tension in the floor beam. The actual moment in the steel floor beam was reduced. A simplified beam analysis was incapable of capturing this behavior, and overestimated the bending in the steel beam.

Two other modified approaches for floor beam analysis were employed in the Chippewa and Frigo bridges. HL-93 analysis was further simplified. Since each of these decks accommodates multiple HL-93 lanes, the load on stringers from the trucks HL-93 truck was assumed to be equally distributed. With a pin end assumption, even though construction details implied a rigid end joint, the HL-93 moments were estimated as 100% high and 9% low in the Chippewa and Frigo bridges respectively.

The OSOW truck impact on the Chippewa floor beams was calculated in the same manner as used for the Cameron bridge. With a pin ended assumption this overestimated the OSOW induced moment by 205%. The 100% error in HL-93 estimate and 205% for the OSOW in the Chippewa is puzzling. A specific source of this error could not be identified.

On the Frigo bridge a different approach was taken for the OSOW loading on the floor beam. The actual stringers were continuous over multiple spans. The wheel line of the OSOW vehicle was applied to a stringer. To determine the stringer reaction on a floor beam, a simplified 2 span model was analyzed and the middle reaction calculated. Then the AASHTO distribution factor for the portion of a wheel line going to a stringer was examined to find a distribution factor of 1.46. A separate analysis looking at the slab as simply supported, as described above for the Cameron bridge, suggested a higher factor. An approximate assumption was made – placing 2 wheel lines over the stringer below the middle of the two trailers, and 1 wheel line on the two adjacent stringers. This provided a moment estimate in the pin ended floor beam simple model that was 28% higher than the 3D estimate. The 28% difference could be attributable to the conservative placement of load as if being transferred by only three stringers.

9.9: Simplified Analysis for Bascule Girder Moments

Moments induced in the girders of the bascule bridges were estimated by placing 2 lanes of HL-93 trucks, symmetrically located transversely, and assuming that each of the two bascule girders resisted one complete truck weight. The bascule girder results are listed in Table 9.9-1. Predictions for the HL-93 loading were accurate – as expected for the simple symmetric loading.

Table 9.9- 1. Bascule girder simple moment prediction error – vs. accurate 3D analysis.

	Error in simplified method	
Bridge	HL-92 load	OSOW dual trailer
Marinette bascule	-3%	+21%
Winneconne bascule	+3%	+29%

The moments calculated under the OSOW loading were obtained in a slightly different process. Since the OSOW Dual500-2 truck and trailer occupied a single lane, assuming that it did not drive down the middle of the bridge, the truck load was applied in an unsymmetrical pattern. To estimate the portion of the truck load resisted by a single girder a simple analysis was followed. The truck wheel loads were applied to a simple supported floor beam and the reaction on the closest girder was calculated as a portion of the truck axle load. Then that portion of the axle load was applied to the bascule girder at each axle location, rather than at the floor beam locations. With such loading on the bascule girder the moment at the support was calculated. The structural model used in this calculation, however, was not just a cantilever girder. Instead the two girders on opposite leafs were both modelled with fixed ends at the abutments and a hinge between girder at midspan. The analysis of this indeterminate girder was

done using software. While the resulting girder moments were over-estimated, by 21 to 29%, this appears to be a simple and conservative method for quick girder analysis.

9.10: Recommended Simplified OSOW Analysis Techniques

Stringers:

No single technique for predicting the moments in stringers was identified. The moment in stringers on a bascule bride with steel grating could not be safely estimated using the AASHTO distribution factors because of the unusual spacing of the OSOW vehicle wheels. In the bridges with concrete decks using the 1996 AASHTO Standard Specifications [9] equation from Section 3.23.2.3.1.5 for a distribution factor for 4 or more stringers supporting a concrete floor provided a conservative estimate of the stringer moment, 16 to 53% high. Part of the error comes due to the AASHTO equation being developed for a truck with wheel spacing of 6ft. rather than the close wheel spacing that can exist in OSW dual trailer vehicles. The inability to more accurately estimate the stringer moment with a simple analysis also comes from the composite character of the stringer. A closer estimate of the moment in the stringer could be obtained by using the following steps in bridges with composite decks:

1. Place the wheel line loading of the vehicle on a single stringer model and calculate the internal moment,
2. Calculate the AASHTO Standard Spec distribution factor for the stringer spacing,
3. Adjust the calculated stringer moment by the distribution factor, and
4. Apply that moment to a composite cross section with steel beam and concrete deck, then calculate the resultant axial force in the steel beam and the moment in the steel beam.

Floor Beams

In bridges with close spacing between floor beams the loading on the floor beam depends on how the stringers carry the truck wheel line loads. With long stringer spans, the portion of the vehicle line load going to a stringer can be estimated using the AASHTO Standard Specifications distribution equation. With short stringer spans it is recommended that the load going to stringers be estimated by assuming that the deck is simply supported, non-continuous, at each stringer. The truck wheel loads from one axle line should be applied to the slabs and reaction on the slabs calculated. The reactions represent the portion of the axle load carried by each girder. Then a representative stringer should be analyzed with a wheel line loading to determine the support reaction. The loads applied to the floor beam by the stringers can be taken as the portion of load on a stringer multiplying the calculated stringer reaction. When these loads are applied to the floor beam the beam moments should be

calculated assuming that the beam is pin ended. Using this approach the floor beam moments may be over-estimated by 50%

Bascule Girder Moments

The moments in bascule girders can be estimated by analyzing a simple, but indeterminate, 2D model of a single girder line. The girders line is made up of two girders, each assumed fixed at the abutments and joined by a pinned connection at the middle bridge joint. The load on each girder can be estimated by first finding the portion of truck weight carried by the girder. This is estimated by analyzing a model of the floor beam, simply supported, with one axle of wheel loads applied to find the portion of the axle weight at a reaction. Then the axle loads of the vehicle are directly applied to the girder but adjusted in magnitude by the portion of axle weight at the floor beam reaction on the girder. This approach resulted in over-estimates of girder moments ranging from 15 to 21%.

10. Summary

A prime observation from this study is that very large overload vehicles, with total gross weights nearly seven times the weight of the basic truck used in bridge design, can be allowed to pass over most of the complex bridges examined. This may be particularly important for the long span bridges, such as the La Crosse Cameron Avenue tied arch. The Leo Frigo Memorial bridge over the Fox River in Green Bay was found to be slightly less robust, but even its truck capacity was not limited by the main structural elements: the arch and the tie beam. There were no cases, of the set of bridges examined, where vehicles with gross weight of up to 500,000lbs caused the arches, tie girders or hangers of these bridges to be overloaded.

The forces developed in the long span bridges by the basic design vehicle, AASHTO HL-93 trucks weighing 72,000lbs in each of the design lanes, exceeded those created by the overweight trucks on all of the bridges examined except for the Frigo Memorial Bridge. It was assumed, however, that when one of these special highly overweight vehicles crossed a bridge all other truck traffic would be held off the bridge and the vehicles would be travelling at slow speeds.

As a general conclusion it appears that the bridge stringers, which support the concrete deck, and the floor beams, which support the stringers, are the critical components that need to be closely examined when an overload vehicle is crossing a bridge. The stringer force capacity limited the bridge load capacity in three of the five bridges that were closely examined. The floor beam force capacity controlled in one.

Two bascule bridges were examined. Under the HL-93 design truck loading, the bridge capacity was found to be limited by the stringer strength in one case and the floor beam strength in the second case. When the large overweight vehicles pass over these bridges, however, the capacity is limited by the strength of the two main bascule girders that support the entire bridge. These observations may be deceptive since a close examination of two complex parts of the bascule bridge, the midspan joint between leafs and the tail beam that prevents the bascule leafs from tipping downward, was not possible in the scope of this project. Though the joints were modelled, the predicted strain conditions didn't match measured values found during truck loading. This indicated that a fine modelling of the stress flows in the regions of the components would be needed to obtain reliable response values. These critical parts may deserve a detailed examination to insure that stresses remain within acceptable limits under heavy truck loading.

An alternate method, based on the empirical data from the load test combined with force predictions from analysis, did indicate that it is highly likely that the tail beam or tail lock could be severely overloaded (to nearly twice the yield stress) under both full factored HL-93 design truck loading

and the OSOW truck loading. The tail lock beam is an essential resisting element in a bascule bridge and needs to be guarded. It appears critical that further investigation of the tail beams on an array of bascule bridges be undertaken.

A general simplified method for estimating forces in stringers and floor beams was not satisfactorily achieved for all loadings. The portion of truck wheel loads carried by a stringer can be estimated by using an AASHTO defined distribution factor (from the AASHTO Standard Specifications) and the stringer moments calculated for HL-93 truck loading will be acceptable for most bridges with standard proportions. When the span to spacing ratio of the stringers exceeds 4, as in the Frigo bridge, then use of the AASHTO factor may produce results that are 25% conservative.

Stringer moments are not successfully predicted using the same AASHTO distribution factor but for the wheel loads of the OSOW trucks examined. It is unlikely that the AASHTO factor would work with any vehicle that has wheel spacing on an axle substantially different from the AASHTO assumed 6ft. spacing. When OSOW trucks were on the bridges examined, the stringer moments could be conservatively predicted using an alternate method that overestimated by 16% to 124%. The alternate method estimates wheel loading on a stringer by considering the bridge deck to act as short simply supported spans between stringers. Calculated reactions from the deck on the stringers, due to wheel loads, are used to calculate the stringer moments. This method conservatively estimated stringer moments in all cases.

Floor beam forces were more difficult to predict than the stringer forces when using a simplified method. One of the primary difficulties is in accounting for the restraint applied to a floor beam by the supporting girders. In cases where the joint was by web connection only, the floor beam could be considered pin ended. When the floor beams were rigidly connected to the girders the assumed support condition was dubious. A fixed end assumption produced a calculation of negative end moments much larger than actually existed, and of course smaller positive moments. A pin ended assumption over-estimated the magnitude of the positive moments. The calculation process is further complicated by the assumption made regarding the wheel load distribution to the stringers as discussed above. Since the stringers apply the load to the floor beams, errors in assumptions regarding stringer load resistance carry into the floor beam calculations. Results for floor beam moment calculations in the bascule bridges were acceptable with HL-93 loading, except in the case of the Chippewa arch bridge. With OSOW vehicle loading the moments were over estimated by 9% to 43% (except with the Chippewa bridge), a conservative result that may be acceptable for judging capacity.

A simple method for estimating moments in the main girders of bascule bridges was identified. The portion of a truck load conducted to any girder was first calculated by applying the truck axle line on a single simply supported floor beam and solving for the portion of total axle load carried to the floor beam's reaction on the girder. Then that portion of the truck load was applied directly on the girder, a contribution from each axle, and the girder moment calculated. The girder moment calculation, however, had to be dome using a model where each girder had a fixed end and was joined to the girder in the opposing leaf by a hinged joint. Existence of an initial small gap in the midspan joint was found to

have little effect on peak forces and stress. With a gap of 0.125in. in the Winneconne bridge, the resulting peak stresses change by only 8%. In bridges with well-maintained joints the effect of an initial gap on the member forces can be ignored.

REFERENCES

[1] Bae, H. and Oliva, M. (2009), "Bridge analysis and evaluation of effects under overload vehicles." Rep. No. CFIRE02-03, Univ. of Wisconsin, Madison, WI.

[2] AASHTO. (2014). "AASHTO LRFD Bridge Design Specifications, 2014", 7th Ed., American Association of State Highway and Transportation Officials, Washington, DC.

[3] Chung, W. and Sotelino, E. (2006), "Three-dimensional finite element modeling of composite girder bridges." Engineering Structures 28 (2006): 63-71.

[4] Wisconsin Department of Transportation, WisDOT Bridge Manual. http://wisconsindot.gov/Pages/doing-bus/eng-consultants/cnslt-rsrces/strct/bridge-manual.aspx

[5] Computers and Structures, INC. CSI Knowledge Base. https://wiki.csiamerica.com/display/csibridge/Home

[6] Murphy, J., "PCBridge", http://joeinmadison.com/sharew/share.htm

[7] QConBridge, Washington State Department of Transportation, www.wsdot.wa.gov/eesc/bridge/software/index.cfm?fuseaction=software_detail&software_id=48

[8] Koglin, T. (2003), "Movable Bridge Engineering." John Wiley & Sons, Inc., Hoboken, New Jersey.

[9] Standard Specifications for Highway Bridges. (1996) American Association of State Highway

[10] Wisconsin Department of Transportation, Highway Structures Information System (HSI). <https://trust.dot.state.wi.us/hsi>

Appendix

Critical Bridge Member Locations

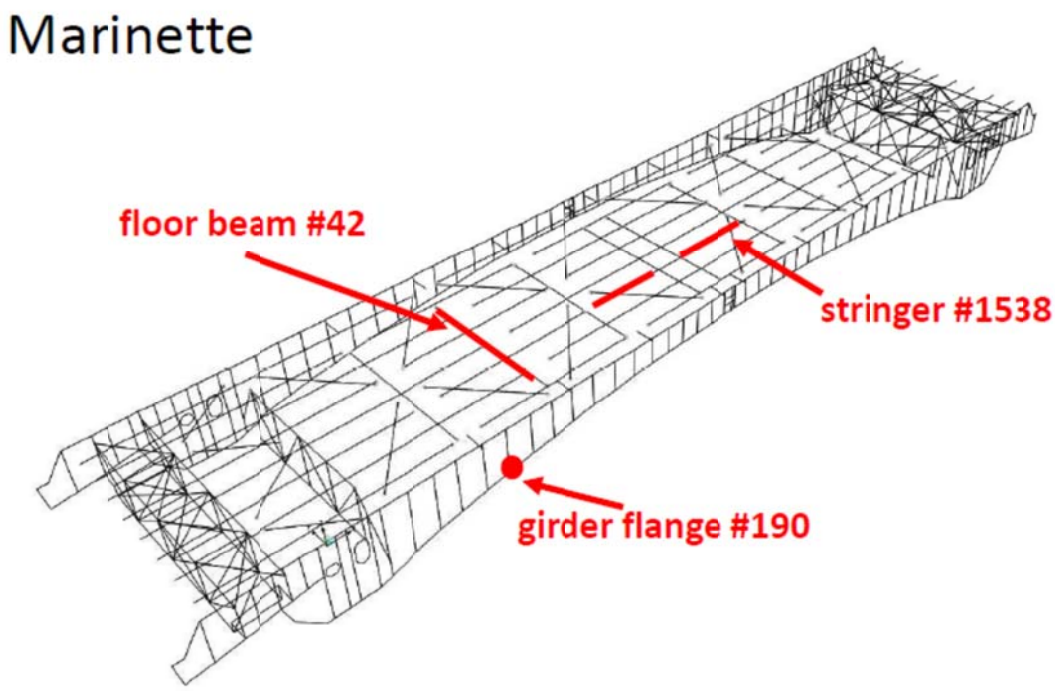
Marinette
floor beam #42
stringer #1538
girder flange #190

Winneconne

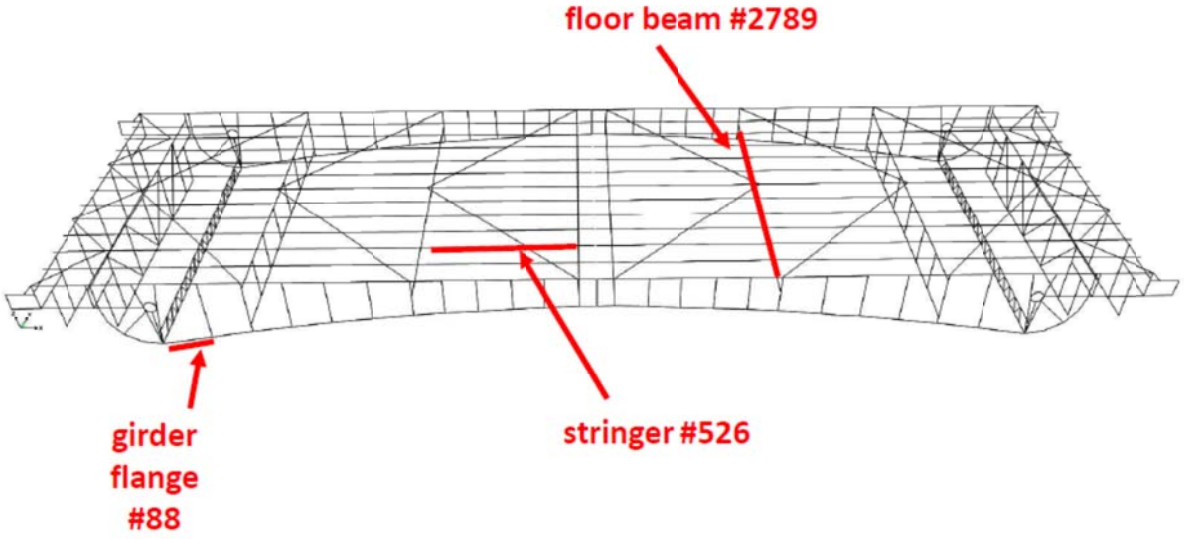

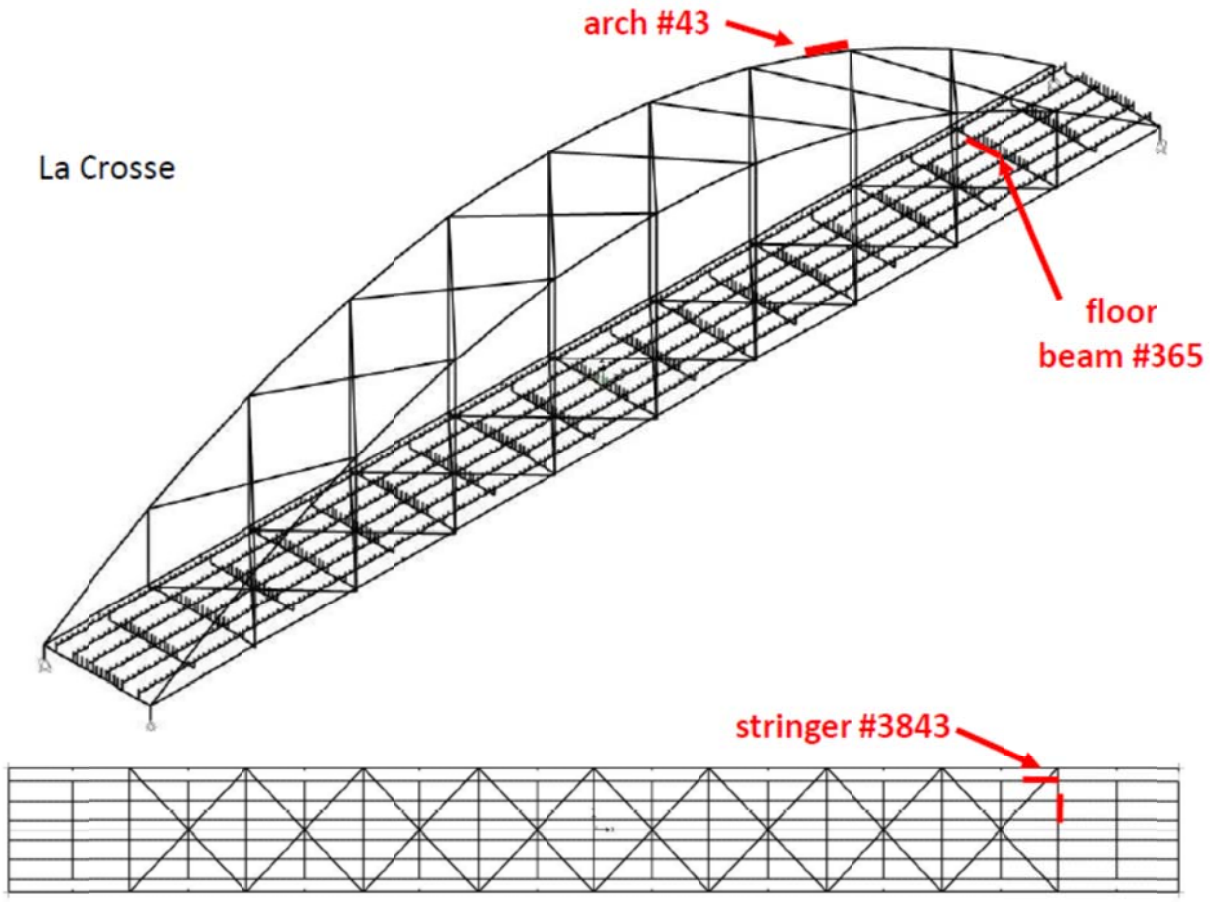
arch #43
La Crosse
floor
beam #365
stringer #3843

Chippewa

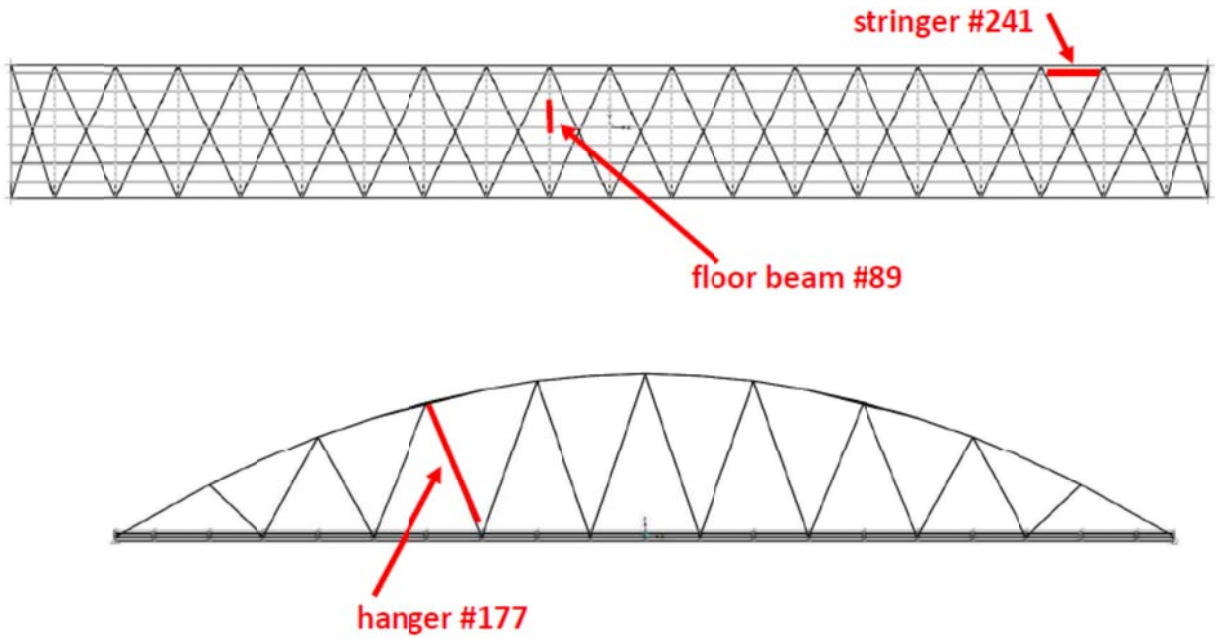

CFIRE

University of Wisconsin-Madison
Department of Civil and Environmental Engineering
1410 Engineering Drive, Room 270
Madison, WI 53706
Phone: 608-263-3175
Fax: 608-263-2512
cfire.wistrans.org